Optimization of Carbon-S-Glass Fiber Epoxy Resin Composites with Varied Carbon Content and Fiber Orientation for Improved Beam Bumper Energy Absorption through Analytical Approach

Haymanot Saketa Negasa

A Thesis Submitted to the Department of Mechanical Engineering
School of Mechanical, Chemical and Materials Engineering

Presented in Partial Fulfillment of the Requirement for the degree of Master of Science in Automotive Engineering

Office of Graduate Studies
Adama Science and Technology University

September, 2023 G.C
Adama, Ethiopia

Optimization of Carbon-S-Glass Fiber Epoxy Resin Composites with Varied Carbon Content and Fiber Orientation for Improved Beam Bumper Energy Absorption through Analytical Approach

Haymanot Saketa Negasa

Advisor: Getachew Alemayehu (PhD)

A Thesis Submitted to the Department of Mechanical Engineering

School of Mechanical, Chemical and Materials Engineering

Presented in Partial Fulfillment of the Requirement for the degree of Master of Science in Automotive Engineering

Office of Graduate Studies

Adama Science and Technology University

September, 2023 G.C

Adama, Ethiopia

DECLARATION

I hereby declare that this Master Thesis entitled "**Optimization of Carbon-S-Glass Fiber Epoxy Resin Composites with Varied Carbon Content and Fiber Orientation for Improved Beam Bumper Energy Absorption through Analytical Approach**" is my original work. That is, it has not been submitted for the award of any academic degree, diploma or certificate in any other university.

All sources of materials that are used for this thesis have been duly acknowledged through citation.

Haymanot Saketa	______________	__________________
Name of the student	Signature	Date

RECOMMENDATION

I, the advisor of this thesis, hereby certify that I have read the revised version of the thesis entitled "**Optimization of Carbon-S-Glass Fiber Epoxy Resin Composites with Varied Carbon Content and Fiber Orientation for Improved Beam Bumper Energy Absorption through Analytical Approach**" prepared under my guidance by Haymanot Saketa submitted in partial fulfillment of the requirements for the degree of Masters of Science in Automotive Engineering. Therefore, I recommend the submission of revised version of the thesis to the department following the applicable procedures.

Getachew Alemayehu (PhD)	________________	________________
Major Advisor	Signature	Date

APPROVAL PAGE

I, the advisors of the thesis entitled "**Optimization of Carbon-S-Glass Fiber Epoxy Resin Composites with Varied Carbon Content and Fiber Orientation for Improved Beam Bumper Energy Absorption through Analytical Approach**" and developed by Haymanot Saketa; hereby certify that the recommendation and suggestions made by the board of examiners are appropriately incorporated into the final version of the thesis.

Getachew Alemayehu (PhD)	________________	____________________
Advisor	Signature	Date

We, the undersigned, members of the Board of Examiners of the thesis by Haymanot Saketa have read and evaluated the thesis entitled "**Optimization of Carbon-S-Glass Fiber Epoxy Resin Composites with Varied Carbon Content and Fiber Orientation for Improved Beam Bumper Energy Absorption through Analytical Approach**" and examined the candidate during open defense. This is, therefore, to certify that the thesis is accepted for partial fulfillment of the requirement of the degree of Master of Science in Automotive Engineering.

____________________	____________________	____________________
Chairperson	Signature	Date
____________________	____________________	____________________
Internal Examiner	Signature	Date
____________________	____________________	____________________
External Examiner	Signature	Date
____________________	____________________	____________________
Head of the Department	Signature	Date
____________________	____________________	____________________
School Dean	Signature	Date
____________________	____________________	____________________
Post Graduate Dean	Signature	Date

ACKNOWLEDGEMENT

First of all, I would like to thank immensely my Lord for all His Provisions and Blessings throughout my life and the thesis work. I would like to express my heartfelt gratitude to my advisor, Getachew Alemayehu (PhD), for his invaluable guidance and expertise. I am deeply thankful to my mother, Wolansa Alemu, and my aunt, Tenagne Alemu, for their unwavering support and belief in my abilities. I also extend my appreciation to friends, whose encouragement and friendship have made this journey more meaningful. Lastly, I acknowledge the contributions of all those who have supported me throughout my MSc thesis work. Your guidance, belief and presence have been instrumental in my success, and I am sincerely grateful for your firm support.

TABLE OF CONTENTS

CONTENTS **PAGE**

LIST OF TABLE

TABLE **PAGE**

LIST OF FIGURES

FIGURE **PAGE**

ACRONYMS AND SYMBOLS

ACP	AnsysCompositePrePost
AISI	American Iron & Steel Institute
AM	Availability of Raw Material
ASTM	American Society for Testing Materials
AVI	Availability of Material Information
AVM	Availability of Material
BBA	Building Block Approach
CAD	Computer Aided Design
CAE	Computer Aided Engineering
CCF	Chopped Carbon Fiber
CFRP	Carbon Fiber Reinforced Polymer
CMH	Composite Material Handbook
CMVSS	Canadian Motor Vehicle Safety Standard
CNTs	Carbon Nanotubes
CS	Cost
CSM	Continuous Strand Mat
DP	Disposal
DS	Density of Material
EA	Energy Absorption
EC	Environmental Consideration
ECE	Economic Commission for Europe
EPP	Expanded Polypropylene
ETP	Engineering Thermoplastic

FEA	Finite Element Analysis
FEM	Finite Element Method
FM	Flexural Modulus
FMSS	Federal Motor Safety Standard
FS	Flexural Strength
GMT	Glass Mat Thermoplast
IIHS	Insurance Institute for Highway Safety
IPM	Ideal Point Method
ITH	Impact Toughness
KBS	Knowledge Based System
KIC	Stress Intensity Coefficient
KMPH	Kilometer per Hour
LCC	Load Carrying Capacity
MP	Manufacturing Process
MPa/GPa	Mega Pascal/Giga Pascal
NHTSA	National Highway Traffic Safety Administration
OEM	Original Equipment Manufacturers
PAN	Polyacrylonitrile
PR	Performance
RC	Resistance to Corrosion
RMC	Raw Material Cost
RY	Re-Cycling
SC	Service Condition

SEA	Specific Energy Absorption
SH	Shape
SMC	Sheet Molding Method
UD	Uni-directional
W	Weight
WA	Water Absorption
$\boldsymbol{V_f}$	Volume Fraction of Fiber
$\boldsymbol{V_m}$	Volume Fraction of Matrix
$\boldsymbol{\varepsilon}$	Young's Modulus of Elasticity
$\vee$	Poisson's Ratio
$\boldsymbol{G}$	Shear Modulus
$\boldsymbol{v_c}$	Volume Fraction of Carbon
$\boldsymbol{v_s}$	Volume Fraction of S-Glass
$\boldsymbol{v_E}$	Volume Fraction of Epoxy Resin
γ	Shear Strain
$\boldsymbol{\rho}$	Density
K	Elastic Constant
$\boldsymbol{E}_k$	Kinetic Energy
V	Velocity
$\boldsymbol{\kappa}$	Spring of Stiffness
$\boldsymbol{F}$	Force
$\boldsymbol{P}$	Pressure
$\boldsymbol{mm}$	Millimeter

ABSTRACT

This MSc Thesis focuses on the redesign and optimization of the bumper beam for the Lifan 520. The objective is to demonstrate an innovative advancement in Composite science by developing a hybrid material made of Carbon-S-Glass fiber Epoxy Resin, replacing the previous steel beam. The aim is to achieve the ideal balance of strength, rigidity, and weight through a laminate structure with a unidirectional fiber arrangement. The optimization procedure involves adjusting the percentages of carbon fiber and S-Glass fiber in the composite material. The fiber-to-matrix ratio is carefully balanced at 60% fiber and 40% matrix. The evaluation process includes analyzing different carbon fiber content ranges (5%, 15%, 25%, 30%, 35%, and 40%) and assessing key characteristics such as internal energy, deformation, equivalent stress, and directional acceleration. The Greys Relational Analysis Technique is employed to evaluate the composite's performance under various scenarios. The optimization procedure reveals that the composition with 5% carbon content stands out prominently and performs exceptionally well achieving the top spot. This result emphasizes the importance of finding the right balance between structural stability and weight savings. Furthermore, an investigation into the influence of fiber orientation is conducted. Unidirectional fiber alignment at 0 degrees consistently holds the top position, demonstrating its remarkable suitability for projected loading circumstances. The 22.5-degree orientation follows closely, confirming its effectiveness in various applications. Additionally, a multidirectional configuration with the coordinates (0, 90, 0, 90, 0) degrees achieves an honorable third place, indicating the potential advantages of multiple fiber orientations. Based on the findings, it is recommended to use a composite material with 25% carbon content for the bumper beam of the Lifan 520. The unidirectional fiber alignment at 0 degrees is suggested as the optimal orientation for achieving the desired performance under projected loading conditions. However, considering the potential benefits, a multidirectional configuration with the specified coordinates may also be considered for certain applications. The analysis of the selected material was conducted using software such as SOLIDWORKS, ANSYS SpaceClaim, ANSYS21R2, ANSYSCompositePrepPost, and LS-DYNA. These tools facilitated the assessment of the material's properties and performance. This MSc Thesis contributes crucial insights to the field of composite material engineering and introduces a paradigm shift in automotive material science. The discoveries made significantly advance our understanding of the intricate interactions between material composition, orientation, and performance outcomes. This research lays the foundation for future advancements in vehicle safety engineering.

Keywords: *Varied Carbon, Grey Relation Analysis, Hybrid, ACP, C5, FEA, Fiber Orient*

CHAPTER ONE

INTRODUCTION

This chapter has the following sections: background of the study, statement of the problem, objective of the study, scope of the investigation, significance of the study, and structure of the study.

1.1. Background

In the automotive sector, bumper beams are used as shock-absorbing elements. The brackets used to fasten them to the front and rear ends of motor vehicles serve as crash-boxes, absorbing loads mostly in the axial direction. The bumper beam is the first component to sustain damage in auto accidents; therefore its specifications are among the most important criteria for determining a car's dependability and safety. Other bumpers are designed using energy absorbers or brackets, while some are made with foam cushioning. The purpose of a car bumper is to stop or reduce physical harm to the front and back ends of a passenger car. In most cases, a bumper is fastened to either end of a car to cushion impact during collisions and protect the occupants. Car bumpers serve as front and rear vehicle shields for occupants and can be composed of steel, aluminum, rubber, or plastic. The bumper system takes the strain even in low-speed collisions to stop or lessen vehicle damage. The bumper, which is positioned either in the front or the back of a car, shields the occupants from the force of an accident by being there (Witteman, 2000).

The bumper subsystem is one technique to accomplish the objective of a light weight vehicle, which is now the main focus. The car bumper subsystem can be improved to carry less weight and absorb more structural energy. The beam bumper can be improved in particular. In today's engineering analysis, it is uncommon for a project to not require a simulation to examine the behavior of the model under predetermined conditions. The practice of replicating real-world situations has several significant benefits. New design concepts can be explored before being translated into drawings by modeling it to see how it will perform under various load circumstances when minimal money has been invested and modifications are affordable. Simulators may evaluate the design in great detail after a detailed 3D model has been produced, reducing the number of prototypes required and saving time and money. Analysis can be used to expedite an engineering change and lower the cost of an existing product that is having a problem in the field or is simply being upgraded (Hosseinzadeh R.M, 68(2005)).

Three key stages make up the finite element approach: (1) pre-processing, where the analyst creates a finite element mesh to break the subject geometry into smaller pieces for mathematical analysis and adds material properties and boundary conditions; (2) solution, where the program derives the controlling matrix equations from the model and solves for the basic quantities; and (3) post-processing, where the analyst verifies the results (Tejasagar Ambati, 2012).

Due to their high specific strength, high modulus, and superior damping properties, fiber reinforced composite materials have been widely used in transportation vehicle structures. These materials are anticipated to lighten vehicles while also lowering noise and vibration levels. Additionally, composites display exceptional resilience to corrosion and fatigue, offering substantial benefits over the conventional usage of different grades of steel for the construction of automotive bodywork (Marzbanrad JM, 2009).

Steel bumper beams have many benefits, one of which is their excellent weight carrying capacity. However, the strength-to-weight ratio is becoming worse. Sources claim that weight reduction and a sufficient improvement in mechanical qualities have made composites a competitive alternative to traditional steel. A very good composite polymeric base bumper has recently replaced the steel beam bumper used on passenger vehicles. Aluminum and composites have already been utilized to lighten vehicles and increase their energy efficiency. Additionally, they offer flexible design options, corrosion resistance, toughness, and durability along with high performance at a reasonable price. This study is performed by using AnsysCompositePrePost and ANSYS LS-DYNA software's for designing of an improved vehicle bumper made from Carbon fiber, S-glass fiber with epoxy resin composite materials, the output parameters were assessed by use of FEM to govern the impact cases (Berrahou Mohamed, 2022).

A typical beam bumper consists of a bumper cover (1) that defines the bumper system's external appearance, an energy absorber (2) made of an elastic material, such as a polypropylene foam body or a urethane foam body, to absorb energy, an impact beam (3) to support the energy absorber, and a stay (4) to connect the impact beam 3 to the car body (Marzbanrad JM, 2009) and (Heinz Heisler, 2002).

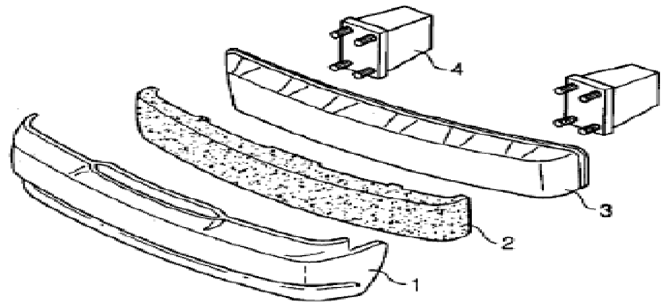

(a)

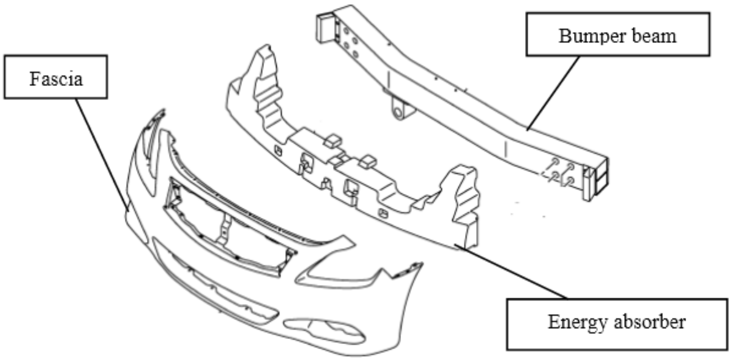

(b)

Figure 1.1: (a&b) Typical Beam Bumper (Marzbanrad JM, 2009) & ((2016)Infinitihelp website.)

1.2. Problem of the Statement

When collisions occur, the bumper beam of the Lifan 520 demonstrates insufficient capacity to absorb energy, leading to potential safety concerns. Utilizing steel as a structural material for the bumper beam would address this issue but would also result in an undesirable increase in the overall weight of the vehicle, leading to higher fuel consumption. Therefore, there is a need to redesign and optimize the bumper beam using an innovative approach in composite science to achieve a balance between strength, rigidity, and weight, thereby improving energy absorption capabilities without compromising fuel efficiency.

1.3. Objectives of the Study

1.3.1. General Objective

The main goal of this thesis is to design and evaluate a beam bumper for light automobiles built of a Hybrid Composite that is Carbon-S-Glass Fiber Reinforced Epoxy Composite, with variable Volume Fraction percentage of carbon fiber and fiber alignment to improve the beam bumper's performance.

1.3.2. Specific Objectives

The specific objectives of the study are;

- To determine the typical mechanical properties of the materials.
- To develop 3D Model of a Hybrid material and laminate beam bumper using Carbon-S-Glass fiber and Epoxy Resin on AnsysCompositePrePost.
- To determine the best-performing percentage of added carbon fiber (explore composite sample with different percentage of carbon fiber i.e. 5%, 15%, 25%, 30%, 35%, & 40% out of the total fiber percentage).
- To examine different fiber alignment technique (22.5^0, 45^0, 67.5^0, & 90^0) and some combined orientations) and analyzing the impact performance for enhanced performance of the already selected fiber percentage.
- To compare and select the optimum ranged (best performing) hybrid composite material with fine and recommend for automotive structural use and further investigation.

1.4. Scope of the Study

The key subjects of this thesis are the effectiveness, advantages, and restrictions of current or previously finished designs. Depending on careful monitoring, the design may be enhanced in terms of shape, size, or material-based design modification goals. The impact weight of the modified beam bumper for a show car will be evaluated using FEM software in accordance with requirements. Additionally, by choosing materials with a lower weight-to-strength ratio, I will improve vehicle performance and lengthen the fatigue life of the bumper beams. For in-depth examination, applications such as SOLIDWORKS, ANSYS.21R2, and Ansys-ACP are employed.

1.5. Significance of the Study

The Significance of this study is to;

- Save the occupants from severe injury.
- Efficient crashworthiness ability or better crash performance of beam bumper.
- Minimize the impact of the collision and shield the other components from additional harm.
- Improve energy absorption

- Lighter in weight resulting fuel economy

Also this paper could be significant for students, academicians, and manufacturers who’re engaged in body design.

1.6. Organization of the Study

There are six (6) chapters in the thesis. The background of the study, the overall purpose of the research, a statement of the issues, the study's objectives, and its significance are all covered in chapter 1. The review of the relevant literature, with an emphasis on earlier investigations on beam bumper, is presented in Chapter 2 of the study. Boundary condition and load determination will be addressed. In Chapter 3, this is about logical reasoning techniques. Using the ANSYS LS-DYNA and AnsysCompositePrePost software, the Finite Element Impact Simulation and Analysis was presented and briefly observed in Chapter 4. The outcomes of the simulation utilizing the ANSYS LS-DYNA software are covered in Chapter 5 and discussed and presented. In the final topic, it talks about the conclusions and provide some suggestions for the future.

CHAPTER TWO

REVIEW OF LITERATURE

Examining various pieces of literature is crucial to comprehending the research of a vehicle's crashworthiness and improvements to composite performance. A literature review primarily comprises various composites research investigations as well as an examination of earlier crashworthiness tests and analyses of various circumstances.

2.1. Theoretical Background

(Gergely Czél, 2015), to enhance the mechanical performance of pseudo-ductile, unidirectional (UD) inter-layer carbon/glass hybrid composites, a novel partially discontinuous architecture is developed. The idea was demonstrated in a number of laminates using S-glass Epoxy UD pre-pegs and high strength, high modulus carbon. The revolutionary hybrid architecture generated pseudo-ductile tensile stress-strain responses with a linear starting portion, a broad plateau, and a second linear part, all of which were connected by smooth transitions. A plateau stress of 860 MPa, a pseudo-ductile strain of 2%, and a modulus gain of 60% over pure glass were all displayed by the best hybrid design. Each specimen design's initial modulus, plateau stress, and overall tensile stress-strain response were foreseen with accuracy.

Understanding the energy-absorbing mechanisms of composite material systems experiencing crush failure was the subject of some study that got started in the 1980s. Since the underlying principles that determine the crushing behavior and energy absorption in composite materials are technically difficult and poorly understood, research in this area has until now only focused on experimental evaluation. This study only takes into account CFRP systems that use thermo-set resin in order to concentrate on advanced structural composites, which are frequently the most popular form of composite used in primary vehicle structures. The brittle crush failure reaction in these kinds of composite material systems is progressive crushing (Feraboli, Vol. 43, No. 19, 2009, pp. 1967–1990)**.**

The major goal of this project is to create a beam bumper that will increase the crashworthiness of the bumper. It also examines the impact behavior of an epoxy composite vehicle bumper beam reinforced with s-glass fibers that has a volume composition of 60% fiber and 40% matrix. The current Lifan 520 model bumper beams are replaced with composite bumper beams. Internal energy is absorbed by steel at a rate of 1200.9 J while it is absorbed by composite materials at a rate of 1960 J, which is 38.7%

higher than that of steel. For the design of the new car bumper made of s-glass fiber reinforced epoxy composite materials, the analysis is done using the LS-DYNA program, and both the total deformation and internal energy absorbed by the materials are calculated (Ashenafi Abuye, 2017)

LS-DYNA, Abacus/Explicit, RADIOSS, and PAM-CRASH are examples of contemporary explicit FEA programs that are used to model the dynamic crushing deformation and damage of both composite and metallic structures (Composite Materials Handbook (CMH-17)), over the past ten years, these codes have developed in the automotive industry into a trustworthy instrument for the modeling of collisions involving metallic structures. In order for these cutting-edge material models to be effective in producing results that are sorely needed as the use of composites in vehicle structures increases, the application of such models in full-scale FEA crash simulations necessitates a cunning strategy and implementation due to the technical challenges presented by the ongoing development of composite material models. When using composite damage material models in crash simulation, the BBA (Building Block Approach) method is used (Du Bois, December 2001).

(Hosseinzadeh R.M, 68(2005)), according to their study, bumper beams are one of the key elements of passenger cars that protect them from front and rear collisions. A commercial front bumper beam manufactured of glass mat thermoplastic (GMT) was examined and described using the E.C.E. United Nations Agreement (Uniform Provisions concerning the Approval of Vehicles with Regard to Their Front and Rear Protective Devices). One of the most typical components of passenger cars that shield them from front and rear collisions, according to studies, is bumper beams. In this work, a commercial for a front bumper beam made of glass mat thermoplastic (GMT) is analyzed and described utilizing modeling using the modeling application LS-DYNA ANSYS. The three main design criteria for this structure are shape, material, and impact conditions. The results are compared to more conventional metals like steel and aluminum. In place of the current GMT, the proposed high strength SMC (sheet molding compound) bumper is utilized to describe the aforementioned aspects.

(Marzbanrad JM, 2009), Discussed the most important parameters including material, thickness, and shape and also impact condition and are studied for design and analysis of an automotive front bumper beam to improve the crash-worthiness design in low-velocity impact. The simulation of original bumper under condition impact is according to the low-speed standard of automotive stated in E.C.E. United Nations Agreement Regulation no.42, 1994 (Feraboli, Vol. 43, No. 19, 2009, pp. 1967–1990). The deflection, impact force, stress distribution, and energy-absorption behavior of a front bumper beam constructed of three materials aluminum, glass mat thermoplastic (GMT), and high-strength sheet molding compound (SMC) are investigated in this study using impact modeling. To determine the optimal choice of material, form, and thickness, the aforementioned features are contrasted with one another. The findings demonstrate that a modified SMC bumper beam can optimize elastic strain energy while minimizing bumper beam deflection, impact force, and stress distribution. Additionally, the impact of passengers on conduct is investigated.

(Witteman, 2000), thanks to advancements in vehicle styling, the overhang of the bumper will be lower, there will be more sweeps, and the bumper system will take up less space overall. In addition to discussing how this novel prototype energy absorber design might be utilized in place of EPP foam, this paper will examine market trends for bumper energy absorbers. A review of the prototype ETP energy absorber's simulated performance as well as a comparison of the actual test findings for an 8 km/h FMVSS Part 581 impact series to the performance of EPP foam packaged in the same environment are also required.

The performance requirements for bumpers vary by nation. According to international safety regulations, a car's safety systems must continue to operate normally following a straight-on pendulum or moving-barrier impact at 4 km/h (2.5 mph) to the front and rear, and at 2.5 km/h (1.6 mph) to the front and rear corners at 45.5 cm (18 in) above the ground with Automobile Beam Bumper Analysis to Improve Energy Absorption (2017) the front and rear corners. It must adhere to 4 KMPH pendulum and barrier impacts in North America (FMSS: Federal Motor Vehicle Safety Standards) and Canada (CMVSS: Canadian Motor Vehicle Safety Standards) (James Jones, 2023).

(Mohapatra, 2005), there is discussion of the shorter development cycles for autos. Finding time-efficient design solutions is the main challenge facing OEMs and suppliers in light of the more intense market competition. Researchers are making many outdated designs better by applying cutting-edge techniques. It is more challenging for R&D departments to generate a number of diverse design possibilities in less time and money than existing designs since there are typically competing performances and cost limitations. Utilizing some of the most contemporary CAD and FEM tools in a CAE environment is the most efficient method to achieve these best solutions. These technologies enable speedy design changes when employed in a virtual setting.

(Andersson R, 2002), Among the items disclosed are a bumper system with a bumper cover, an energy absorber made of synthetic resin using a foam molding process, an impact beam made of glass mat thermoplastic with a "C" shaped section supporting the energy absorber, and a stay attaching the impact beam to a vehicle body. On the impact beam's front upper and lower portions, tips are generated, and in between the tips is a web portion. An inner surface of the energy absorber has tip insertion grooves where the tips are placed, and the inner surface also has a pressure receiving surface that corresponds to the web part.

(Butler M, 2002), The emphasis on enhancing crash performance in automotive vehicles necessitates the adoption of innovative methods and materials. In order to effectively mitigate the impact of crashes, the crash safety components should possess the capability to either transmit or absorb energy. The energy absorption capacity of a component relies on its geometry and material properties. Therefore, it is crucial to select materials with high yield strength and a relatively high elongation to fracture for these components. Given these requirements, the utilization of high strength stainless steels is gaining popularity as they fulfill the necessary criteria and address the evolving needs in automotive safety.

(Morgan, 1999), Bumper system technologies will need to develop new strategies to fit into the smaller package spaces while still maintaining the vehicle performance and cost criteria as automakers continue to be more aggressive with the style of new cars. This paper's goal was to present cutting-edge expanded polypropylene (EPP) foam technology and procedures.

(Masoumi A, 2011), This thesis discusses the design of a new frontal vehicle architecture that loads the second unloaded longitudinal component with the axial force of an offset accident's asymmetric impact force. Only when longitudinal elements and a pattern of progressive folding are used together may enough energy be absorbed in the front structure. This prevents the passenger compartment from deforming. The new longitudinal members include two functional parts that work together to prevent premature bending collapse: an inside square crushing column for a normal, steady axial force level and a stiff outer sliding supporting structure that provides the extra bending resistance that is required. The force is transferred to the other longitudinal part via an integrated cable system. With this cutting-edge design idea, a vehicle may withstand full, offset, and oblique collisions with a front structure that can absorb the same amount of energy.

(O. G. Lademo), explains a "rib-reinforced beam" a thin walled, hollow beam with ribs that might be used as a car bumper. Using numerical simulation of the bending behavior under impact loads, the crashworthiness of the rib-reinforced beam is compared with thin-walled hollow tube-like beams filled with and without foam materials (empty beam and foam-filled beam). Investigating the effects of the reinforced rib's shape and performing shape optimization design are done to increase energy absorption and decrease the first peak force. The development of a multi-objective crashworthiness optimization method based on the Ideal Point Method (IPM) that considers the least initial peak force, maximum energy absorption, and maximum specific energy absorption. A normalized cubic spline function is used to provide the reinforced rib's ideal design. According to numerical example results, the optimized rib-reinforced beam has a higher energy absorption capability and a lower initial crash force than empty and foam-filled beams of equal weight. It has been discovered that for rib-reinforced beams, small rumple forms around compressed indentions, which helps to delay side wall collapse and results in more energy absorption.

(Nitin S. Gokhale, 2007), Aluminum extrusions are frequently created through a series of procedures in the soft W-temper condition before the components are artificially aged to reach the T6 condition, which is the material's peak hardness, to manufacture bumper systems. For accurate finite element (FE) modeling of the crash performance of the final systems, it is probably necessary to use geometry that is derived from a FE model that closely follows the process route, i.e., includes simulation of all significant forming processes. Additionally, the forming processes lead to the uneven evolution of various internal variables (such the effective plastic strain) in the produced components. Tensile studies show that plastic straining in W-temper causes a considerable shift in the T6 work-hardening curves. The tests also reveal a reduction in the elongation of the T6 specimens due to the plastic pre-deformation. These process effects have been incorporated in the current work's user-defined elasto-plastic constitutive model in LS-DYNA along with some ductile fracture criteria, a state-of-the-art anisotropic yield criterion, the associated flow rule, and a non-linear isotropic work hardening rule.

(Ramazan Karakuz, 2010), We used numerical modeling and practical laboratory analysis to perform research on the damage prediction in glass/epoxy laminates subjected to low velocity impact loading. The Fractovis plus impact testing device was used for the experimental laboratory test, which used 20 J of impact energy. Their study examines quantitatively the impact behavior of unidirectional laminated glass/epoxy composite plates with $[0/\pm\theta/90]_S$ fiber orientation at equal energies of 40J, 2m/s, and 5kg of impact mass. They selected five distinct fiber directions (15°, 30°, 45°, 60°, and 75°) to test the stacking effect. To investigate the impact behavior of glass/epoxy composite plates, three different plate thicknesses at 2.9 mm, 5.8 mm, and 8.7 mm were chosen. The stress and contact pressures on composite plates during impact events are computed numerically using the transient finite element code 3D IMPACT. Choi and Chang failure/damage criterion can also be used to forecast the threshold of impact damage and commencement. The developers of this code employ an eight-point brick element and a direct gauss quadrature integration approach to account for the variation in material properties from layer to layer. Step-by-step time integration is also performed using the New-mark approach. The Newton Raphson method is additionally combined with a contact law to determine the contact forces upon impact. The academics get the conclusion that the numerical results are often consistent with the outcomes of the experimental investigation when they compare them to those results.

(Idicula, 2006), They have shown that adding natural fiber to glass fiber considerably enhances the composite materials' capacity to transfer heat. Cicala et al. have investigated the characteristics and abilities of different Hybrid glass/natural fiber composites for use in curved pipes. Flax fiber/polypropylene composites' mechanical characteristics were assessed by Arbelaiz et al., who also looked at the effects of fiber/matrix alteration and glass fiber hybridization. According to their findings, the glass/flax ratio affects the tensile strength and modulus of hybrid glass/flax polypropylene composites.

(JFA Madeira, 2019) This study aims to determine the ideal ply fiber orientations to reduce maximum out-of-plane displacement under such loading conditions and to assess the mechanical performance of hybrid carbon-glass composite plates under combined bending and torsion loading. Hybrid composite plates with 10 plies each and different stacking sequences were made using hand lay-up and reinforced with carbon and glass fibers in an epoxy matrix. Two experimental setups (with two separate boundary conditions) are explored here to test the composite plates, both exhibiting combined bending and torsion force. The experimental tests were numerically simulated in ABAQUS and validated using experimental data. Then, using the ply fiber orientations as design variables, global and local optimization with direct search (GLODS) was used to optimize the hybrid composite plates. The objective function of limiting the maximum out-of-plane displacement is carried out through an interactive function. As required, switch between (GLODS) and (ABAQUS). Additionally, three ideal laminate specimens were produced for experimental verification. The hybrid composite plates' performance was enhanced by the optimization strategy. The cost savings over some non-optimized plates is greater than 30%.

(Katkar A.D., 2015)**,** In order to improve the crashworthiness design in low-velocity impacts, the most crucial design parameter, thickness, was examined for the design and analysis of a car front bumper beam in this article. According to the low-speed automobile standard outlined in E.C.E. United Nations Agreement, Regulation No. 42, 1994, the simulation of the original bumper under the condition of impact thickness was conducted. In these studies, an impact analysis is used to estimate the deflection and plastic strain caused in a front bumper beam made of three different thicknesses (4mm, 4.5mm, and 5mm). To determine the optimal option of bumper thickness, the aforementioned features are contrasted with one another.

(George C. Jacob, 2004), A composite material's capacity to absorb energy is essential for enhancing human safety in auto accidents. The ability of a structure to endure impacts and safeguard its occupants is referred to as crashworthiness. For the purpose of comparing the crashworthiness in terms of specific energy absorption (SEA), chopped carbon fiber (CCF) composite material systems were put up against other fiber resin systems, such as graphite/epoxy cross-ply laminates (CP#1 and CP#2), a graphite/epoxy braided material system (O), and a glass-reinforced continuous-strand mat (CSM). How many of these material systems would be necessary for a midsize car driving at various speeds was calculated and compared. Among all the composite materials examined, the chopped carbon fiber composite material's SEA was the greatest. It was determined that, in the event of a collision at 15.5 m/s (35 mph), only 4.27 kg of it would need to be installed at precise locations inside the vehicle to guarantee passenger safety. This logically led to the crucial practical conclusion that the required amount of this composite material to achieve the appropriate impact performance criterion is merely a reasonable amount. Both of the requirements a large magnitude of energy absorption and a safe acceptable rate of this energy absorption that must be accomplished before a material is certified extremely crashworthy were met by the CCF composite when tested at 5mm/min crushing speed.

(Berrahou Mohamed, 2022), discussed, the primary goal of this work is to repair a composite material structure by bonding composite patches with varied fiber orientations. The effects of stress distribution, damaged area ratio, stress intensity factor KIC, and enforced stacking sequence were highlighted in a thorough analysis that had two sides, an applied experimental side and a numerical model side. 8-layer graphite/epoxy, glass/epoxy, and boron/epoxy plates with various angles are among the composite materials plates examined in this work. The results obtained show unmistakably that the orientation of the fibers affects the ultimate strength of failure and that fibers oriented longitudinally in the direction of the tensile strength provide us a good performance of the composite material on the experimental side. Regarding the model, the effects of the stress intensity factor, together with the interaction between the damaged area and the fiber orientation, on the effectiveness of these patches, were investigated. We can conclude from this study that fiber orientation plays a major impact in the performance of the composite material and its repair efficiency.

(Yonggang, 2015, Vol. 7(6)), This article examines the bumper beam, the most important part of the car's front bumper system, in order to enhance its crashworthiness performance in low-velocity accidents. The low-speed automobile norm specified in E.C.E. United Nations Agreement, Regulation No. 42 is followed when doing the low-velocity impact simulation using finite element analysis. The fundamental goal of this article is lightness. First, the steel and carbon fiber composite bumper beams are analyzed to determine their deformation, weight, force of impact, capacity to absorb energy, and impactor acceleration. As a result, the impact behavior of the carbon fiber composite bumper beam is improved. Second, bumper beams with varying thicknesses, including 5.4, 6, 6.6, and 7.2mm, are studied for lightweight purposes. According to the findings, the 5.4mm bumper beam is the best option without compromising impact performance. Thirdly, to achieve superior lightweight outcomes, the thickness distribution of the bumper beam is altered in accordance with the stress distribution. It appears that the weight of the upgraded bumper beam is much lower yet the impact performance is unaffected.

(M.M. Davoodi, 11 April 2012), In low-speed impacts, bumper beams deflect the unintentional kinetic energy, and in high-speed impacts, they deform, absorbing it. The complicated nature of bumper system design increased as a result of new environmental restrictions on "end-of-life vehicles" and safety criteria for "low-, high-speed, and pedestrian impacts." The new bumper design must be flexible enough to decrease passenger and occupant injury and remain intact in low-speed crashes, in addition to being strong enough to disperse the kinetic energy in high-speed impacts. Before going into mass manufacturing, the reinforcing beam must be confirmed using finite-element analysis (FEA) and experimental tests because it is crucial to safety. The strength, weight, and potential for using biodegradable and recyclable materials to prevent environmental pollution can all be optimized by careful bumper beam design and analysis of useful characteristics. The development of appropriate design and analysis techniques eliminates the need to modify the design. On the other hand, research into the factors that contribute most to high bumper beam strength improves the effectiveness of product creation. Some important design factors in bumper beam fabrication are cross section, longitudinal curvature, fixing method, rib thickness, and strength. To determine the best bumper beam design procedure, this study thoroughly reviews the pertinent bumper design literature. It focuses in particular on the important design factors for bumper beams and the best values or ranges of values for each. The findings can support functional study of the bumper beam determining variables by designers and researchers.

2.2. Composite Materials

The definition of a composite material is a structural material comprised of two or more components that, when combined, produce desired attributes that none of the components can achieve alone (Kaw, 2006) (J.N.Reddy, 2004). These composite materials go through two main phases: the matrix phase and the reinforcing phase. The substance used for reinforcing might be continuous or discontinuous and can be in the form of fibers, particles, or flakes. The materials used in the matrix stage are normally continuous and are used to scatter the fibers and transfer load to the reinforcing phase material. Reinforcing materials are strong and have low densities, while matrix materials are frequently hard or ductile.

A substance comprised of two or more macroscopically linked phases that are not chemically soluble in one another is referred to as a composite. The second phase, into which the reinforcement has been included, is referred to as the matrix. Continuous threads, woven material, short length fibers, particles, or flakes can all be used as reinforcement. In general, the matrix is continuous. A unidirectional lamina has all of its fibers aligned in the same direction. The layers of unidirectional lamina in cross ply laminate are aligned at right angles to each other (Dr.Shivanand N. Pujar, 2022).

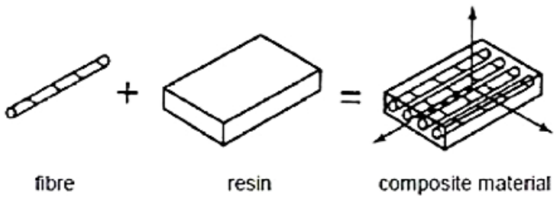

Figure 2.1: Typical Composite Materials (Jones, 1999)

Composite materials are normally classified into two broad categories: natural fiber composites and synthetic fiber composites (Kaw, 2006). Synthetic composites are formed by mixing two or more materials in specific quantities under controlled conditions; examples include carbon, glass, and so on; natural composites are made of naturally occurring fibers such as sisal, bamboo, and so on.

2.2.1. Composites with Fiber Reinforcement

S-glass fibers coupled with an epoxy resin matrix are used to reinforce composite materials called S-glass fiber reinforced epoxy materials. Silica, alumina, and magnesium are combined to generate S-glass, a high-performance fiber. They exceed traditional E-glass fibers in terms of mechanical properties like stiffness, temperature resistance, and better tensile strength.

Table 2.1: Frequently utilized natural fibers and polymer composites (Mueller, (2003))

Natural Fiber Composites	Cellulose (Plant) fiber	Bast	Flax, Hemp, Kenaf, Jute & etc.
		Leaf	Sisal, Banana, Abacca, Pineapple & etc.
		Seed	Cotton, Kapok, Poplar, Colatropis
		Fruit	Coir, Luffa
		Wood	Hardwood, Softwood
		Grass	Wheat, Bamboo, Corn, Bagasse
	Matrix Materials	Thermoplastic s	Polypropylene, Polyamide, Polyethylene, Polyvinylchloride
		Thermo-setting Plastic	Phenolic, Epoxy, Polyester, Polyimide, Polyurethane
		Biopolymers & Rubbers	Carbohydrate, Proteins, Polyphenol-resins, India-rubber

Epoxy resins are thermosetting polymers with excellent chemical resistance, adhesion, and durability. Epoxy resins provide a strong and long-lasting matrix with S-glass fibers, which increases the mechanical properties of the composite material. Natural Fiber Composites: Natural fiber composites use natural fibers as reinforcing components and a polymer matrix to bind the fibers together, such as epoxy or polypropylene. These composites are lightweight, renewable materials with high specific strength and stiffness.

2.2.2. Energy Absorption of Fiber Reinforced Composites

Fiber reinforced composites can absorb and dissipate energy emitted following an impact or loading event. The amount of energy that a composite can absorb is affected by the type and arrangement of fibers, the matrix material, and the overall design of the composite. The following are some important factors concerning energy absorption in fiber-reinforced composites (Jones, 1999):

1. ***Fiber Orientation***: To absorb energy, a composite's fiber orientation is essential. When subjected to tensile, compressive, or shearing processes, fibers oriented in the direction of the applied load can absorb energy and effectively resist deformation. On the other hand, improper alignment of the fibers may result in a decrease in their absorption capacity.
2. ***Volume Fraction and Fiber Type***: The composite's fiber type has an impact on how much energy is absorbed. When it comes to absorbing energy, stronger fibers like carbon or the aramid fibers have an advantage over weaker ones. The capacity for energy absorption is also influenced by the volume fraction of fibers; a larger fiber volume fraction typically results in increased strength and stiffness, which improves energy absorption.
3. ***Matrix Material***: The matrix material in a fiber-reinforced composite also contributes to energy absorption. In order to avoid early fiber failure, the matrix can assist in distributing and transferring loads between fibers. While brittle matrices, like some thermo-setting resins, may fracture and restrict energy absorption, ductile matrix materials, like some thermoplastics, can experience plastic deformation and dissipate energy through plastic strain.
4. ***Inter-facial bonding***: Effective energy absorption depends on the bond formed between fibers and the matrix. Fiber pull-out, fiber/matrix de-bonding, and matrix cracking are examples of energy dissipation mechanisms that are made possible by a

strong inter-facial bond between the fibers and matrix. Inadequate inter-facial bonding can impede the absorption of energy and cause an early breakdown.

5. ***De-lamination and Fiber Breakage***: Both of these processes can aid in the absorption of energy. De-lamination is the separation of layers or plies in a composite. Whereas fiber breakage can release energy through fiber fracture and fiber/matrix de-bonding, de-lamination can absorb energy by generating pathways for crack propagation.
6. ***Architecture of Composites***: Energy absorption may be impacted by the composite's general architecture and design, including the layer thickness and stacking arrangement. Specific applications can maximize the load-bearing capacity and energy absorption characteristics by customizing the composite layup and thickness distribution.

Fiber reinforced composites' energy absorption capability can be modified for specific purposes by modifying variables such as matrix material, fiber type, orientation, volume %, and composite architecture. The selection and optimization of these characteristics are influenced by the intended performance, application, and cost aspects.

2.3. Unidirectional Lamina Engineering Constants

In laminated fiber-reinforced composite materials, a laminate is the fundamental building component. Understanding laminated fiber-reinforced structures thus requires an understanding of the mechanical behavior of a lamina (Jones, 1999).

Composite laminates, as defined in materials science, are assemblies made up of layers of fiber composite materials that can be bonded to provide the necessary engineering attributes, such as strength, coefficient of thermal expansion, bending stiffness, and in-plane stiffness.

High-strength fibers in a polymeric, metallic, or ceramic matrix material make up each of the individual layers. Graphite, glass, boron, and silicon carbide are common fibers that are utilized, whereas epoxies, polyamides, aluminum, titanium, and alumina are some examples of matrix materials.

Hybrid laminate can be created by layering various materials. Following that, the laminate displays orthotropic, quasi-isotropic, or anisotropic characteristics (with primary properties having varying directions). Typically, the individual layers are orthotropic (that is, with principal properties in orthogonal directions) or transversely isotropic (with isotropic properties in transverse plane). Quasi-isotropic laminates exhibit isotropic (that is, independent of direction) in plane response but are not restricted to isotropic out-of-plane (bending) response.

The laminate can show coupling between in-plane and out-of-plane response depending on how the different layers are stacked. The existence of curvature resulting from in-plane force is an illustration of bending-stretching coupling.

A lamina of composite is typically between 0.1 and 5 mm thick and is constructed with either unidirectional or bidirectional reinforcement. It is employed in the creation of laminates, the specifications of which (such as thickness, number plates, orientation, etc.) are established based on the demands of a certain project. Therefore, understanding the mechanical behavior of individual lamina, especially its constitutive equations, is necessary for the analysis of a laminate (Raiano, www.aerospacengineering.net, 2013).

The primary distinction between anisotropic and orthotropic materials is that the former exhibit distinct outcomes when analogous stimuli are applied in all directions, while the latter exhibit similar results when applied in just three mutually perpendicular directions. Anisotropy is the property of being directionally dependent (its characteristics vary continuously), as opposed to isotropy, which implies identical properties in all directions. (Raiano, www.aerospacengineering.net, 2013)

Specifically, a material is referred to as orthotropic if its three planes of symmetry are mutually orthogonal. The two primary directions (the direction of the fibers and the direction of the orthogonal reinforcement for unidirectional fiber) are parallel to the central plane of the lamina, which in a composite laminate identifies the plans. Observing, for instance, that applying a tensile load to an element with a prismatic form and made of anisotropic material results in deformations and variable flows along all element sides can help one better understand the differences between an anisotropic material and an orthotropic material. This happens irrespective of the specific direction in which the loading is applied. Alternatively, if the material is orthotropic, it can be characterized by three mutually orthogonal directions that, when a tensile stress is applied in them, result in a constant deformation without distortion in the plans indicated by these (Figure 2.1) (Raiano, www.aerospacengineering.net, 2013).

An orthotropic material is a continuous, unidirectional lamina of composite reinforced fibers. For an orthotropic material, there are *nine (9)* separate material constants, as is covered in Stress-Strain Relations of Materials. The planar stress assumption is valid for thin plates like laminas, and the number of independent constants can be further decreased from 9 to 4.

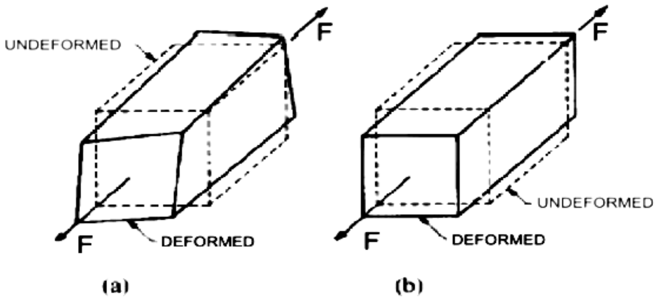

Figure 2.2: Deformation

To sum up, the constitutive equations of an *anisotropic material* comprise 21 elastic constants (a symmetric matrix of size 6×6); an *orthotropic material's* elastic constants involve 9 (6×6 sparse matrix); in the case plan, they decreased to only 4 (3×3) sparse matrices. In any case, it is more complex than isotropic materials, which only involve two elastic constants (**ε**, ***V***) due to its two-dimensional and three-dimensional nature. (Raiano, www.aerospacenginering.net, 2014).

There are just two independent engineering constants for isotropic materials: Poisson's ratio (ν) and Young's modulus of elasticity (**ε**). On the other hand, orthotropic laminas feature *nine* different engineering parameters: *three shear Moduli* (G_{12}, G_{13}, G_{23}), three independent *Poisson's ratios* (ν_{12}, ν_{13}, ν_{23}), and *three Young's Moduli* along the three primary materials directions (ε_1, ε_2, ε_3).

2.3.1. Stiffness Assessment by Material Mechanics

The engineering constants of a unidirectional lamina include longitudinal elastic modulus ε_1, transverse elastic modulus ε_2, in-plane shear modulus G_{12}, transverse shear modulus G_{23}, longitudinal Poisson's ratio ν_{12} and transverse Poisson's ratio ν_{23}.

An orthotropic material is a continuous unidirectional fiber reinforced composite lamina. There are 9 independent material constants for an orthotropic material, as explained in Stress-Strain Relations of Materials. The planar stress assumption is true for a thin plate such as a lamina, and the number of independent constants can be lowered from ***9 to 4*** (Jones, 1999).

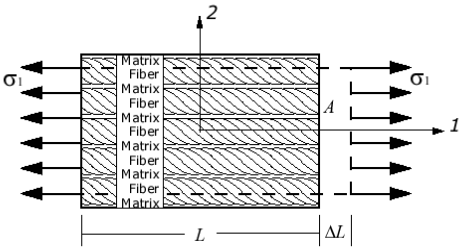

Figure 2.3: Volume Element Loaded in the 1-Direction (Jones, 1999)

A fracture between the fibers and the matrix is inferred if the strains were not the same. So, there is merit to the assumption. It is evident that sections normal to the 1-axis that were plane before straining remain plane after stressing since the strains in the matrix and fiber are the same. Our predictions for the apparent orthotropic Moduli of a unidirectional fiber-reinforced composite material, namely ε_1, ε_2, V_{12}, and G_{12}, are derived on the basis of this information. Keep in mind that each prediction has a concrete foundation that is not based on wishful thinking (Chamis, 2021).

A) $\boldsymbol{\varepsilon_1}$ ***Determination***

Assuming that the bonding between the fibers and the matrix is excellent, the strains of the fibers and the strains of the matrix must be equal in the fiber direction (i.e.,$\boldsymbol{\varepsilon_f = \varepsilon_m = \varepsilon_1}$) when the lamina is exposed to a uniaxial force along the fiber direction.

The total force applied on the lamina is,

$$P_1 = \sigma_1 A_1 = \sigma_f A_f + \sigma_m A_m \qquad \dots\dots\dots\dots\dots\dots\dots \qquad (2.1)$$

Where A_f and $A_m$are the fiber and matrix cross section areas, respectively. The *Young modulus* $\boldsymbol{E_1}$ can then be obtained,

$$\varepsilon_1 = \frac{\sigma_1}{\varepsilon_1} = \frac{{P_1}/{A_1}}{\varepsilon_1} = \frac{\sigma_f A_f + \sigma_m A_m}{A_1 \varepsilon_1} \qquad \dots\dots\dots\dots\dots\dots\dots \qquad (2.2)$$

$$= \frac{\sigma_f}{\varepsilon_1}\frac{A_f}{A_1} + \frac{\sigma_m}{\varepsilon_1}\frac{A_m}{A_1} \quad = \frac{\sigma_f}{\varepsilon_f}\frac{LA_f}{LA_1} + \frac{\sigma_m}{\varepsilon_m}\frac{LA_m}{LA_1} \quad = E_f V_f + E_m V_m \qquad \dots. \qquad (2.3)$$

Where **V** is the volume percentage and **L** is the length of the lamina. Keep in mind that

$v_f + v_m = 1$ This is predicated on the no-void assumption.

B) $\boldsymbol{\varepsilon_2}$ ***Determination***

Again, assuming perfect fiber-matrix bonding, when the lamina is exposed to a uniaxial force, the stress of the fiber and the stress of the matrix are equal in the *transverse direction* of the fiber ($\boldsymbol{\sigma_f = \sigma_m = \sigma_2}$):

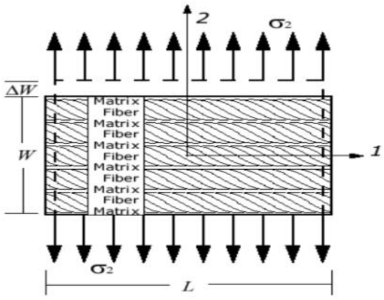

Figure 2.4: Volume Element Loaded in the 2-Direction (Jones, 1999)

The *transverse strain* is the sum of the fiber and matrix contributions, which are proportional to their respective volume fractions:

$$\varepsilon_2 = V_f \varepsilon_f + V_m \varepsilon_m \qquad \dots\dots\dots\dots\dots\dots. \qquad (2.4)$$

Using the serial-spring model, the *Young's modulus* $\boldsymbol{\mathcal{E}_2}$ can be calculated:

$$\mathcal{E}_{\mathbf{2}} = \frac{\sigma_2}{\varepsilon_2} \quad = \frac{\sigma_2}{V_f\varepsilon_f + V_f\varepsilon_m} \quad = \frac{1}{\frac{V_f\varepsilon_f + V_m\varepsilon_m}{\sigma_2}} \quad = \frac{1}{\frac{V_f\varepsilon_f}{E_f\varepsilon_f} + \frac{V_m\varepsilon_m}{E_m\varepsilon_m}}$$

$$= \frac{1}{\frac{V_f}{E_f} + \frac{V_m}{E_m}} \quad = \frac{\mathcal{E}_f\mathcal{E}_m}{V_f\mathcal{E}_m + V_m\mathcal{E}_f} \qquad \dots\dots\dots\ \dots\dots \qquad (2.5)$$

C) $\mathbf{v_{12}}$ ***Determination***

The analysis for $\boldsymbol{\varepsilon_1}$'s analysis is used to determine the so-called main ***Poisson's ratio***, or $\boldsymbol{\nu_{12}}$. The primary Poisson's ratio is

$$\nu_{\mathbf{12}} = -\frac{\boldsymbol{\varepsilon_2}}{\boldsymbol{\varepsilon_1}} \qquad \dots\dots\dots\dots\dots\dots\dots\dots\dots. \qquad (\mathbf{2.6})$$

As stated in the Determination of ***E₁*** section, we have, $(\boldsymbol{\varepsilon_f = \varepsilon_m = \varepsilon_1})$

And, $\qquad \varepsilon_2 = V_{f\varepsilon} f_2 + V_m \varepsilon_{m2}$

$$= -\left(\boldsymbol{V_f v_f \varepsilon_f + V_m v_m \varepsilon_m}\right) \qquad \dots\dots\dots\dots\dots\dots. \qquad (\mathbf{2.7})$$

The major Poisson's ratio is then expressed as,

$$v_{12} = -\frac{E_2}{E_1} = \frac{V_f\, v_f \varepsilon_f}{E_f} + \frac{V_m v_m \varepsilon_m}{E_m} \quad \ldots\ldots\ldots\ldots\ldots\ldots \quad (2.8)$$

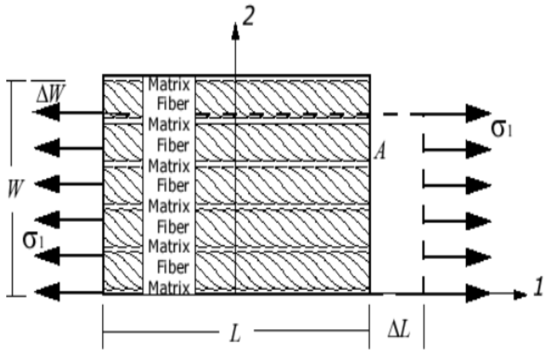

Figure 2.5: Typical Volume Element Loaded in the 1-Direction (Jones, 1999)

D) **G_{12}** ***Determination***

In the mechanics of materials approach, the in-plane shear modulus of a lamina, $\mathbf{G_{12}}$, is calculated on the assumption that *the shearing stresses on the fiber and the matrix are equal*.

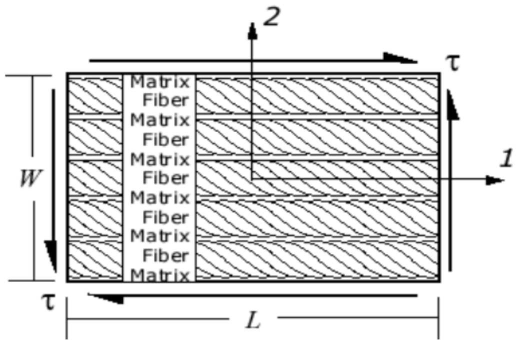

Figure 2.6: Shear-Loaded Representative Volume Element (Jones, 1999)

Expressed as, $\tau = G_f \gamma_f = G_m \gamma_m$

The shear strain is the total of the fiber and matrix contributions, which are proportional to their respective volume fractions: $\gamma = V_f \gamma_f + V_m \gamma_m$

The serial-spring model can thus be used to compute the shear modulus G_{12}:

$$G_{12} = \frac{\tau}{\gamma} = \frac{1}{\frac{v_f}{G_f} + \frac{v_m}{G_m}} = \frac{G_f G_m}{v_f G_m + v_m G_f}$$

After estimating the first three parameters, the minor Poisson's ratio V_{21} is easily determined.

$$\frac{v12}{E1} = \frac{v21}{E2}, v21 = \frac{v12}{E1} E2 \quad \ldots\ldots\ldots\ldots. \quad (\mathbf{2.9})$$

2.4. NHTSA and IIHS Crashworthiness

The National Highway Traffic Safety Administration (NHTSA) assesses the crashworthiness of vehicles and trucks each year. The NHTSA selects brand-new cars with strong sales volume forecasts or upgraded safety features. The governing organization in the United States is the National Highway Traffic Safety Administration (NHTSA). Due to the fact that accidents are covered by motor insurance, the Insurance Institute for Highway Safety (IIHS) also conducts comprehensive testing and uses a star rating system (up to five stars) to assess the safety of vehicles.

In terms of vehicle safety, IIHS assesses two factors: crashworthiness (how well a car protects its occupants in a collision) and crash avoidance and mitigation (how well a car's technology can stop a collision or minimize its severity). The IIHS also offers an annual Top Safety Pick, based on car segment, in addition to its star rating system. The IIHS evaluates a car using a series of tests that look at frontal crash, side crash, roof strength, head restraints and seats, and front crash prevention in order to assign it a star grade. In a few of these tests, the vehicle's structural layout is specifically analyzed. The other two tests that determine how a car will handle a frontal crash are the driver-side small overlap test and the passenger-side small overlap test. Both of these tests are designed to simulate what occurs when a car's front left or right corner strikes another car or an object like a tree or utility pole. The moderate overlap test, in which the vehicle is driven at 40 mph toward a barrier, is the third test.

Vehicle producers design and test their models in a variety of collision situations, including front, rear, and side impacts as well as rollovers, in order to comply with the safety criteria of the NHTSA and IIHS. The purpose of creating an automobile's crash management systems was not to keep the car from becoming damaged. Instead, the intention is to create a body structure that can absorb or deflect energy to the greatest extent possible in order to protect the passenger compartment.

To assess how successfully occupants are safeguarded in a head-on accident, tests are carried out. A rating of one to five stars is assigned to the vehicle based on the test results, with five stars representing the best protection and one the worst. The usefulness of the crash test scores depends on whether two vehicles are in the same weight class. According to federal law, all passenger vehicles must withstand a frontal collision at 30 mph, while the NCAP test involves colliding with a fixed object at 35 mph.

The truck is equipped with instruments to capture the structure's reaction to the collision.

In order to conduct the test, anthropomorphic dummies are installed in the driver's and passenger's seats. These dummies quantify the force of the impact to the chest, head, and leg. Based on these readings, a five-star rating was assigned. The test program exclusively evaluates crash-worthiness, which measures how well a vehicle's occupants are protected in a frontal collision.

2.5. E.C.E. United Nations Agreement, Regulation No. 42

Regulations set forth by the United Nations economic commission for Europe (UNECE) include "identical guidelines for the front and rear protection of vehicles that are approved." To improve their safety and lower the danger of harm to pedestrians and other vulnerable road users in the event of a collision, motor vehicles must comply with the requirements for front and rear protection set forth in Regulation No. 42.

When a passenger car is engaged in a low-speed collision, this regulation is applicable to how specific front and rear structural components behave. Protective devices, which are simply components found at the front and back ends of vehicles and created in such a way to allow contacts and minor shocks to occur without causing any severe damage, ensure exterior protection.

There are three annex documents that come before the regulation program is put into action. A vehicle type's front and rear protection devices (bumper beams, etc.), as approved by regulation No. 42, are the main subject of this message, which may also refer to a vehicle type's denial, withdrawal of permission, or definitive halt in production. Following the Low-speed Impact Test procedure, comes the installation of approval marks. During this test, a frontal and rearward low-speed collision with another vehicle will be simulated. The test must enable the ability to confirm that the vehicle's safety features adhere to the Regulation's requirements (E.C.E.(United Nation), 20 March 1958)

2.6. Research Gap

Low speed collisions are an area in which many researchers have conducted their work using the pendulum test. In order to increase the energy absorption, some of these studies have focused instead of the strengthening beam, on the fascia of the bumper beam and the energy absorber.

Certainly, those are some general potential research gap points related to bumper beams;

- **Material Advancement Characterization**: To understand their potential as bumper beam materials and how they stack up against more conventional choices in terms of crash performance and cost-effectiveness, researchers are examining the behavior of novel and advanced materials, such as composite materials with customized features.
- **Design Integration**: Examining the integration of bumper beams into the overall structure of the vehicle while taking into account issues like compatibility with other safety systems, simplicity of assembly, and design implications.
- **Multidisciplinary Optimization:** developing research that combine elements of material science, structural engineering, and vehicle dynamics in order to provide optimized bumper beam designs that balance safety, weight, and cost.
- **Real-world Crash Scenarios:** identifying particular collision scenarios that the current bumper beam design does not sufficiently address through the analysis of actual crash data. This can lead to the development of specialized bumper beam designs for particular accident types.
- **Energy-Efficient Manufacturing:** researching waste and energy-saving, environmentally friendly methods for producing bumper beams that increase sustainability and cost savings.
- **Evolving Safety Regulations:** Examine the design of bumper beams for any potential effects of changing safety laws and standards. This can entail anticipating modifications and creating bumper beams that not only adhere to present regulations but also consider requirements for the future.
- **Structural Health Monitoring:** investigating the installation of sensors and a monitoring system inside bumper beams to evaluate the stability of the structures over time. This might give insight into the necessity for maintenance and guarantee long-term crash performance.
- **Human-Centric Design:** exploring how bumper beam designs might be modified to reduce injuries to pedestrians and cyclists who are involved in collisions with automobiles as well as crash scenarios.
- **Validation of Simulation Models:** To provide precise forecasts of collision performance and behavior, bumper beam analysis computer simulation models are validated against data from actual crash tests.

- **Impact of Vehicle Electrification:** examining potential variations in weight distribution, collision behavior, and interaction with battery systems and how these can affect the bumper beam design as the automotive industry moves toward electric and hybrid vehicles.

Those research gap points can help guide further exploration and advancement in the design and performance of bumper beams in the automotive industry.

In other way round there is a deficiency of researchers on the moderate speed impact analysis. Based on a review of the literature, numerous writers have determined the mechanical and tribological characteristics of glass fiber reinforced composites through material substitutions. And therefore, in order to increase the materials' mechanical strength, some materials were chosen for this job.

In the case of these thesis, on Lifan 520 (2011 model) the bumper is originally made of steel and research is made by changing the bumper beam to S-Glass fiber composite material (which is 60% fiber and 40% matrix) and evaluated the Total Deformation, Equivalent (von-Mises) stress, Equivalent Elastic strain, Internal Energy. As a limitation the following points were seen:

In the case of these Thesis as a Gap;

- There is a restriction on the evaluation of material testing for bumper beams that only enables one composite material to be evaluated for that particular automobile model i.e. Lifan 520. The opportunity to test and investigate the potential advantages of additional high-performance materials is sadly limited by this restriction.
- Although the study's research of a bumper beam made of epoxy resin composites with s-glass fiber reinforcement is its main focus, it's crucial to recognize the variety of materials that the automotive industry has to offer (adding carbon fiber or hybridizing the element).
- It can also be evaluated by changing the fiber alignment in different directions in order to attain better and greater performance.
- The meshing was very coarse and it should be much finer.
- The change of the weight of newly developed material was not investigated.
- There was no any optimization method used.

CHAPTER THREE

MATERIAL AND METHOD ANALYSIS

This chapter explains about the materials to be used and the methodology to be followed through this work.

3.1. MATERIALS

In the production process of a product, particularly a Hybrid product, the choice of materials is crucial. It will be vital to make sure that the product's design conforms to all necessary technical, safety, and regulatory standards in addition to picking the right materials. The product must also be produced cheaply, sold for a profit, and appropriately disposed of after its useful life is over (Md Abdul Maleque, 2013).

The Principal Elements of the Materials to Be Employed

• S-Glass Fiber • Carbon Fiber • Matrix (Epoxy Resin) • Optimum range for Matrix- Fiber mixture and fibers in a Hybrid • Fiber Alignment • Compatibility of Hybrid Composites (Carbon-S-Glass-Epoxy Composite)	• Composite Selection Method • Engineering constants for a lamina that is unidirectional • **ANSYS LS-DYNA** (program for impact testing, analysis, and simulation of the current and new bumper beam load conditions) • **ANSYS Composite PrePost**

3.1.1. Glass Fibers

Glass fibers are composed of incredibly tiny glass fibers, a non-crystalline substance with a short-range network structure (Fig.3.1). As a result, it lacks a distinguishable microstructure and possesses isotropic mechanical characteristics that are mostly influenced by composition and surface finish. There are other categories of glasses, including silica, oxy-nitride, phosphate, and halide glasses, but from the perspective of composite technology, only silica glasses are now significant (Seo, 2011).

Glass fiber is a material consisting of numerous extremely fine fibers of glass. It is a special type of synthetic fiber which is very strong. Also known as fiberglass that is a material consisting of numerous extremely fine fibers of glass. The Versatility of glass as a fiber makes it unique industrial textile material. Glass fiber in fabric form offers an excellent combination of properties from high strength to fire resistance (Ever Barbero, 2011).

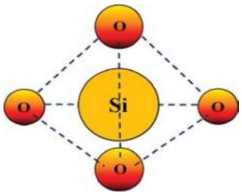

Figure 3.1: Molecular Structures of Glass Fibers (Seo, 2011)

Glass, **carbon**, and ***aramid*** fibers are the most common types of fibers. Other synthetic fibers are constructed of polymers that, because to their limited mechanical qualities, are not utilized in structural applications (Gibson, 1994). Despite having weaker mechanical qualities than other grades of glass fibers, e-glass (electrical glass), which is inexpensive, is the material used to make the most glass fibers in the industry. However, although costing more to create, structural glass (S-glass) has a much stronger strength and somewhat higher modulus (Gibson, 1994). C-glass (chemical glass) has an improved durability against alkali and acid assaults.

When silica-based or other glass formulations are extruded into many fibers with tiny diameters suited for textile production, glass fibers are created. Although the process of melting and drawing glass into fine fibers has been around for ages, it is only recently that these fibers have been used for textile purposes. Up until this point, all glass fibers had been produced as staple, which is a name for naturally occurring wool fiber clusters or locks. Glass fibers were first produced for sale in 1936. The Owens-Corning Fiberglas Corporation was established in 1938 as a result of the merger of Corning Glass Works and Owens-Illinois Glass Company. Continuous filament glass fibers were introduced when the two businesses collaborated to create and market glass fibers (C.Y. Li, Mechanics Of Materials , 2004). Owens-Corning is still the major glass fiber producer in the market today (C.Y. Li, Composites Science and Technology, 2003).

Varieties of Glass Fiber

Glass fibers can be divided into two groups: expensive special-purpose fibers and inexpensive general-purpose fibers. Over 90% of glass fibers are used for common purposes. These fibers are referred to as E-glass and are governed by ASTM regulations. (ASTM). The remaining glass fibers are high-end, specialty items. Many have letter designations that imply specific qualities, such as E-glass (Gupta, 1988). Some have trade names, but not all are subject to ASTM specifications.

E-glass is a type of calcium aluminum borosilicate glass that contains less than 1% of the alkali oxide Na2O. The fluoride found in most glasses helps to dissolve raw materials and brings down the glass's liquid's temperature. The E-glass occasionally has a refractive index of 1.562 and a density of 2.62 g/cm3.

The composition of E-glass after long producing time is varying as a result of some factors that encourage or force manufacturers to revise the formulation. Also, the need to improve some properties like corrosion resistance and higher mechanical performance leads to production of new types of glass fibers, Table 3.1, 3.2 (Lowenstein, Amsterdam (1983)) (Ed., New York 2010).

Table 3.1: Glass fibers by commercial melt process (Donaldson, 2001)

Fiber	Composition, wt%												
	SiO_2	B_2O_3	Al_2O_3	CaO	MgO	ZnO	TiO_2	Zr_2O_3	Na_2O	K_2O	Li_2O	Fe_2O_3	F_2
General-purpose fibers													
Boron-containing E-glass	52–56	4–6	12–15	21–23	0.4–4	...	0.2–0.5	...	0–1	Trace	...	0.2–0.4	0.2–0.7
Boron-free E-glass	59.0	...	12.1	22.6	3.4	...	1.5	...	0.9	...	...	0.2	...
	60.1	...	13.2	22.1	3.1	...	0.5	...	0.6	0.2	...	0.2	0.1
Special-purpose fibers													
ECR-glass	58.2	...	11.6	21.7	2.0	2.9	2.5	...	1.0	0.2	...	0.1	Trace
D-glass	74.5	22.0	0.3	0.5	...	...	...	...	1.0	<1.3	...	...	...
	55.7	26.5	13.7	2.8	1.0	...	...	...	0.1	0.1	0.1	...	...
S-, R-, and Te-glass	60–65.5	...	23–25	0–9	6–11	...	...	0–1	0–0.1	...	...	0–0.1	...
Silica/quartz	99.9999	...	...	...	...	...	...	...	...	...	...	...	...

As it is seen in the table different types of glass fibers were made to fulfill the industrial needs and this just was possible by modifying formulations.

Table 3.2: Physical and Mechanical Properties of Commercial Glass Fibers (Donaldson, 2001)

Fiber	Coefficient of linear expansion,	Specific heat,	Dielectric constant at room temperature	Dielectric strength,	Volume resistivity at room temperature	Refractive index	Weight loss in 24 h in 10%	Tensile strength at 23 °C (73 °F)		Young's modulus		Filament elongation at break, %
	10^{-6}/°C	cal/g/°C	and 1 MHz	kV/cm	$\log_{10}$ (Ω cm)	(bulk)	H_2SO_4, %	MPa	ksi	GPa	10^6 psi	
General-purpose fibers												
Boron-containing E-glass	4.9–6.0	0.192	5.86–6.6	103	22.7–28.6	1.547	~41	3100–3800	450–551	76–78	11.0–11.3	4.5–4.9
Boron-free E-glass	6.0	…	7.0	102	28.1	1.560	~6	3100–3800	450–551	80–81	11.6–11.7	4.6
Special-purpose fibers												
ECR-glass	5.9	…	…	…	…	1.576	5	3100–3800	450–551	80–81	11.6–11.7	4.5–4.9
D-glass	3.1	0.175	3.56–3.62	…	…	1.47	…	2410	349	…	…	…
S-glass	2.9	0.176	4.53–4.6	130	…	1.523	…	4380–4590	635–666	88–91	12.8–13.2	5.4–5.8
Silica/quartz	0.54	…	3.78	…	…	1.4585	…	3400	493	69	10.0	5

The types of glass fibers most commonly used are mainly **E-glass** (alumino-borosilicate glass with less than 1 wt.% alkali oxides mainly used for glass-reinforced plastics), but also **A-glass** (alkali-lime glass with little or no boron oxide), **ECR-glass** (alumino-lime silicate with less than 1 wt.% alkali oxides, has high acid resistance), **C-glass** (alkali-lime glass with high boron oxide content used, for example for glass staple fibers), **D-glass** (borosilicate glass with high dielectric constant), **R-glass** (alumino silicate glass without MgO and CaO, with high mechanical requirements), and **S-glass** (alumino-silicate glass without CaO but with high MgO content with high tensile strength) (Shindo, Amesterdam 2000). The Compositions of some typical glasses which are used in the manufacturing of fibers are given in (Table 3.3).

Despite being a fully viable material for glass and glass fiber, pure silica must be handled at very high temperatures, which is a disadvantage unless certain chemical qualities are required. In order to lower the glass's operating temperature, impurities are frequently added to the glass in the form of other substances. Additionally, these components provide the glass a number of other qualities that could be useful in a variety of contexts. Soda lime glass, often known as A-glass, was the first form of glass used for fiber. It was not very alkali resistant. A new variety of E-glass was created; it is an alkali-free, 2% aluminum borosilicate glass (M.F. Yu, (2000)), (E. Hernandez, (1998)). This was the first glass formulation used for continuous filament formation. E-glass still makes up most of the fiberglass production in the world. Its particular the components may differ slightly in percentage but must fall within a specific range. The letter E is used because it was originally for electrical applications. S-glass known as R-glass in Europe is based on this S_iO 2-Al_2O 3-MgO system; this fiber has higher stiffness and strength (hence the designation S) than E-glass (Table 3.3). It also retains its improved properties to higher temperatures.

Table 3.3: Typical composition and properties of glass fibers (Seo, 2011)

	E-glass (%)	S-glass (%)	AR-glass (%)
SiO_2	54	65	64
TiO_2			3
ZrO_2			13
Al_2O_3	14	25	1
B_2O_3	9		
MgO	5	10	
CaO	18		5
Na_2O			14
Modulus (GPa)	70	80	75
Strength (MPa)	2200	2600	1700
Density (Mg/m^3)	2.54	2.49	2.70

It also retains its improved properties to higher temperatures. However, it is more difficult to draw into fibers due to its limited working range and is therefore more expensive. S-glass fibers are still used for some specialist applications but they have been largely superseded by the fibers such as carbon andaramidwithsuperiormechanicalproperties.C-glasswasdevelopedtoresist attack from chemicals mostly acids that destroy E-glass (E. Hernandez, (1998)). T-glass is a North American variant of C-glass. A-glass is an industry term for cullet glass, often bottles, made in to fiber. AR-glass is alkali-resistant glass. Most glass fibers have limited solubility in water but are very dependent on PH. Chloride ions will also attack and dissolve E-glass surfaces.

Since E-glass does not really melt, but soften, the softening point is defined as ‘the temperature at which a 0.55–0.77 mm diameter fiber 235 mm long, elongates under its own weight at 1 mm/min when suspended vertically and heated at the rate of 5 ^{0}C per minute’ (Li CY, 2004). The strain point is reached when the glass has a viscosity of 1014.5 Poise. The annealing point, which is the temperature where the internal stresses are reduced to an acceptable commercial limit in 15min, is marked by a viscosity of 1,013 poise (Li CY, 2004).

The vitreous and crystalline states of silica (glass and quartz) have similar energy levels on a molecular basis also implying that the glassy form is extremely stable. In order to induce crystallization, it must be heated to temperatures above 1,200 ^{0}C (2,190^{0}F) for long periods of time.

Glass fibers are useful because of their high ratio of surface area to weight. However, the increased surface area makes them much more susceptible to chemical attack. By trapping air within them, blocks of glass fiber make good thermal insulation with a thermal conductivity of the order of 0.05 w/ (m.K.). The strength of glass is usually tested and reported for 'virgin' or pristine fibers those that have just been manufactured. The freshest, thinnest fibers are the strongest because the thinner fibers are more ductile. The more the surface is scratched, the less the resulting tenacity (E. Hernandez, (1998)). Because glass has an amorphous structure, its properties are the same along the fiber and across the fiber (M.F. Yu, (2000))**.** Humidity is an important factor in the tensile strength. Moisture is easily adsorbed and can worsen microscopic cracks and surface defects and lessen tenacity.

In contrast to the carbon fiber, glass can undergo more elongation before it breaks (M.F. Yu, (2000)). There is a correlation between the bending diameter of the filament and the filament diameter. The viscosity of the molten glass is very important for manufacturing success. During drawing (pulling of the glass to reduce fiber circumference), the viscosity should be relatively low. If it is too high, the fiber will break during drawing. However, if it is too low, the glass will form droplets rather than drawing out into fiber.

The use of glass fibers as reinforcement in the thermoplastic polymers likes polyamides, polyesters or polypropylene yields materials with very attractive properties (P. Zhang, (2002) 3893), (B.I. Yakobson, (1997)). Glass fiber containing thermoplastic compounds show high strength and stiffness while maintaining a high level of impact strength. Combined with their low specific weight, ease of processing and tailor-made properties, these materials find widespread use in automotive applications and household/electronic appliances.

3.1.2. Carbon Fiber (T-230)

Carbon fiber is made up of thin, long strands of carbon atoms that are crystallinity bound together. These fibers are incredibly robust while being lightweight. Because of its superior strength-to-weight ratio, carbon fiber is stronger than many metals while being substantially lighter. In industries such as aerospace and automotive, this feature is highly valued (Michael Heine, January 2008).

Carbon fibers come in a variety of shapes and sizes, with variable characteristics. Carbon fibers with normal modulus, intermediate modulus, high modulus, and ultra-high modulus are the most common Carbon fiber is defined as a fiber containing at least 92 wt. % carbons, whereas graphite fiber contains at least 99 wt. % carbons.

Carbon fibers offer good tensile qualities, low densities, and high thermal and chemical stabilities in the absence of oxidizing agents, as well as good thermal and electrical conductivity and creep resistance (Yang W, 2011).

Carbon fiber has a high tensile strength, stiffness, and deformation resistance. It is also extremely fatigue resistant and has good load-bearing characteristics. Carbon fiber, unlike metals, is not corroded by moisture or chemicals, making it appropriate for applications in severe settings. Carbon fiber is a great electrical conductor. However, depending on the type of carbon fiber and the production process, its electrical conductivity can vary.

Carbon fiber has an extremely low coefficient of thermal expansion, which means that when exposed to temperature fluctuations; it does not expand or contract considerably. This characteristic is important in situations that require dimensional stability (Prince M Patel, 2013).

Carbon fibers, commonly known as graphite fibers, are strong and lightweight fibers with great chemical resistance. Carbon fiber mechanical properties are dictated by the atomic configuration of carbon chains and their linkages, which is similar to graphite crystal structure. Carbon fiber strength is managed by aligning carbon atomic structures with their strongest atomic connections along the carbon fiber direction (Ever Barbero, 2011).

Carbon fibers, which are frequently made from Polyacrylonitrile (PAN), are well-known for their high strength and light weight. These fibers, with diameters ranging from 6 to 10 micrometers, are produced in a multi-step process that includes spinning, stabilization, carbonization, and, in some cases, graphitization (Mohammad Irshad Ali and J. Anjaneyul, 2018,). PAN precursor fibers are first spun using wet or dry spinning processes, and then stabilized at high temperatures to form thermosetting structures. Subsequent carbonization at high temperatures removes non-carbon components, increasing the strength and stiffness of the fibers. Because of their superior mechanical qualities, PAN-based carbon fibers are widely employed in a variety of industries, making them a favored choice for applications requiring high-performance composite materials.

One of the most exciting materials ever discovered is carbon nanotubes (CNTs), the result of recent study in the field of carbon technology. The arrangement of carbon atoms in CNTs is managed so that a completely cylindrical atomic structure of about 1nm diameter and about 1 m length is formed, with the strong carbon bonds oriented along the cylinder axis. Because of this regulated nanostructure, the intrinsic flaws that arise in every material and are primarily responsible for strength limitations are almost eradicated.

3.1.3. Matrix (Epoxy Resins)

The matrix in a composite performs several functions, including holding the fibers into the composite part shape, protecting the fibers from direct exposure to the environment, transferring stresses to the fibers via the fiber-matrix interface, and resisting some of the applied load, particularly transverse normal stresses and inter-laminar shear stresses (Ever Barbero, 2011) (LChung., 2010).

A chemical compound known as an 'epoxy' is made up of two previously chemically linked carbon atoms and an oxygen atom. The name 'alpha-epoxy' or '1, 2-epoxy' refers to the three-member ring structure that makes up the basic type of epoxy. The most recognizable feature of any increasingly complicated epoxy molecule is its idealized chemical structure, which is depicted in Fig. 4 below.

A typical epoxy's idealized chemical structure is depicted in Fig. 3.2 & 3.3. Keep in mind that the ester groups are absent from the molecular chain.

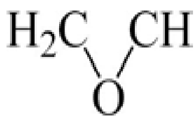

Figure 3.2: Idealized Chemical Structure of a Simple Epoxy (ethylene oxide) (Seo, 2011)

Epoxies are different from polyester resins in that they are cured by a 'hardener' rather than a catalyst. By using an "addition reaction," which involves both components in the chemical process, the hardener-often an amine is employed to cure the epoxy. Two epoxy sites typically attach to each amine site in this reaction due to the chemistry involved.

Since the amine molecules "co-react" with the epoxy molecules in a predetermined ratio, it is essential to establish the right mix ratio between the resin and hardener to guarantee that a complete reaction takes place. Unreacted resin or hardener will remain in the matrix and affect the final attributes after cure if the amine and epoxy ratios are incorrect. In order to facilitate in the correct mixing of the resin and the hardener, manufacturers often formulate the materials to provide a simple mix ratio that is easily obtained by measuring out by weight or volume.

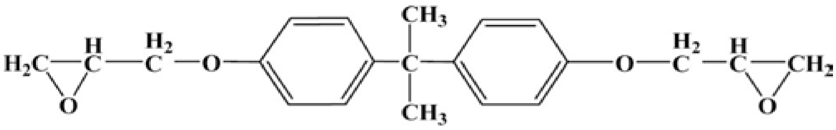

Figure 3.3: Idealized chemical structure of a typical epoxy (di-glyceryl ether of bisphenol-A)

Epoxy resins have a proven track record in repairing concrete and a variety of composite component structures. The resin's structure can be altered to produce a variety of products with differing degrees of performance.

Epoxy resins can be blended with other epoxy resins to achieve specific performance features, can be formulated with different materials, and have lower shrinkage than unsaturated polyester resins. Typically, the epoxies are cured by addition of an anhydride or an amine hardener as a 2-part system. Different hardeners as well as quantity of a hardener produce a different cure profile and give different properties to the finished composite.

For high performance aerospace applications, epoxy resins are combined with a variety of fiber reinforcing elements, including as glass, carbon, and aramid. Fiber reinforced epoxies are used in the sport and recreation industry in addition to replacing reciprocating metal parts, particularly in the weaving industry. The majority of composite production processes, such as filament winding, vacuum-bag molding, autoclave molding, pressure-bag molding, compression molding, and hand lay-up, are compatible with epoxy resins.

At both low and high temperatures, epoxy-based composites work well. Epoxy resins can function effectively in temperatures between 200 and 250 ^{0}F, and some of them can even do so at 400 ^{0}F. Epoxy resins for high-temperature and high-performance applications cost more, but they also provide superior chemical and corrosion resistance.

The epoxy, a conserved thermo-set resin, encloses the functional group of epoxy. Epoxy resin and the hardener, which cures it, are typically combined together prior to use. Epoxy is used in numerous industries, including high tension electrical insulators, electronic and electrical components, metal coatings, and structural adhesives. The most common polymer utilized with advanced composites is epoxy resin. They are widely used principally because of their outstanding mechanical qualities, great adhesion, and good potential for using addition-type processes, minimal cure shrinkage, and low blow cost.

3.1.4. AISI Steel (1006)

Carbon steels are a class of iron and carbon alloys that have residual amounts of other elements and are combined with particular amounts of elements for deoxidization, with the maximum carbon content being 1.65% and the maximum amount of iron being up to 1%. (Principle of Corrosion Engineering and Corrosion control, 2006). About 0.05 to 2.1 percent of the weight of steel is made of carbon. What the American Iron and Steel Institute (AISI) define as carbon steel is as follows:

- To get the desired alloying effect, any element can be added, including chromium, cobalt, molybdenum, nickel, niobium, titanium, tungsten, vanadium, zirconium, and others, with no minimum amount necessary.
- Copper's minimum requirement is set at 0.40%.
- Alternatively the maximum content allowed for any of the subsequent parts doesn't go over the indicated percentage: copper 0.60%, silicon 0.60%, and manganese 1.65% (Classification of Carbon and Low-Alloy Steel, Nov-2001).

Uses of Carbon Steel, it is an essential material in the automotive industry, where it is used to make parts such as engine blocks, transmission components, and suspension parts.

AISI into four classes (Classification of Carbon and Low-Alloy Steel, Nov-2001).

- *Low-carbon steel*

Classification; Based on the amount of carbon in the steel, carbon steel is divided

0.05% to 0.15% carbon (Plain Carbon Steel) content

- *Medium-carbon steel*

Used for large parts, forgings, and automotive components, it has a carbon content of roughly 0.3% to 0.5%, balances ductility and strength, and has good wear resistance. (Nishimura & Murase, 2012) (Engineering fundamentals page on medium-carbon steel)

- *High-carbon steel*

Approximately 0.6 to 1.0% carbon content (Classification of Carbon and Low-Alloy Steel, Nov-2001). Extremely robust; utilized in high-strength wires, sharp instruments, and springs (Engineering fundamentals page on high-carbon steel.)

- *Ultra-high-carbon steel*

Approximately 1.25 - 2.0% Carbon content (Classification of Carbon and Low-Alloy Steel, Nov-2001). It is a kind of steel that tempering can significantly harden, used in specialized applications like punches, axles, and knives (not for industrial use). It is power metallurgy that is used to make the majority of steel that has more than 2.5% carbon content.

3.1.5. Optimal Range for Matrix-Fiber Mixture and Fibers in a Hybrid

The optimal proportion of carbon fiber and S-glass fiber to combine for improved performance in a composite material is determined by a number of criteria, including the mechanical qualities desired, the intended use, production issues, and cost considerations. There is no one-size-fits-all solution because the appropriate mix can vary depending on various characteristics. However, it’s offered some broad principles to assist and identify a suitable fiber content range (N Kumar, 2020).

Mechanical Properties: Carbon fiber has a high strength and stiffness, but S-glass fiber has a strong impact resistance. Depending on the desired balance of these qualities, it can be explored a total fiber content range of 40% to 60% (combining carbon and S-glass fibers) (YG TG, 2021).

Application: If stiffness and strength is the key concerns, it's meant to use a higher percentage of carbon fiber (e.g., 50% to 60% carbon fiber) and if impact resistance is important (as with automobile bumpers), a more balanced composition should be sought.

Manufacturability: A high carbon fiber composition might provide additional manufacturing obstacles, such as fiber dispersion and processing difficulties. It is critical to strike a balance between fiber content and production convenience.

Cost: Carbon fiber is more expensive than glass fiber in general. It is critical to balance performance and cost-effectiveness, so a combination of both fiber types that achieves performance needs while remaining within budget limits should be explored.

Composite Design: Factors such as fiber orientation, stacking sequence, and resin type can all have an impact on the overall performance of the composite. The design and manufacturing method of your composite will have an impact on how well it performs.

Furthermore, material testing and analysis are required to determine the specific composition that best meets your needs. Begin with a few compositions within the specified range and evaluate performance using mechanical testing (such as tensile, flexural, and impact tests). Simulations using Finite Element Analysis (FEA) can also help predict how different compositions will behave to specific loads.

3.1.6. Fiber Orientation

Matrix materials and reinforcing fibers are the two main components of fiber-reinforced composite materials. A fiber is often used as a matrix binder and has a high modulus and strength. This form preserves the fibers' and matrix’s’ physical and chemical identities while providing a combination of attributes that would be impossible to achieve with just one of the components functioning alone (Dr.Shivanand N. Pujar, 2022). Fibers are typically the main components that carry loads, and the matrix that surrounds them serves as a load transfer medium, maintains the fibers in the proper position and orientation, and shields the fibers from environmental damage such high humidity and temperatures (Kaw, 2006) (Berrahou Mohamed, 2022).

Large-scale fiber insertion into a thin matrix layer to create a lamina (ply) was the first step in the manufacturing of a fiber-reinforced composite material. Most laminate have a thickness of between 0.1 and 1 mm (Kaw, 2006) (Mallick P. , 2007). Either continuous (long) or discontinuous (short) fibers are used to build the laminas, as seen in *figure 3.4 below*.

The continuous fibers are placed in three different orientations: **multi-directional** (i.e., fiber in more than two directions), **bidirectional** (i.e., fibers in two directions, usually perpendicular to each other), and **unidirectional** (i.e., all fibers in one direction). When unidirectional fibers are arranged in a lamina, the composite material has the highest strength and modulus in the longitudinal direction. Nevertheless, its strength and modulus are very low in the transversal direction. By varying the quantity of fibers in both the longitudinal and transverse directions, the strength and modulus of a lamina with bidirectional fibers can be adjusted. These characteristics are the same in both directions for a balanced lamina (N Kumar, 2020).

A. Unidirectional Continuous fibers
B. Bidirectional Continuous fibers
C. Multidirectional Continuous fibers
D. Unidirectional Discontinuous fibers
E. Random Discontinuous fibers

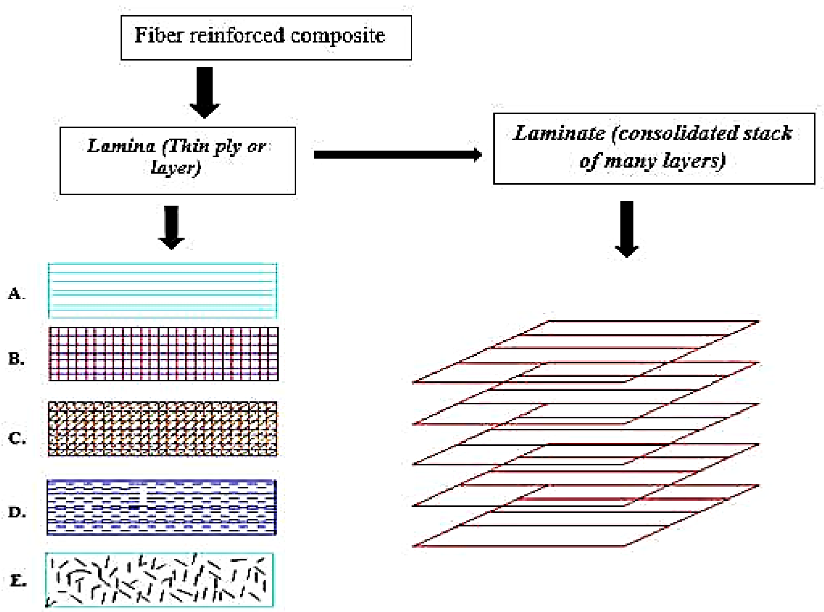

Figure 3.4: Principal Component of Fiber-reinforced Composites (Mallick P. , 2007)

In a fiber-reinforced composite construction, the thickness needed to carry a certain load or maintain a given deflection is acquired by stacking many laminas in a predetermined order and then consolidating them to form a laminate. A laminate's laminas can have fibers oriented in several directions or all in one direction (Gergely C, 2015).

A next of studies are being carried out to establish the ideal fiber alignment for the best performing carbon composite with carbon content. Two different types of fiber alignments are being assessed: multi-directional, in which each lamina has a different fiber alignment i.e. (45^0, 0^0, 45^0, 0^0, 45^0), (0^0, 90^0, 0^0, 90^0, 0^0), (-45^0, 45^0, -45^0, 45^0, -45^0), (-45^0, 45^0, 0^0, -45^0, 45^0) and unidirectional, in which all the laminae have the same fiber alignment but vary in angle by a degree of 0^0, 22.5^0, 45^0, 67.5^0, and 90^0. These tests ignore the inter-laminar interaction that generally affects overall performance in favor of evaluating the mechanical characteristics of the composite. The objective is to comprehend how various alignment patterns impact the mechanical properties of the composite by taking fiber alignment into account. The goal of this study is to pinpoint the ideal fiber alignment for enhancing the mechanical performance of carbon composites with ideal carbon content.

3.1.7. Compatibility of Hybrid (Carbon-s-glass fiber epoxy resin)

It’s the ability of diverse types of fibers and matrix to efficiently collaborate in a composite material. Hybrid composites are made up of multiple kinds of fibers, each with its own set of properties, and a matrix substance such as epoxy resin. Compatibility is critical for achieving optimal mechanical performance, durability, and other required composite material qualities (Gergely Czél, 2015).

Combining carbon and S-glass fibers with epoxy resin can result in a hybrid composite material that could be utilized to make a beam bumper. Carbon and S-Glass fibers, each with their own distinct qualities, can be combined to provide a balanced and optimum solution for beam bumper applications.

Hybrid composite compatibility is a complicated component of composite material engineering that necessitates a thorough understanding of material qualities, processing procedures, and the required final product performance characteristics. It entails meticulous thought and testing to guarantee that the final composite fits the planned aims and requirements (Mehmet Bulut, 2 February 2018).

The following are key factors concerning hybrid composite compatibility (Gergely Czél, 2015) (Mohamad Fotouhi, July 2016):

Material Recruitment: It is critical to select fiber types and matrix materials that are chemically and mechanically suitable. The materials must bond well in order to prevent de-lamination and ensure good stress transfer.

Inter-facial Adhesion: For load transfer, the contact between the fibers and the matrix is crucial. A suitable matrix should evenly moisten the fibers, facilitating good adhesion and reducing the possibility of fiber pullout or de-bonding.

Thermal Expansion Matching: The coefficients of thermal expansion of different fiber kinds can vary. The matrix should serve to buffer the thermal expansion mismatch between fibers, minimizing the possibility of de-lamination during temperature variations.

Fatigue Durability: The compatibility of the fibers and matrix determines the composite's long-term performance. Over its intended lifespan, the composite should be resistant to deterioration, moisture absorption, and environmental influences.

Surface Treatment: Depending on the qualities of the fibers, surface treatment may be required to improve adhesion with the matrix. The degree to which the surface treatment sticks to the fibers is a measure of compatibility.

Mechanical testing, such as tensile, flexural, and impact tests, can demonstrate how well the fibers and matrix interact. Material testing and finite element analysis can be used to determine compatibility. Also optimization of the volume and weight ratio and collaboration with different material expertise will have or ensures the optimal Hybrid/Composite mixture compatibility.

Combining carbon and S-glass fibers with epoxy resin can result in a hybrid composite material that could be used to make a bumper beam. Carbon and S-Glass fibers, each with their own distinct qualities, can be combined to provide a balanced and optimum solution for bumper beam applications (Olagoke Olabisi, Spring 2000).

Carbon fibers are well-known for their high strength and rigidity, which are critical characteristics for a beam bumper that must absorb and disperse impact forces. S-glass fibers can also contribute to this strength. S-Glass fibers are known for their high impact resistance and energy absorption characteristics. This can improve the bumper beam's ability to survive crashes and safeguard the vehicle's occupants (Putu Suwarta, 20-25th August 2017).

The hybrid composite can be developed to produce an excellent strength-to-weight ratio. The lightweight natures of carbon fibers can assist reduce the overall weight of the bumper beam, improving fuel efficiency and vehicle performance. The durability and resistance to environmental variables of epoxy resin are well recognized. This improves the bumper beam's long-term performance. S-glass fibers are frequently less expensive than high-performance carbon fibers. You can potentially produce a cost-effective solution while keeping acceptable performance by adopting a hybrid blend of both fiber kinds.

A high-performance composite material made of s-glass fibers and epoxy resin matrix has the following advantages (Mallick P. K., 2007 Third Edition) (K.L. Loewenstein, 1993 3rd Edition) (Ever Barbero, 2011) (LChung., 2010);

1. *Stiffness and strength*: The composite's overall mechanical properties are improved by the high tensile strength of S-glass fibers. Because of this, S-glass fiber reinforced epoxy composites are suitable for structural applications that call for strength and stiffness.

2. *Impact resistance*: The composites have good impact resistance because to the S-glass fibers and epoxy resin matrix, which enables them to withstand unforeseen loads and impacts without suffering significant damage.

3. *Excellent fatigue resistance*, which is essential in applications where the material would be subjected to cyclic loading or recurrent stress, is displayed by S-glass fibers.

4. *Temperature resistance:* S-glass fibers have a higher melting point and are more thermally stable than E-glass fibers. This allows for the use of S-glass fiber reinforced epoxy composites in high-temperature applications.

5. *Chemical resistance:* Composite materials made of epoxy resins are suitable for hostile environments because they exhibit great chemical resistance over a broad PH range.

Among the industries that utilize S-glass fiber reinforced epoxy composites are those that produce cars, sporting goods, marine structures, and aerospace and automotive components. These composites are valuable due to their combination of high strength, light weight, and resistance to harsh conditions.

Mechanical Properties of the Materials

It is obvious that there are a number of elements that will affect the accuracy or quality of the findings produced by FEA. The type of elements used, the quality of the elements used, the quantity of elements used, and the modeling of boundary constraints and loading conditions will all have an impact on the findings that are meaningful or useful (Loughlana J, 2008).

The shell element is the greatest option for meshing because of the thickness of the beam bumper. The best kind of element is a solid element, even though the impactor is a three-dimensional solid.

Table 3.4: General Material Properties (Pascault JP, 2010) (Chamis, 2021) (Chou T.-W. K., 2010)

Material Properties	**Used Materials**		
	S-Glass Fiber	**Carbon Fiber**	**Epoxy**
Young's Modulus of elasticity (GPa)	86	200 – 500	2 – 6
Tensile Strength, Yield (MPa)	2600	3220	54.6
***Poisson's Ratio* (v)**	0.22	0.26 – 0.28	0.29 – 0.34
Fatigue Strength (MPa)	50 – 150	No fatigue limit	35 – 70
Tensile Strength, Ultimate (MPa)	4600	2500 - 7000	86.04
Elongation (% Strain)	5.7	1.7 – 2.5	1 - 8.5
Shear Modulus (GPa)	37	12.5	1.6
Shear Strength (MPa)	_	4.05	29
Density (kg/m^3)	2490	1750	1100

3.1.8. Typical Mechanical Properties of the Materials

Some of typical material properties that are found in Hybrid composite made of Carbon-S-glass fiber and epoxy resin are listed below. Also it should be noted that those properties can vary based on factors such as the fiber volume fraction, the specific epoxy resin used, manufacturing process, and testing conditions.

These values are calculated with the volume fraction of 40% of epoxy resin and volume fraction of fiber with 60% amount.

Other properties like *Fatigue Resistance* and *Water Absorption*, Hybrid composites can offer improved fatigue resistance due to the combination of different fiber types. Epoxy-based composites generally have low water absorption, but it can increase over time if exposed to moisture (Chou T. W., 2010) (Zhu, 2008).

The composite composition i.e. 60% fiber (Carbon & S-glass) and matrix (Epoxy resin)

The following are basic expectations of how the typical mechanical qualities might change by modifying the percentage of carbon fiber (while keeping the S-glass percentage complimentary to preserve the overall 60% fiber content).

- ***Young's Modulus*** (*$\mathcal{E}$*): Raising the amount of carbon fiber while keeping the overall fiber content constant is likely to raise the Young's Modulus of the composite. When compared to glass fibers, carbon fibers have a greater Young's Modulus. The overall stiffness of the composite will likely increase as the proportion of stronger carbon fibers increases.
- ***Shear Modulus*** (***G***): The shear modulus of a material represents its resistance to shear deformation. It is a measure of a material's resistance to altering shape when subjected to shear pressures. As the percentage of carbon fiber in the composite changes but the overall fiber content remains constant at 60%, the shear modulus may change as follows:

  Carbon fibers often have a *lower* shear modulus than glass fibers. As a result, increasing the percentage of carbon fiber in the composite could result in *decrease* in shear modulus.
- ***Density*** (***ρ***): Carbon fibers are significantly lighter than glass fibers. As the amount of carbon fiber in the composite increases, the density of the composite may decrease significantly, *contributing to a lightweight structure.*
- ***Poisson's Ratio*** (***V***): Poisson's ratio is a measure of the lateral contraction of a material when stretched in one direction. It describes how much a material compresses laterally when deformed axially.

  Because of structural variations, carbon fibers and glass fibers might have differing Poisson's ratios. The Poisson's ratio of the composite will be influenced by the Poisson's ratios of both fiber types and the matrix.
- ***Compressive Strength***: It is the greatest compressive stress that a material can bear before failing under compression. It is the greatest compressive stress that a material can bear before failing under compression. Carbon fibers are generally strong in both tension and compression. Increasing the percentage of carbon fiber might lead to an increase to composite's compressive strength.
- ***Tensile Strength***: Carbon fibers are more durable than glass fibers. Raising the proportion of carbon fiber in the composite may result in an increase in tensile strength. In general, carbon fibers are stronger than glass fibers. Increased carbon fiber content may result in increased tensile strength of the composite.
- ***Impact Resistance***: Because of the differing failure mechanisms of carbon and glass fibers, impact resistance may vary. Because of the intrinsic strength of carbon

fibers, increasing the proportion of carbon fiber could potentially improve impact resistance.

- ***Strain to Failure*** (***ε_f***): Strain to failure is the amount of deformation a material can withstand before failing under tensile loading. It's critical to understand how far a material can stretch before breaking. The strain to failure may be modified as you vary the quantity of carbon fiber in your composite while maintaining the overall fiber composition constant at 60%:
  Increasing the proportion of carbon fiber in the composite may cause changes in the strain to failure. Carbon fibers, on average, have a lower strain to failure than some glass fibers. As a result, increasing the percentage of carbon fiber in the composite may result in a lower strain to failure.

Calculations of the characteristics of composite materials

The structure of composites determines whether a composite material is isotropic or anisotropic.

- *Isotropic* substance is one whose properties do not change depending on the direction of measurement.
- *Anisotropic* material is one whose properties vary depending on whether they are measured along an axis or parallel to a plane.

The Rule of Mixtures

It's a method of approximating the qualities of composite materials based on the concept that a composite property is the volume weighted average of the properties of the phase.

For example, suppose the carbon amount is fixed to 25% while the S-glass fiber proportion remains complimentary to preserve the overall fiber content of 60%.

$\mathbf{0.6 + 0.4 = 1}$ 60% - *fiber* and 40% - *matrix*

When, $\mathbf{5\%}$ - 0.6 $\left(\frac{5}{100}\right) = 0.03$, (0.6 – 0.03) = 0.57

Fiber of (**0.03**$_{\text{carbon}}$ + **0.57** $_{\text{S-glass}}$) & matrix of **0.4**$_{\text{Epoxy Resin}}$ total of 1

When, $\mathbf{15\%}$ - 0.6 $\left(\frac{15}{100}\right) = 0.09$, (0.6 – 0.09) = 0.51

Fiber of (**0.09**$_{\text{carbon}}$ + **0.51** $_{\text{S-glass}}$) & matrix of **0.4**$_{\text{Epoxy Resin}}$ total of 1

When, **25%** - $0.6\left(\frac{25}{100}\right) = 0.15$, $(0.6 - 0.15) = 0.45$

Fiber of ($\mathbf{0.15}_{\text{carbon}}$ + $\mathbf{0.45}_{\text{S-glass}}$) & matrix of $\mathbf{0.4}_{\text{Epoxy Resin}}$ total of 1

When, **30%** - $0.6\left(\frac{30}{100}\right) = 0.18$, $(0.6 - 0.18) = 0.42$

Fiber of ($\mathbf{0.18}_{\text{carbon}}$ + $\mathbf{0.42}_{\text{S-glass}}$) & matrix of $\mathbf{0.4}_{\text{Epoxy Resin}}$ total of 1

When, **35%** - $0.6\left(\frac{35}{100}\right) = 0.21$, $(0.6 - 0.21) = 0.39$

Fiber of $\left(\mathbf{0.21}_{\text{carbon}} + \mathbf{0.39}_{\text{S-glass}}\right)$ & matrix of $\mathbf{0.4}_{\text{Epoxy Resin}}$ total of 1

Finally, **40%** - $0.6(\frac{40}{100}) = 0.24$, $(0.6 - 0.24) = 0.36$

Fiber of $\left(\mathbf{0.24}_{\text{carbon}} + \mathbf{0.36}_{\text{S-glass}}\right)$ & matrix of $\mathbf{0.4}_{\text{Epoxy Resin}}$ total of 1

- $\boldsymbol{Younge's\ Modulus\ of\ Composite}(\boldsymbol{\varepsilon})$

$$= V_c\varepsilon_c + V_S\varepsilon_S + V_E\varepsilon_E \quad \ldots\ldots\ldots\ldots\ldots\ldots \quad (3.1)$$

$$where \quad V_f + V_m = 1$$

- $\boldsymbol{Density\ of\ Composite}(\boldsymbol{\rho})$

$$= \left(\frac{1}{\left(\frac{V_C}{\rho_C}+\frac{V_S}{\rho_S}\right)+\frac{V_E}{\rho_E}}\right) \quad \ldots\ldots\ldots\ldots\ldots\ldots \quad (3.2)$$

- $\boldsymbol{Poisson's\ Ratio}\ (\vee)$

$$= (\boldsymbol{V_c}\vee_{\boldsymbol{c}}) + (\boldsymbol{V_S}\vee_{\boldsymbol{S}}) + (\boldsymbol{V_E}\vee_{\boldsymbol{E}}) \quad \ldots\ldots\ldots\ldots\ldots\ldots \quad (3.3)$$

The shear Modulus of the composite can be computed using the volume fraction results of Poisson's Ratio and Young's Modulus.

- $\boldsymbol{Shear\ Modulus\ of\ composite}\ (\boldsymbol{Gc})$

$$G_{xy} = \frac{\varepsilon_Z}{2 + 2\mu_{xy}}, \qquad G_{xz} = \frac{\varepsilon_Y}{2 + 2\mu_{xz}}, \qquad G_{yz} = \frac{\varepsilon_x}{2 + 2\mu_{yz}}$$

$$= \frac{\boldsymbol{\varepsilon}}{\boldsymbol{2+2\mu}} \quad \ldots\ldots\ldots\ldots\ldots\ldots \quad (3.4)$$

Calculated Values

The density Table demonstrates that when the amount/percentage of carbon in the hybrid composite grows, the total density of the composite drops due to the lower value of the carbon fiber density.

Table 3.5: Constants of Elasticity of carbon, S-Glass, and Epoxy Resin (Courtesy of Zweben, 2011) (Chou T.-W. K., 2010)

Constants of Elasticity		**Giga Pascal**		
		Carbon	**S-Glass**	**Epoxy Resin**
Young's Modulus	***X***	**230**	**90**	**3.78**
	Y	**23**	**90**	**3.78**
	Z	**23**	**90**	**3.78**
Poisson's Ratio	***XY***	**0.2**	**0.22**	**0.35**
	XZ	**0.4**	**0.22**	**0.35**
	YZ	**0.2**	**0.22**	**0.35**
Shear Modulus	***XY***	**9**	**36.8**	**1.4**
	XZ	**8.2**	**36.8**	**1.4**
	YZ	**9**	**36.8**	**1.4**
Density (Kg/m³)		**1800**	**2500**	**1160**

Table 3.6: Density of Carbon-s-glass fiber epoxy with varying carbon value

Density	25% C	30% C	35% C	40% C	15% C	5% C
	1644.3 Kg/m³	1631.78 Kg/m³	1619.45 Kg/m³	1607.3 Kg/m³	1669.929 Kg/m³	1696.369 Kg/m³

Table 3.7: calculated constants of elasticity when the carbon amount varies

Constants of Elasticity		**Giga Pascal**					
		C-25%	**C-30%**	**C-35%**	**C-40%**	**C-15%**	**C-5%**
Young's Modulus	**X**	76.5	80.7	84.9	84.9	68.1	59.7
	Y	45.5	43.5	41.4	41.4	49.5	53.5
	Z	45.5	43.5	41.4	41.4	49.5	53.5
Poisson's Ratio	**XY**	0.269	0.268	0.268	0.267	0.2702	0.2714
	XZ	0.299	0.304	0.310	0.315	0.2882	0.2774
	YZ	0.269	0.268	0.268	0.267	0.2702	0.2714
Shear Modulus	**XY**	17.913	17.129	16.344	16.352	20.138	21.806
	XZ	17.499	16.656	15.820	15.755	20.066	21.782
	YZ	30.147	31.816	33.488	33.504	20.138	21.806

3.2. METHODS

3.2.1. The Fundamental Steps in Approach

A Mechanical structure analysis technique that makes use of mathematical operations is finite element analysis. In order to perform FEA, you must divide a bigger, more complex entity into smaller, easier-to-manage portions. You gain a better understanding of how the object will react to stressors as you continue to split the structure. The finite element method (FEM) is the process of disassembling a structure for FEA (Gigante, 2022, Nov 30).

Here are the basic steps to be followed;

- **Step 1 _ Modeling**

When modeling an object, it is necessary to leave off the intricate geometrical details in order to emphasize the thing's fundamental structure. Be wary of characteristics that serve structural needs rather than aesthetic ones. Understand why one geometrical feature should be kept and another should be eliminated.

- **Step 2 _ Material Definition**

The name of the phase implies that material attributes should be defined here. These are based on the type of analysis being conducted (AnsysCompositePrePost).

- **Step 3 _ Defining Loads**

This stage helps you discover which external pressures are acting on the structure and how they affect different components of the structure.

- **Step 4 _ Boundary Conditions**

As we have done in earlier mathematical issues, setting the conditions under which the structure will exist primarily serves to reduce the complexity of the issue. If we are familiar with the circumstances beforehand, we can compute considerably more quickly.

- **Step 5 _ Meshing**

Finite elements, drum-roll, please is the smallest shapes that make up your structure's geometry. Meshing is the process of connecting these finite components' computations to form a mesh structure.

Note; the more precise your results will be, the denser your mesh structure must be. The complexity of calculations will rise as nodal points are added, though.

- **Step 6 _ Solution**

Partial differential equations can easily be transformed into algebraic equations. As a result, matrices will make equations simpler to understand. The singular matrices are then concatenated into a single global matrix to solve for unknown variables.

The item will now have a representation thanks to the work of FEM computing software. To choose the design that best meets your needs, keep comparing various options.
The following diagram provides a summary of the Basic design study framework along with some suggestions for improvement.

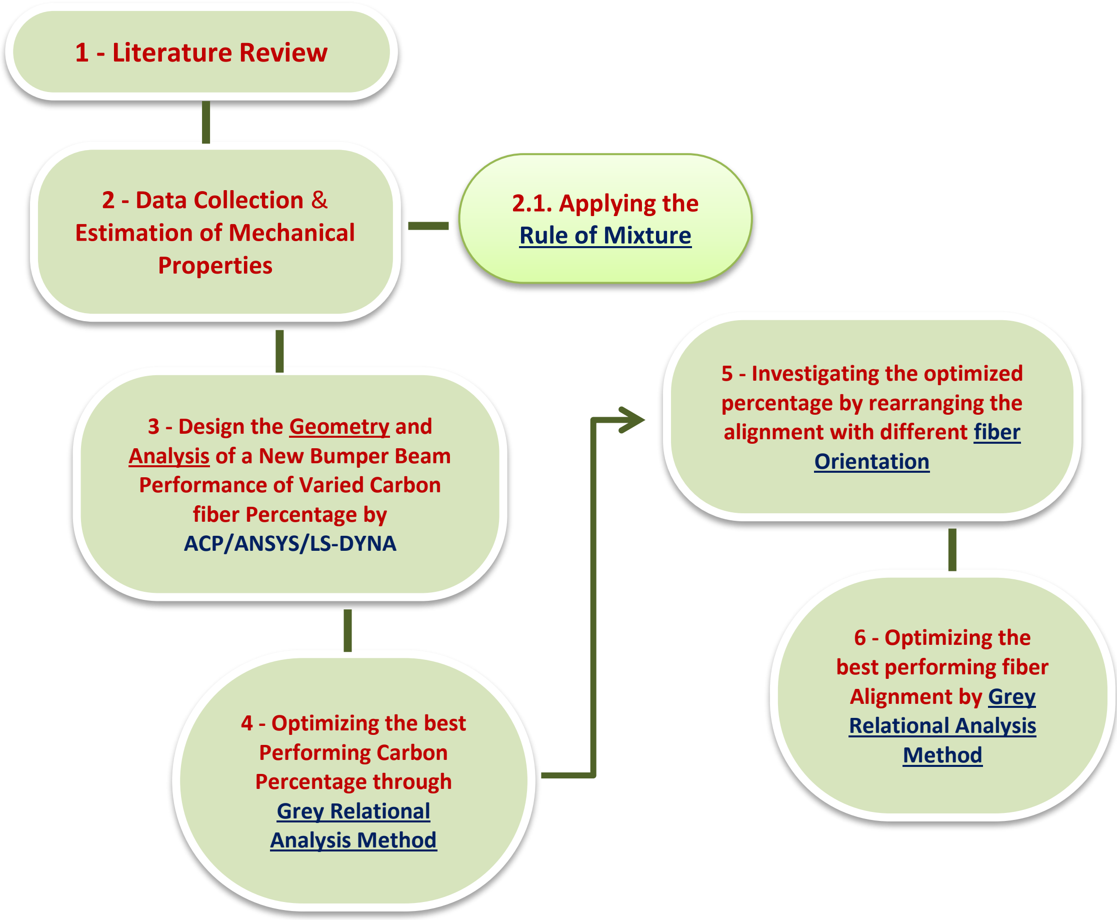

Figure 3.5: Design Framework

N.B. Continuous **design iterations** are performed adjacent to an analytical stage with the objective of improvement and improved results.

3.2.2. Impact Mode

Based on the nature and direction of the impact, frontal car crashes are classified into three main kinds. Vehicle-to-vehicle collisions can have a variety of impact forms. Only frontal collisions are evaluated in this study. In fact, in most collisions between two vehicles, the smaller vehicle is generally more severely damaged and its occupants are subjected to greater loads. Here are some examples of common frontal vehicle collisions:

1. *Full Frontal Collision*: this happens when the front ends of two cars hit immediately, resulting in a head-on collision. It usually occurs when two automobiles going in opposite directions crash head-on.
2. *Off-set Frontal Collision*: in an off-set frontal collision, when the front ends of two cars contact at an angle rather than directly head-on, an impact occurs. This type of collision occurs frequently when one vehicle veers into the path of another.
3. *Angular Frontal Collision*: This type of collision occurs when the front of one vehicle collides at an angle with the side of another vehicle. It can happen when a car fails to yield at an intersection and is hit by a vehicle moving on the opposite side of the road.
4. *Rear-End Collision*: Rear-end crashes, while not exactly frontal accidents, and involve the front of one vehicle colliding with the rear of another vehicle. This sort of collision is typical when one car fails to stop or quickly slows down, and the following vehicle is unable to stop in time.

Each form of frontal car collision has its unique set of dynamics and impact characteristics, which can influence the severity of the crash and the damage to the vehicles involved. Understanding these crashes aids in the analysis of accident scenarios, the implementation of safety measures, and the design of cars that are more crashworthy.

3.2.3. Mathematical Models for Frontal Collision

The dynamic behavior of a system as a function of time is described using mathematical models. When a *frontal collision* occurs, the impediment causes an impulsive force to be applied to the vehicle. The body's ability to deform absorbs some of the impact's energy during an impact. It is suggested that two mathematical models be used to examine the frontal collision of two cars. The component parts of the frontal compartmental structures are considered independently in the mathematical model. There are suggested two two-degrees-of-freedom numerically simplified models. The table-spring type is represented by the first mathematical model, and the table-spring with shock absorber type is represented by the second mathematical model.

The vehicle's structure is built with certain places that can dissipate kinetic energy through deformation during an impact. Elastic and plastic deformations, also known as elasto-plastic deformations, are common in accidents involving two cars (MalenD, 2011) (Du Bois P, 2004)

Two different types of crash tests are performed by the National Highway Traffic Safety Administration (NHTSA) as part of the New Car Assessment Program.

- **35mph frontal contact** - The car strikes a sturdy concrete barrier head-on at 35 mph (56 kmph). This is the same as one car striking another car of same weight traveling at 35 mph.
- **35mph side impact** - A deformable 'bumper' equipped 3,015Pound (1,368Kg) sled collides with the side of the test vehicle. The tires of the sled are inclined. In the test, an automobile crossing an intersection is simulated as getting sideswiped by a vehicle that is disregarding a red signal. In spite of the fact that the sled is actually moving at 38.5 mph, mathematical calculations show that this speed is equivalent to a side hit that would occur at 35 mph.

A. Simplified Numerical Models with two Degrees of Freedom and two Vehicles

Two bodies (two vehicles) make up the simplified numerical model with two degrees of freedom (Du Bois P, 2004). The frontal collision between two automobiles will affect how they behave. The bodies are joined together by elastic components of the helical spring type, each with a rigidity of k_1 and k_2. The streamlined model for analyzing the collision between two cars is shown in figure below.

Where: $\mathbf{m_1}$ denotes the mass of **vehicle 1**; $\mathbf{m_2}$ denotes the mass of **vehicle 2**; $\mathbf{x_1}$ denotes the motion of vehicle 1; $\mathbf{x_2}$ denotes the motion of vehicle 2; $\boldsymbol{k_2}$ denotes the elastic constant corresponding to the area of vehicle 1 deformable; $\boldsymbol{k_2}$ denotes the elastic constant relating to the area of vehicle 2.

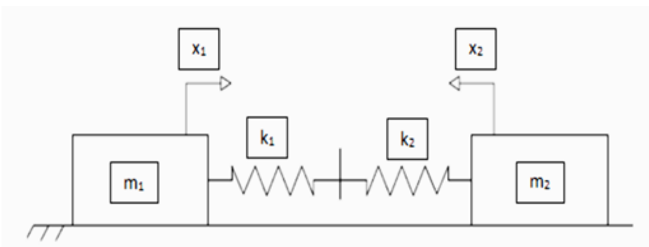

Figure 3.6: a two-degree-of-freedom & simplified mass-spring numerical

On the basis of Lagrange's generalized equation, the motion equations for the vehicles involved in the crash are determined (IlieS, 2012) (RadesM, 2008):

$$\frac{d}{dt}\frac{\partial E_c}{\partial \dot{x}_l} - \frac{\partial E_c}{\partial x_i} + \frac{\partial V}{\partial x_i} = 0 \qquad \ldots\ldots\ldots\ldots\ldots\ldots.. \qquad (3.5)$$

Where: $\boldsymbol{E_C}$ is the system's kinetic energy, $\boldsymbol{V}$ its potential deformation energy, and $\boldsymbol{x_i}$ are its generalized coordinates (the separations between the bodies' centers of gravity in longitudinal directions, $\boldsymbol{x_1}$ and $\boldsymbol{x_2}$).

The system of the two vehicles' combined kinetic energy is (AlecuA, 2014)

$$\boldsymbol{E}_c = \frac{1}{2}m_1\dot{x}^2{}_1 + \frac{1}{2}m_2\dot{x}^2{}_2 \qquad \ldots\ldots\ldots\ldots\ldots\ldots\ldots\ldots \qquad (3.6)$$

$\dot{x}_1, \dot{x}_2$, are the speeds corresponding to both vehicles.

The two elastic elements connected in series are used to represent the potential deformation energy of the system created by the two vehicles. Thus, $k_s = \frac{k_1\, k_2}{k_1+k_2}$ is considered to be the equivalent elastic constants of the two elastic elements $\boldsymbol{k_1}$ and $\boldsymbol{k_2}$ (AlecuA, 2014).

$$\boldsymbol{v} = \frac{1}{2}k_s(x_1 + x_2)^2 \qquad \ldots\ldots\ldots\ldots.\ldots\ldots\ldots.. \qquad (3.7)$$

The remaining forces are thought to be insignificant in comparison to the collision force, which is the only force thought to affect the cars during impact.

The Generalized Lagrange Equation for the two vehicles will be applied below:

$$\begin{aligned} \frac{d}{dt}\frac{\partial E_c}{\partial \dot{x}_1} - \frac{\partial E_c}{\partial x_1} + \frac{\partial V}{\partial x_1} = 0 \\ \frac{d}{dt}\frac{\partial E_c}{\partial \dot{x}_2} - \frac{\partial E_c}{\partial x_2} + \frac{\partial V}{\partial x_2} = 0 \end{aligned} \qquad \ldots\ldots\ldots\ldots\ldots\ldots\ldots.. \qquad (3.8)$$

The equations of motion for the vehicles engaged in a frontal collision are found by solving this system of equations and substituting the kinetic energy and potential deformation energy with the relevant formulae.

$$\begin{cases} m_1\ddot{x}_1 + k_s(x_1 + x_2) = 0 \\ m_2\ddot{x}_2 + k_s(x_1 + x_2) = 0 \end{cases} \qquad \ldots\ldots\ldots\ldots\ldots\ldots. \qquad (3.9)$$

The end result is a system of two degree II differential equations where the two vehicles' individual accelerations are unknown:

$$\ddot{X}_1 = \frac{-k_s(x_1 + x_2)}{m_1}$$
$$\ddot{X}_2 = \frac{-k_s(x_1 + x_2)}{m_2} \quad \ldots\ldots\ldots..\ldots\ldots\ldots.. \quad (3.10)$$

B. Modeling in Mathematics of the Mass-Spring-Damper Kind

Two bodies (two vehicles) are connected to each other by elastic spring-type elements with stiffness $\mathbf{k_1}$ and $\mathbf{k_2}$, and two damping elements with damping constants $\mathbf{c_1}$ and $\mathbf{c_2}$ make up the simplified numerical model with two degrees of freedom (Du Bois P, 2004) (Deac S C, 2017). The streamlined model for analyzing the collision between two cars is shown in figure below.

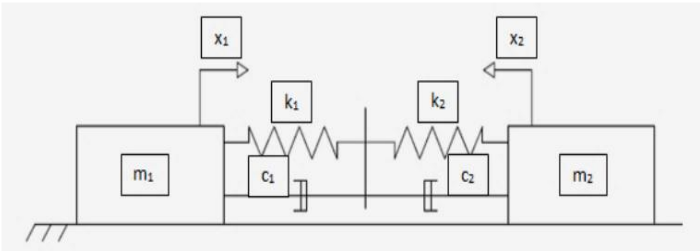

Figure 3.7: Simplified mass-spring-damper type numerical models with two degrees of freedom

where: $\boldsymbol{m_1}$ denotes the mass of vehicle ***1***; $\boldsymbol{m_2}$ denotes the mass of vehicle ***2***; $\mathbf{x_1}$ denotes the movement of vehicle ***1***; $\mathbf{x_2}$ denotes the movement of vehicle ***2***; $\mathbf{k_1}$ denotes the elastic constant corresponding to the deformable area of vehicle ***1***; $\mathbf{k_2}$ denotes the elastic constant corresponding to the area of vehicle ***2***; $\mathbf{c_1}$ denotes the damping constant corresponding to the deformable area of the vehicle ***1***; $\mathbf{c_2}$ the damping constant corresponding to the deformable area of the vehicle ***2***.

On the basis of Lagrange's generalized equation, the motion equations for the vehicles involved in the collision are determined (IlieS, 2012) (RadesM, 2008):

$$\frac{d}{dt}\frac{\partial E_c}{\partial \dot{x}_i} - \frac{\partial E_c}{\partial x_i} + \frac{\partial E_a}{\partial \dot{x}_i} + \frac{\partial V}{\partial x_i} = 0 \quad \ldots\ldots\ldots\ldots\ldots\ldots. \quad (3.11)$$

Where; $\mathbf{E_c}$ – is the kinetic energy of the system; $\mathbf{E_a}$ is the energy dissipated by the damping elements; $\dot{x}_i$ are the corresponding speeds of the vehicles; V – is the potential deformation energy of the system; $\boldsymbol{x_i}$ – are the generalized coordinates (distances of the centers of gravity of the bodies in the longitudinal direction $\boldsymbol{x_1}$ and $\boldsymbol{x_2}$).

The kinetic energy of the system formed by the two vehicles is (AlecuA, 2014):

$$\boldsymbol{E_k} = \frac{1}{2} m_1 \dot{x}^2{}_1 + \frac{1}{2} m_2 \dot{x}^2{}_2$$

Where: $\dot{x}_1, \dot{x}_2$ are the speeds corresponding to the two vehicles!

The two elastic elements connected in series are used to represent the potential deformation energy of the system created by the two vehicles. Thus, $k_s = \frac{k_1 k_2}{k_1 + k_2}$ is considered to be the equivalent elastic constants of the two elastic elements $\boldsymbol{k_1}$ and $\boldsymbol{k_2}$ (AlecuA, 2014).

$$v = \frac{1}{2} k_s (x_1 + x_2)^2$$

It is assumed that the two dampers are connected in series to calculate the energy lost by the damping components of the system made up of the two cars. Thus, $\boldsymbol{CC_s} = \frac{c_1 c_2}{c_1 + c_2}$ $\mathbf{C_1}$ and $\mathbf{C_2}$ are two depreciation factors, and is regarded as their equivalent depreciation constant.

$$\boldsymbol{E_a} = \frac{1}{2} c_s (\dot{x}_1 + \dot{x}_2)^2 \qquad \dots\dots\dots\dots\dots\dots \qquad (3.12)$$

The Generalized Lagrange Equation for the two vehicles will be applied below:

$$\begin{cases} \frac{d}{dt}\frac{\partial E_c}{\partial \dot{x}_1} - \frac{\partial E_c}{\partial x_1} + \frac{\partial E_a}{\partial \dot{x}_1} + \frac{\partial V}{\partial x_1} = 0 \\ \frac{d}{dt}\frac{\partial E_c}{\partial \dot{x}_2} - \frac{\partial E_c}{\partial x_2} + \frac{\partial E_a}{\partial \dot{x}_2} + \frac{\partial V}{\partial x_2} = 0 \end{cases} \qquad \dots\dots\dots\dots\dots\dots\dots\dots \qquad (3.13)$$

The equations of motion for the involved vehicles in a frontal collision are produced by solving this system of equations and substituting the kinetic energy and potential deformation energy with the relevant formulae.

$$\begin{cases} m_1 \ddot{x}_1 + c_s (\dot{x}_1 + \dot{x}_2) + k_s (x_1 + x_2) = 0 \\ m_2 \ddot{x}_2 + c_s (\dot{x}_1 + \dot{x}_2) + k_s (x_1 + x_2) = 0 \end{cases} \qquad \dots\dots\dots\dots\dots \qquad (3.14)$$

The result is a system two differential equation in which the accelerations of the two vehicles are unknown,

$$\begin{cases} \ddot{X}_1 = \frac{-C_s (\dot{x}_1 + \dot{x}_2) - k_s (x_1 + x_2)}{m_1} \\ \ddot{X}_2 = \frac{-C_s (\dot{x}_1 + \dot{x}_2) - k_s (x_1 + x_2)}{m_2} \end{cases} \qquad \dots\dots\dots\dots\dots\dots \qquad (3.15)$$

In conclusion, it has been demonstrated that the mathematical models developed for the investigation of the frontal collision between two cars can aid in the advancement of passive safety. With a minimal investment of resources, satisfactory outcomes can be attained by applying fundamental concepts from classical mechanics. The finite element method's structural analysis can also be used to study these two models.

The generalized inertia load is equal to the acceleration times the mass (inertia), as stated by Newton's equation of inertia. Therefore, the inertia load distribution has temporal features.

The second order ordinary differential equation of motion can be used to build the overall governing equation for this circumstance.

$$\mathbf{F} = [\mathbf{A}]\,[\ddot{\mathbf{u}}] + [\mathbf{B}]\,[\dot{\mathbf{u}}] + [\mathbf{C}]\,[\mathbf{u}]$$

Where, **F** is the load Vector, **A** is the structural mass matrix, **B** is the structural dumping matrix, **C** is the structural stiffness matrix. For the motion function, $\ddot{\mathbf{u}}$ acceleration vector, $\dot{\mathbf{u}}$ velocity vector and $\mathbf{u}$ displacement vector. The concept of energy conservation is applied in elastic impact; the kinetic energy of the impactor and the car at their maximum deflection is preserved and transformed into elastic energy before impact.

$$\boldsymbol{K_E} = \frac{1}{2}m_A v^2{}_A + \frac{1}{2}m_B v^2{}_B - \frac{1}{2}m_A v^2{}_A - \frac{1}{2}m_B v^2{}_B \quad \dots\dots\dots\dots\dots \quad (3.16)$$

The pendulum is simply described as a rigid solid with mass ***M*** and kicking off velocity ***V***. Otherwise, the automobile is represented by a hard solid with comparable mass ***M***. The stiffness of the beam bumper, on the other hand, is included in the model as a spring of stiffness ***K***.

This stiffness can be determined analytically or empirically. The stiffness of the beam is determined by material mechanics, $\boldsymbol{\kappa} = \frac{48\mathcal{E}I}{\boldsymbol{L}^3}$ when its center is exposed to the external load.

- $\boldsymbol{\mathcal{E}}$ – the Young's Modulus of the material
- ***I*** – the moment of Inertia, and ***L*** **-** the total length of the beam bumper.

C. Determination of the Load

Impact force determination in the event of a collision

The transfer or exchange of energy between the colliding bodies,

$$K_E = \frac{1}{2}m_A v^2{}_A + \frac{1}{2}m_B v^2{}_B - (\frac{1}{2}m_A v^2{}_A + \frac{1}{2}m_B v^2{}_B)$$

Where; $\boldsymbol{m_A}$ and $\boldsymbol{m_B}$ are the two colliding masses (vehicles) with velocities($\boldsymbol{V_A}$) and($\boldsymbol{V_B}$). Because both $\boldsymbol{m_A}$ and $\boldsymbol{m_B}$ have similar masses and the vehicle ($\boldsymbol{m_B}$) is at rest (impactor),

Then, m_1 and m_2 are equal and the velocity of the impactor ($\boldsymbol{V_B}$) is zero. The mathematical expression for the conserved energy would be;

$$\boldsymbol{K_E} = \frac{1}{2}mV^2{}_1 \qquad \text{………………………….} \qquad (3.17)$$

The total mass of the specimen (vehicle) has taken from the manufacturer manual and is equal to ***1275*** Kg. Maximum traveling Vehicle Speed, $\boldsymbol{V_1}$ = 48 km/h = 13.3 *m/s* (moderate vehicle speed) This speed is in accordance with Federal Motor Vehicle Safety Standards, FMVSS 208- Occupant Crash Protection, the purpose and scope of which defines requirements to provide impact protection for passengers (George C. Jacob, 2004) (Zhang Jingwen, 2017,).

The Force will be calculated $F = \frac{K_E}{t}$, where $\boldsymbol{t}$ is the time taken for the impact and mostly is taken as **0.1** or less (in our case **0.3**second).

$$= \frac{\frac{1}{4}(\mathbf{1275})(\mathbf{13.3})^2}{\mathbf{0.3}} = 187{,}945.625\ N = \mathbf{187.9}\ KN$$

The Design Factor of Safety (FSd) was determined to be 1.5. This is relatively high value accounts for ambiguity in the nature of forces.

$= 1.5 \times 187.9 = \mathbf{281.85}\ \boldsymbol{KN}$ **,** as a result, for the sake of design, force is assumed

F = 281,850 N

Area of the front face of a beam bumper = (1200 x 50 x 45) mm^3

= 2,700,000 mm^3 = 0.0540000 m^2

The **Pressure** that acted on the beam bumper $P = \frac{\boldsymbol{F}}{\boldsymbol{A}} = \frac{281{,}850\ \text{N}}{0.0540000\ \text{m}^2} = \mathbf{5.2195}\ MPa$

3.2.4. AnsysCompositePrepPost & ANSYS LS-DYNA

In addition to taking a lot of time and being expensive, crash testing necessitates the destruction of a number of test vehicles. Computer simulated crash testing is one relatively recent technology that is rapidly gaining favor. Here, a FE (Finite Element) model of the vehicle is created in place of a real vehicle and is used to conduct the various tests that were performed before utilizing real vehicles.

One of the most well-known software programs, LS-DYNA from Livermore Software Technology Corporation, is capable of handling the crash testing of cars. Automobile manufacturers and their suppliers can test automobile designs using LS-DYNA, saving time and money by eliminating the need to tool up or test a prototype experimentally. Its roots and core competencies are in highly nonlinear transient dynamic finite element analysis (FEA) utilizing explicit time integration, despite the fact that the package keeps adding more and more options for the calculation of several complicated, real-world situations. Many different industries use LS- DYNA in their processes.

The purpose of this work is to demonstrate the dynamic analysis of a vehicle performed using the LS-DYNA program, as well as to suggest potential substitute materials that may be used to lessen impact shock, increase the body sections' durability, and reduce weight.

A solver for finite element analysis (FEA) is LS-DYNA. According to the user's input, the motor is what produces the outcomes. In other words, it is not a program that can construct a mesh or plot stress contours, but rather the most advanced and complicated FEA solver ever developed. The process is to supply LS-DYNA with an ASCII text-based deck that includes nodes, elements, loads, constraints, material laws, etc. (with a suffix of *.k or *.dyn), after which LS-DYNA solves this input and produces a second file (*.f06) with the desired results (Satish Pathy, 2022)

Any text editor can be used to read an LS-DYNA analysis deck. The LS-DYNA Keyword Manual Vol. 1 contains a wealth of relevant knowledge on the LS-DYNA code and its structure. Reading the Introduction and Getting Started sections is recommended for all new users. It gives some really great context for the LS-DYNA code.

LS-DYNA is a finite element code for non-linear transient dynamics that has both explicit and implicit solvers. An *implicit* strategy can solve both the dynamic and the static problem (**no mass**), whereas *explicit* only works when there is **acceleration of mass** (dynamic).

Table 3.8: explicit vs. implicit solver: pros and cons

Explicit		Implicit	
Pros	**Cons**	**Pros**	**Cons**
It solves directly since the solution marches forward.	Solution time step controlled by wave speed and element mechanics.	Large time steps can be used since the solution is iterative.	Requires iterative process to converge.
Dynamic solution	Long run times for simulations that require long event times.	Static and Dynamic solutions	Requires iterative process to converge which can lead to long run times.
Extreme nonlinearity is easily handled.	Of course, solution can blow up due to twisted elements or contact problems.	Linear and Nonlinear solutions	Implicit struggles with extreme nonlinearity
Pretty much all physics can be solved.	W.R.T. multi-physics, no real cons since you are solving the impossible.	Provides the missing link in LS-DYNA to solve standard linear static and dynamic problems.	Focused on solid mechanics so don't expect to see meshfree methods anytime soon.

ACP tools, which are used to model composite models in Ansys software, as well as their applications and usages. ANSYS Composite PrePost is a plug-in module for modeling layered composite structures. Ansys Composite PrePost (ACP) is a Workbench platform integrated tool for modeling composite laminates (Pre) and enhanced analysis results (Post) using dedicated failure tools.

3.2.5. Grey Relational Analysis (Method of Composite Optimization)

Grey relational analysis is a method for calculating the grey relational degree and estimating the contribution measure of the system's main behavior or the degree of impact between system variables (Kuo Y, 2008).

Grey correlation degree is a measure of the degree of correlation between two components or two systems. The changing trend, size, and speed of grey correlation degree show the relative change of components in the system development process. When the contrasting shifts of two factors or systems have the same trend of change, the two factors have a higher degree of grey correlation; otherwise, they have a lower degree of grey correlation (Hsin-HungWu, 2002).

On this study, many of the output parameters influencing the functioning of hybrid composite material sharing are related to system development and change.

There are forty two (6 x 7 = 42) variables to describe the character output of the composite and to solve the change law of the system. The thorough evaluation approach of grey correlation analysis is used to calculate the node's local trust degree.

Procedure and Process of Grey Relation Analysis Application

According to relevant publications (Pakkar M S, 2017) (Shi K, 2017) (Zhou L, 2017), grey relational analysis often includes the following calculations and processes:

1. Convert the original data to the evaluated data. First, we must remove the various dimensions of the original data and convert it into data that can be compared to each other.
2. Determine the reference data sequence. The reference sequence is chosen based on the application.
3. Calculate the absolute difference, as well as the minimum and maximum value of the corresponding element, between the data sequence and the reference data sequence of each evaluated object one by one, and then compute the correlation coefficients of the two sequences at the corresponding element positions.
4. Determine the degree of grey correlation. The grey correlation degree of the two sequences is calculated as the arithmetic average of the correlation coefficient between the data index of each location and the corresponding elements of the reference sequence to reflect the relationship between the evaluation objects and the reference sequence.
5. Rearrange all the grey correlation degrees in the order of, large-to-small or small-to-large.
6. Analyze the findings. If the optimal value of each index is used to select the reference sequence, the sequence with a high correlation degree outperforms the sequence with a low correlation degree. Otherwise, the conclusion is illogical.

To determine the best performance percentage of carbon fiber (i.e. C5%, C15%, C25%, C30%, C35%, and C40%), the **'Equivalent (Von-Mises) Stress**,' **'Strain,'** '**Deformation**,' **'Internal Energy**,' **'Weight,'** **'Acceleration,'** and '**Cost'** of the created hybrid composite materials with each percentage should be compared. As a result, some parameters were chosen when their value was higher, while others were considered when their value was lower. That is the initial explanation as to why to use the Grey Relational Analysis Method to compare output data and choose the best performing hybrid material.

The following mathematical equations were used collectively in Grey Relation Analysis to determine the best performing composite material.

- If the required comparison result would be selecting the ***lower value***, these equation is used:

$$x = \frac{(X_{max} - X)}{(X_{max} - X_{min})} \quad \ldots\ldots\ldots.\ldots \quad (3.18)$$

- If the required comparison result would be selecting the ***higher value***, the formula used will be:

$$x = \frac{(X - X_{min})}{(X_{max} - X_{min})} \quad \ldots\ldots\ldots\ldots\ldots \quad (3.19)$$

Both the above equations were used for Normalization of the Data.

- The ***delta*** is then be calculated, as a result it will give the real contrasted value assigned between 0.5 and 1 (i.e. if 'Lower is Best' the lower value will get 0.5 and the higher will get One the remaining elements as in between),

$$\delta = X_{max} - X \quad \ldots\ldots\ldots\ldots\ldots\ldots\ldots \quad (3.20)$$

- The next step would be the '***Grey Relation Coefficient***' in other word ranking the given result depending on the delta, also from Zero to One i.e. (for example on 'Lower is Best' command that assigned as Zero will get the first rank i.e. **1** same for the other results);

$$\boldsymbol{\gamma} = \left(\frac{\delta_{max} + \delta_{min}}{\delta_{max} + \delta}\right) \quad \ldots\ldots\ldots\ldots\ldots.. \quad (3.21)$$

- The final step is **ranking** the result data based on grey relation coefficient by taking the average value of the result discussed on the relation coefficient with the equation of,

$$\eta = \frac{1}{n}\sum \gamma \quad \ldots\ldots\ldots\ldots\ldots. \quad (3.22)$$

The whole set of parameters and mathematical equations were loaded into Microsoft Excel for simplification and automatic result collection.

CHAPTER FOUR

FE INVESTIGATION USING SIMULATION SOFTWARE

The finite element approach consists of three key stages: First, Pre-processing, in which the researcher develops a finite element mesh to split the subject geometry into smaller sections for mathematical analysis and adds material properties and boundary conditions to the subject geometry, then, Solution, in which the program solves for the primary quantities by deriving the governing matrix equations from the model; Finally Post-processing, in which the analyst validates the results.

4.1. The Basic Geometry and Meshing of the Beam Bumper

4.1.1. Geometry

The basic three dimensional model of the beam bumper is developed using Ansys SpaceClaim. The dimensioning of the geometry is all in Centimeter (i.e. length- 120cm, height- 4.5m, and the thickness of the beam is 5cm).

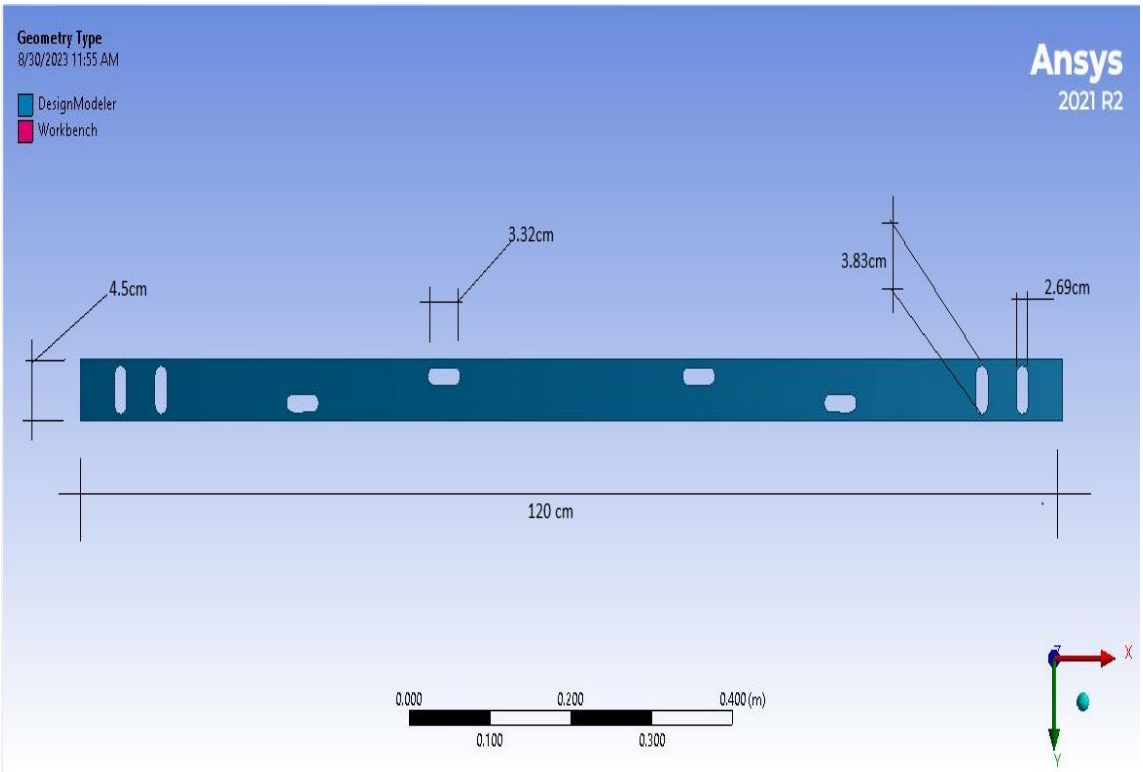

Figure 4.1: Frontal Projection

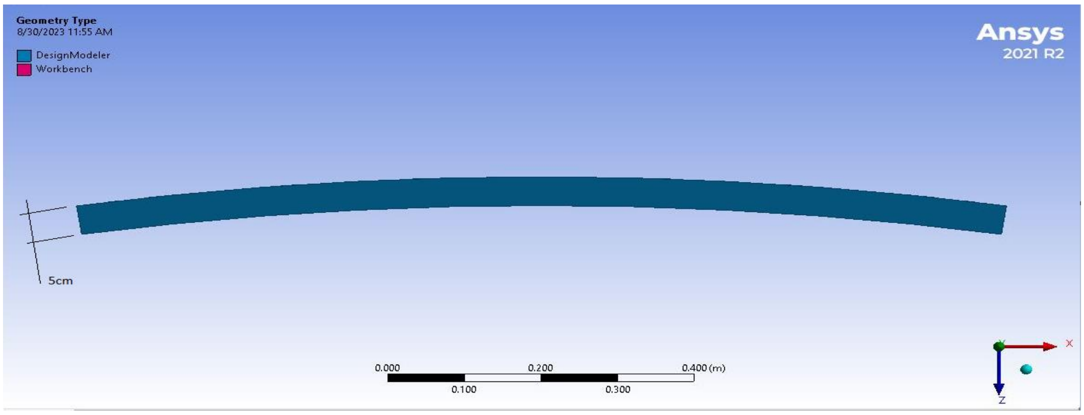

Figure 4.2: Top View

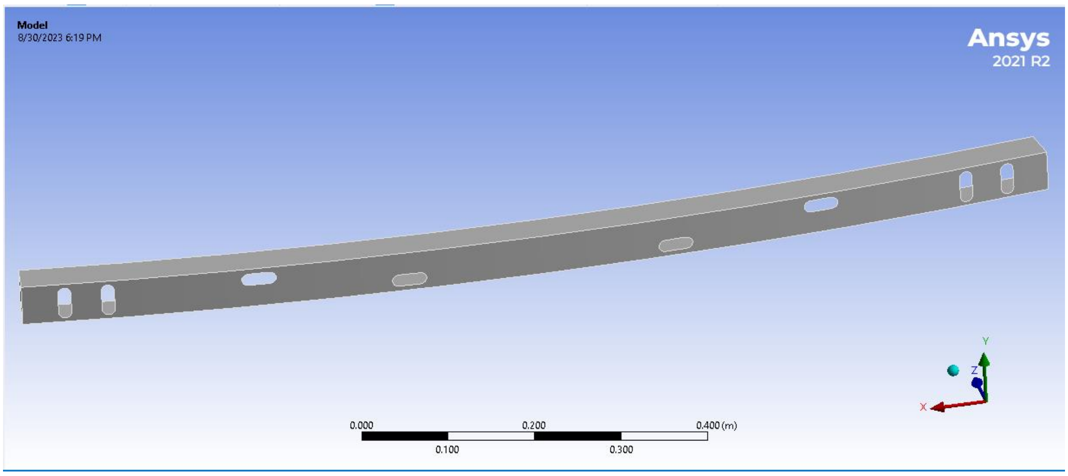

Figure 4.3: 3D isometric View

4.1.2. Meshing

It is ideal to begin the analytical technique with a coarse mesh, but for better and enhanced results, finer meshes (meshes with very small pieces) should be used wherever possible.

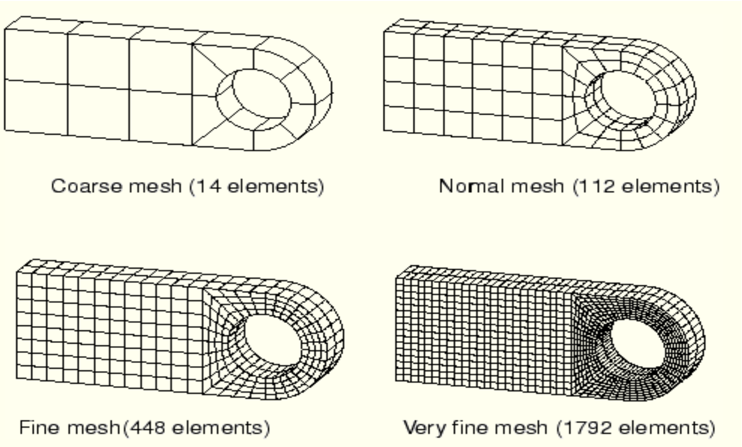

Figure 4.4: Types of Mesh

Although a finer mesh will demand more computer resources to solve, it can still be used as a more accurate verification and check on the given loads and constraints. Mesh refinement, in its most basic form, is the process of resolving the model using increasingly finer meshes. In the instance of this thesis, the number of elements is fixed at **74,856** and the Nodal value is **75,907**. The finer the mesh, the better and more accurate the output would be.

Figure 4.5: Meshed Projection

4.1.3. The Boundary Condition and Impact Load

Beam bumper is attached on a vehicle body position, a fixed support is installed. As a boundary condition for the study, a fixed support was used. One car was moving, while the other was stopped (taken as impactor).

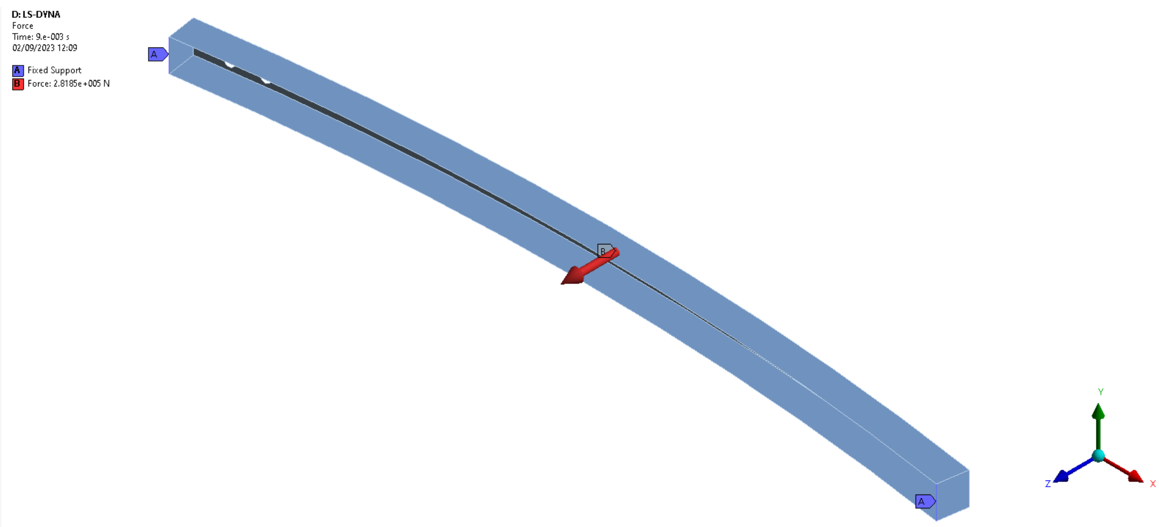

Figure 4.6: Fixed Support Projections

The fixed support was installed on the vehicle body at the attachment location of the automobile beam bumper. This support stabilized the bumper and provided a secure foundation for the analysis.

CHAPTER FIVE

RESULTS AND DISCUSSIONS

In order to thoroughly analyze the mechanical behavior of hybrid composite materials varying carbon contents, the thesis made use of the combined capabilities of front-line modeling technology. The use of two widely recognized finite element analysis (FEA) software tools ACP (AnsysCompositePrePost) and ANSYS 2021R2 aided in the time-consuming setup of composite lay-ups and material properties. ACP, as our pre-processing component, ensured that complicated composite architectures were accurately represented. This indication of our ANSYS.2021R2 simulations enabled extensive investigation of structural reactions. In addition, to further our study, we used LS-DYNA, powerful finite element software designed for dynamic simulations.

This multidisciplinary approach allowed for an in-depth analysis of how varying carbon content affects structural integrity, deformation properties, and energy absorption under on a given of loading circumstances. The methodology, which combines ACP, ANSYS.21R2, and LS-DYNA inside a FEA framework, simulates the dynamic nature of automotive collisions, revealing insights critical to the ongoing improvement of bumper beam materials and designs.

5.1. Original Steel 1006 Bumper Beam Simulation Results

The steel bumper simulation results revealed noteworthy insights. The equivalent stress was determined to be 29,342 MPa, showing that the bumper was subjected to significant stress levels. The deformation reached 63.609 mm, demonstrating the magnitude of structural displacement under applied stresses.

The internal energy was calculated to be 4892.5 J, which represents the energy stored within the system. The steel bumper weighs 6.6906 Kg and contributes to the overall mass of the car. Finally, the acceleration measured was 829.98 mm/s^2, providing significant information about the bumper's dynamic response. These findings give light on the steel bumper's performance, structural integrity, and weight implications within the context of the study.

5.1.1. The Total Deformation and Equivalent (von-Mises) Stress

The structural displacement under applied forces was demonstrated by a deformation of 63.609mm. The equivalent stress was calculated to be 29,342MPa, indicating that the bumper experienced considerable stress levels.

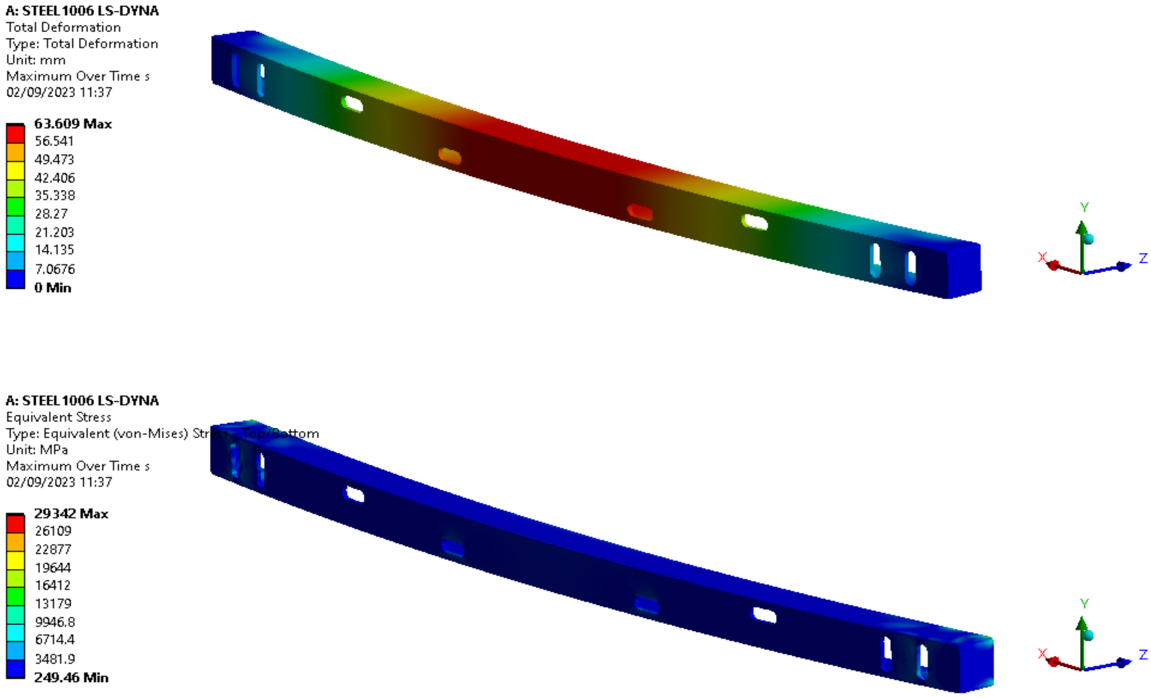

Figure 5.1: Total deformation and Equivalent stress of Steel 1006

5.1.2. Internal Energy and Acceleration

The measured acceleration was 829.98 mm/s^2, which provided important information on the bumper's dynamic response.

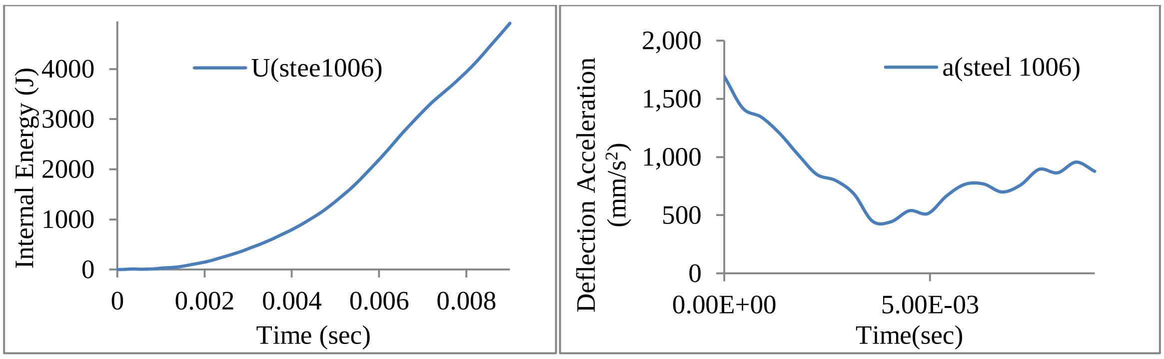

Figure 5.2: Internal Energy and Acceleration for steel 1006

The internal energy, which reflects the energy stored within the system, was calculated to be 4892.5 J.

5.1.3. Results of Weight Evaluation

Many studies have been conducted to carefully examine and optimize the weight of the bumper in order to find a balance between structural integrity, safety, and overall vehicle performance. Manufacturers want to improve the car's efficiency, handling qualities, and overall driving experience by reducing the weight of the steel bumper.

The weight of the steel bumper, assessed at 6.6906 Kg, contributes significantly to the overall mass of the car. The weight of the bumper is an important factor to consider in automotive design since it has a direct impact on numerous aspects of vehicle performance. The weight of the bumper has an effect on acceleration, handling, and fuel efficiency. A heavier bumper may increase the vehicle's inertia, necessitating more energy for acceleration and deceleration. Furthermore, the bumper's extra weight might change the distribution of weight throughout the vehicle, affecting its balance and stability.

5.2. Simulation Results of a Hybrid Composite Containing 25% Carbon

The percentage of carbon is varied to 25% while keeping the S-Glass percentage complimentary to maintain the remaining overall percentage of 60% fiber content $f_f (0.15_c+0.45_s) +m_f (0.4)=1$. Several essential characteristics were observed by altering the carbon percentage to 25% while adjusting the S-Glass percentage to maintain a composite fiber percentage of 60%. The resulting equivalent stress was 43,192 MPa, demonstrating a substantial increase above earlier experiments. The total deformation was 264.48 mm, indicating a significant shift in structural displacement.

The reported internal energy was 25,456 J, indicating a significant increase in energy stored within the system. Surprisingly, the weight dropped significantly to 1.3975 Kg, indicating a significant weight reduction as compared to the steel bumper. However, the acceleration was measured at -6935 mm/s^2, indicating a possible decrease in the bumper's dynamic response. It should be noted that as carbon is added to the epoxy resin and S-Glass fiber composite, the cost is projected to rise due to the greater cost of carbon fiber materials.

5.2.1. The Equivalent (Von-Mises) Stress and Total Deformation

In these test, the carbon-S-Glass composite showed significant improvements. The equivalent stress increased drastically to 43,192MPa, indicating a significant increase in stress levels. Similarly, total deformation was measured at 264.48mm, showing a considerable shift in structural displacement as compared to the steel bumper.

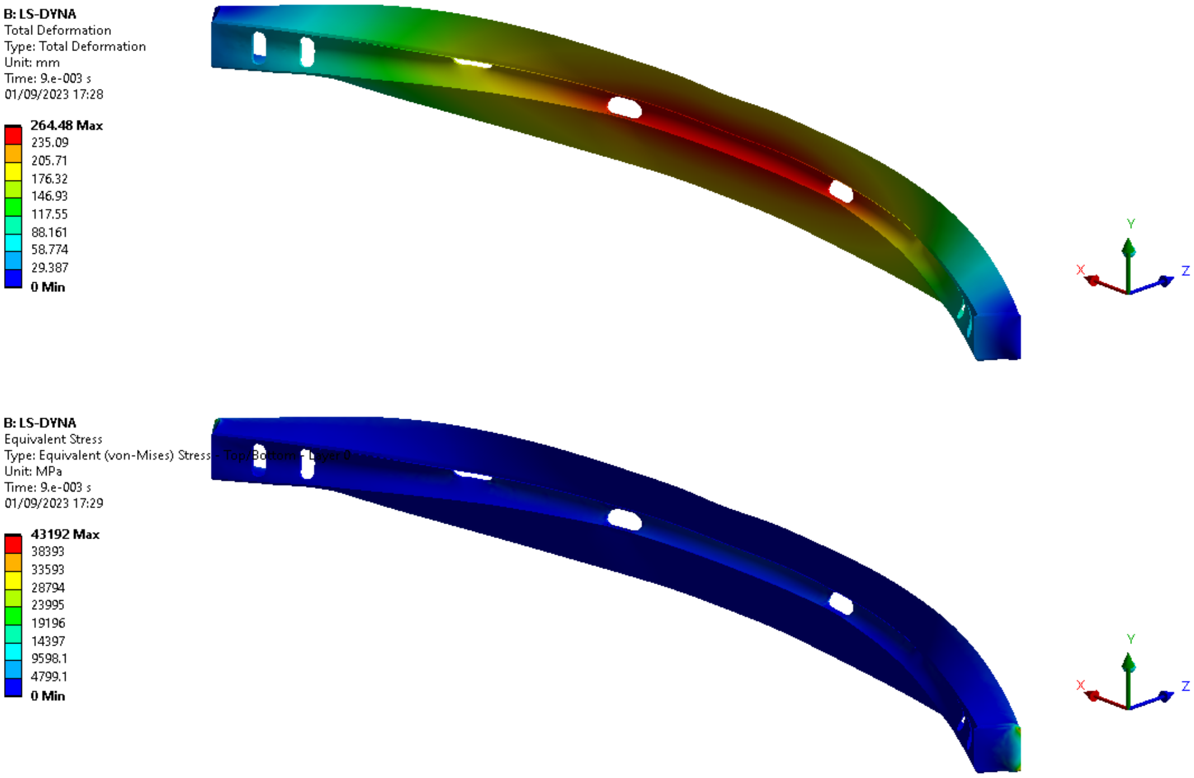

Figure 5.3: Total deformation and Equivalent Stress of 25% Carbon

These findings emphasize the carbon-S-Glass composite's improved strength and deformation characteristics, revealing its potential for improved performance and impact resistance.

5.2.2. Acceleration and Internal Energy Results from Simulation

In comparison to the steel bumper, the carbon-S-Glass (with 25% carbon) composite had a much lower acceleration of -6935 mm/s^2, reflecting a potential decrease in the bumper's dynamic response.

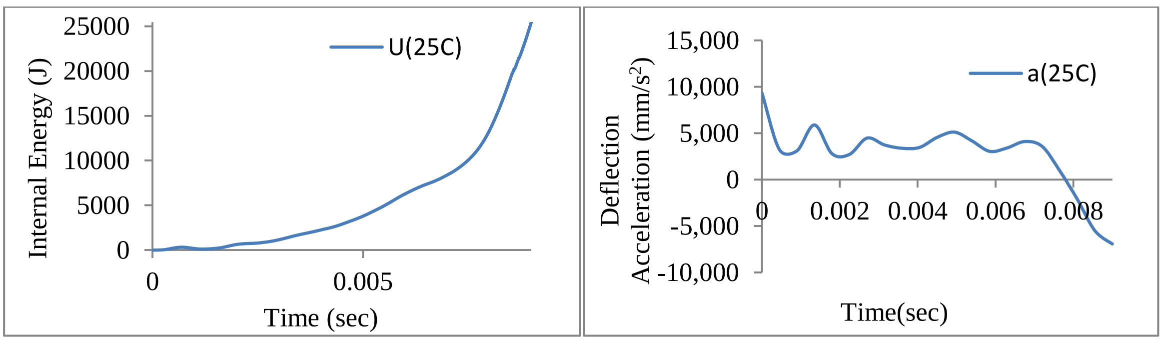

Figure 5.4: Internal Energy and Acceleration for 25% carbon

On the other hand, the composite's internal energy grew significantly to 25,456 J, indicating a significant increase in energy stored inside the system. These findings imply that, while the carbon-S-Glass composite outperforms the steel bumper in terms of structural properties and energy absorption capacity, there may be a trade-off in terms of dynamic responsiveness.

5.2.3. Weight Assessment Results

Surprisingly, the carbon-S-Glass composite weighed just 1.3975 Kg, compared to 6.6906 Kg for the steel bumper (79.12% of the weight is minimized). This large weight reduction emphasizes the composite's potential for lightweight construction and contributes to total vehicle weight reduction. The use of carbon fibers and S-glass fibers in the composite structure improves strength and stiffness while reducing weight. This weight reduction allows for enhanced fuel efficiency, agility, and mobility, making the carbon-S-Glass composite an enticing alternative for automotive applications.

5.3. Results of a 30% Carbon Hybrid Composite Simulation

The percentage of carbon is varied to 30% while keeping the S-Glass percentage complimentary to maintain the remaining overall percentage of 60% fiber content $f_f (0.18_c+0.42_s) + m_f (0.4)=1$. Several major discoveries resulted from the inquiry in which the carbon percentage was reduced to 30% while keeping a complimentary S-Glass percentage to obtain an overall fiber percentage of 60%. The resulting equivalent stress was calculated to be 36,541 MPa, suggesting that the composite displayed a considerable stress level. This discovery emphasizes the composite's capacity to properly withstand and distribute external stresses. Furthermore, the total deformation was 448.82 mm, indicating a significant extent of structural displacement when compared to earlier trials. This shows that the composite material may absorb and transfer energy well during impact occurrences, reducing possible damage.

The internal energy measured was 22,857 J, suggesting a significant amount of energy held within the system and indicating the composite's ability to absorb and discharge energy efficiently. Furthermore, the weight of the composite material was 1.3869 Kg, suggesting a considerable weight decrease when compared to both the steel bumper and earlier studies. This weight reduction leads to overall vehicle weight reduction, which may lead to increased fuel efficiency and performance. However, it is worth mentioning that the acceleration was measured at -4930 mm/s^2, indicating that the dynamic reactivity of the composite material may have decreased. This discovery emphasizes the significance of carefully weighing the trade-offs between weight reduction and dynamic performance when choosing materials for bumper applications.

5.3.1. The Equivalent (von-Mises) Stress and Total Deformation for 30% Carbon Fiber

The resulting equivalent stress was calculated to be 36,541MPa, indicating that the composite was under significant stress. This discovery highlights the composite's ability to endure and distribute external forces properly.

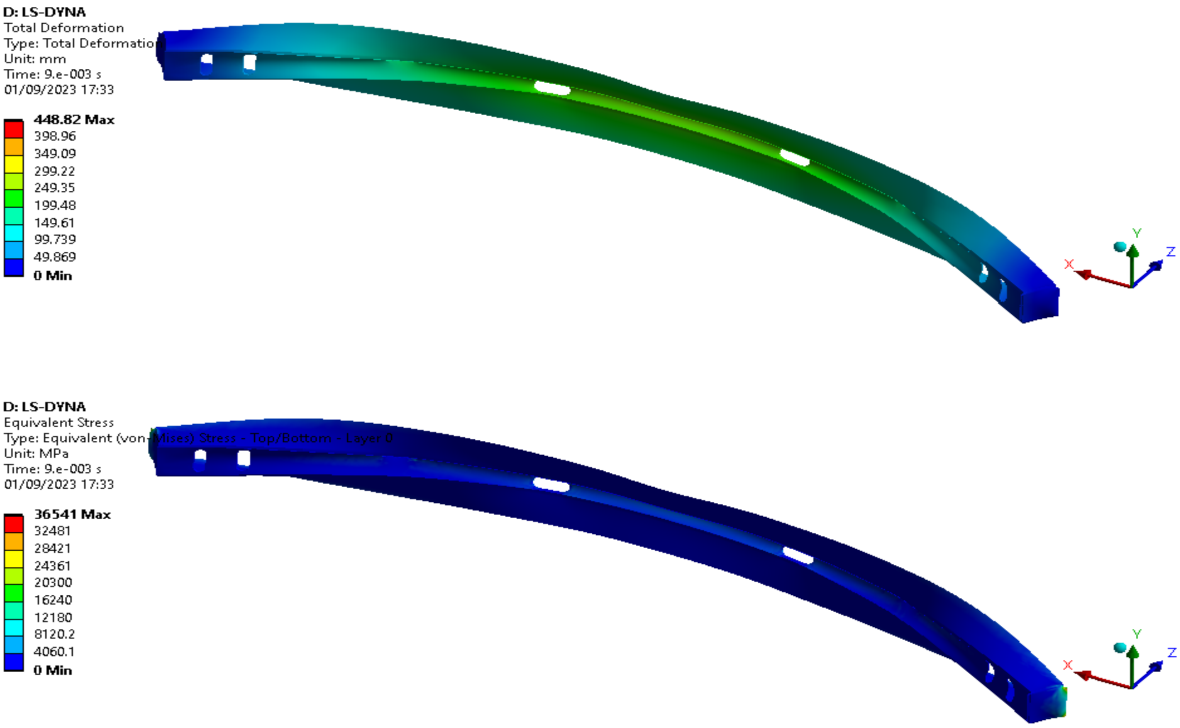

Figure 5.5: Equivalent stress and Total Deformation for 30% Carbon

Furthermore, when compared to previous trials, the overall deformation was 448.82mm, showing a substantial extent of structural displacement. This demonstrates that the composite material can absorb and transfer energy effectively during impact events, limiting potential damage.

5.3.2. Simulation Results for Acceleration and Internal Energy

It is significant to note that the acceleration reported at -4930 mm/s^2 represented a possible decrease in the composite material's dynamic reactivity. This finding shows that the composite may respond to external forces more slowly than in prior studies.

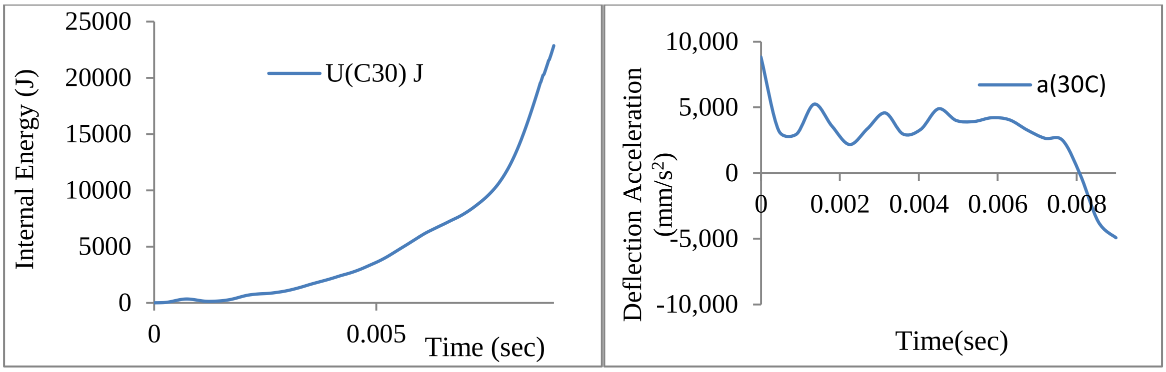

Figure 5.6: Internal energy and acceleration for 30% Carbon

The measurement of 22,857 J for internal energy, on the other hand, suggested a considerable quantity of energy stored within the system. This observation emphasizes the composite's remarkable ability to absorb and release energy, highlighting its potential as an efficient energy-dissipating material. The combination of decreased acceleration and increased internal energy helps to a thorough understanding of the composite's dynamic behavior and impact resistance.

5.3.3. Simulation Results of Weight

Moreover, the weight of the composite material was 1.3869 Kg, indicating a significant weight reduction as compared to the steel bumper and previous tests (when the amount of carbon varied/increased to 30%, the percentage reduction of the weight was improved to 79.27% which is slightly greater than the previous scenario i.e. 25%). This weight reduction leads to a reduction in overall vehicle weight, which may result in improved fuel efficiency and performance.

5.4. Simulation Results of a Hybrid Composite With 35% Carbon

The percentage of carbon is varied to 35% while keeping the S-Glass percentage complimentary to maintain the remaining overall percentage of 60% fiber content f_f $(0.21_c+0.39_s) + m_f\,(0.4)=1$.

The carbon content was raised to 35% while the S-Glass content was changed to maintain an overall fiber content of 60% in order to investigate the impacts of changing the carbon percentage in a composite material. The equivalent stress reduced to 22,982MPa as a result of this adjustment, and the total deformation increased to 10,879mm. The internal energy also decreased to 19,385J, and the acceleration increased to -4062 mm/s^2. The weight of the composite also decreased to 1.3764kg.

It is interesting to notice that, despite an increase in acceleration and overall deformation, the composite's stress, internal energy, and weight reduced as a result of the change in carbon content. These results indicate that changing the carbon content of the composite directly affects its mechanical properties, with various parameters responding to the adjustment in various ways.

5.4.1. The Total Deformation and Equivalent (von-Mises) Stress for 35% Carbon Fiber

Equivalent Stress: The characteristics of the S-Glass fibers are responsible for the reduction in equivalent stress (to 22,982MPa). Since S-Glass fibers are renowned for having great strength and stiffness, adding more of them to the composite may have improved the material's overall strength, lowering the stress value.

Overall Deformation: The higher carbon content can be used to explain the rise in overall deformation (to 10,879mm). Carbon fibers are renowned for their outstanding flexibility and deformation resistance. The composite may have become more flexible by increasing the carbon content, resulting in a higher overall deformation under applied stresses.

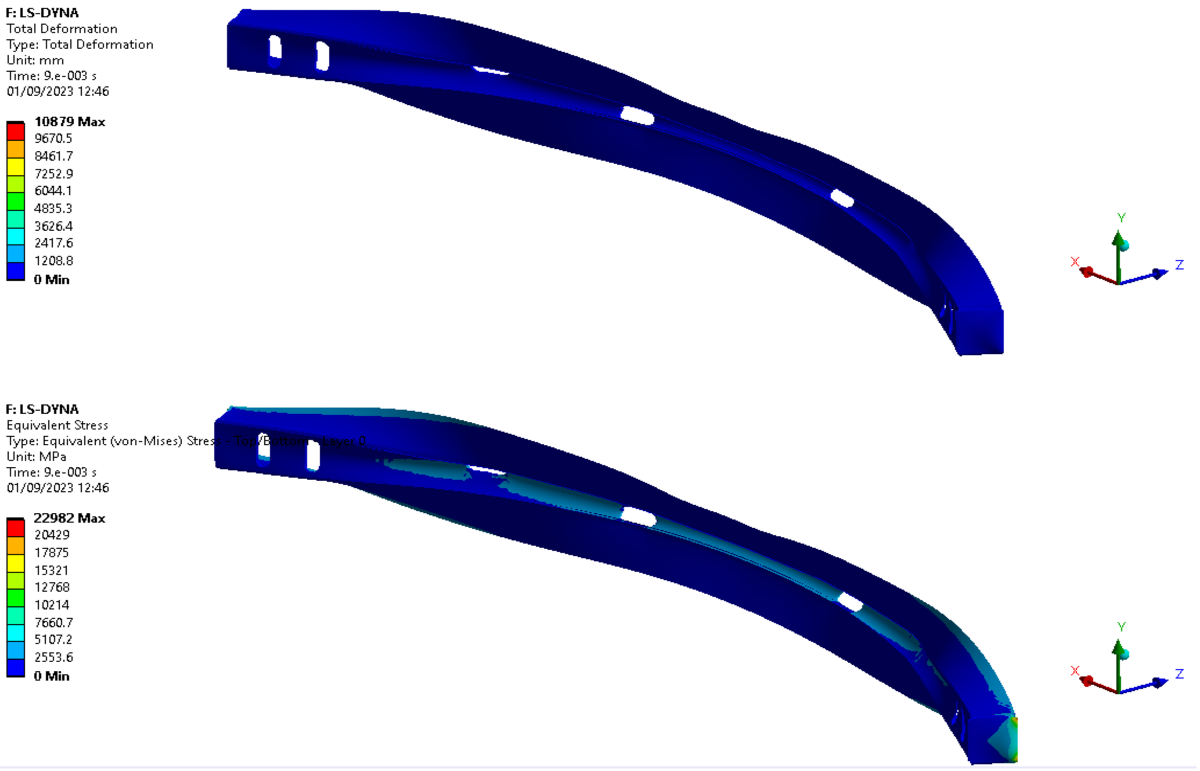

Figure 5.7: Total deformation and Equivalent Stress for 35% Carbon

5.4.2. Acceleration and Internal Energy Simulation Results

Internal Energy: The alteration in the composite's composition is to blame for the drop in internal energy (to 19,385J). The internal energy of the composite can be affected by the particular stiffness and energy-absorbing qualities of carbon and S-Glass fibers. The energy absorption properties may have been impacted by the change in carbon %, leading to a reduced internal energy value.

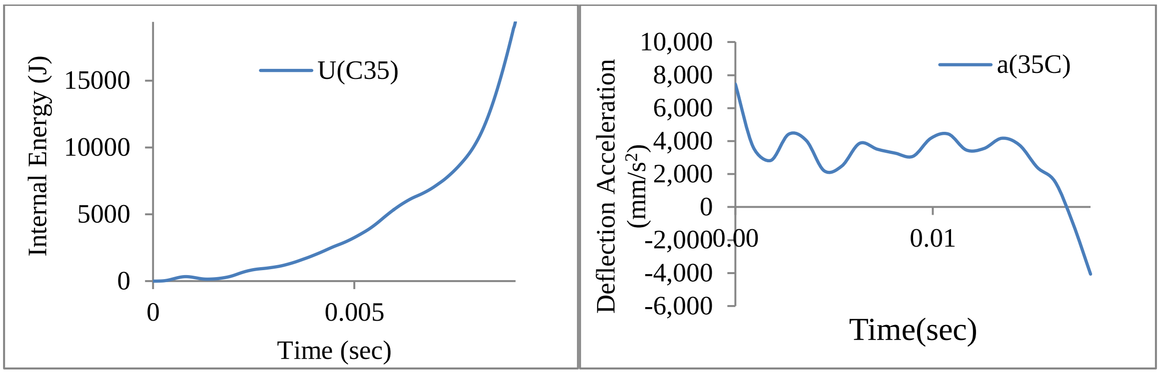

Figure 5.8: Internal energy and Acceleration for 35% Carbon

Acceleration: The change in the composite's mechanical characteristics is probably what caused the acceleration to increase (to -4062 mm/s^2). The increased acceleration may have resulted from the material's enhanced flexibility and deformability, which may have been a result of the higher carbon content.

5.4.3. Weight Assessment Results

Weight: The difference in density between carbon and S-Glass fibers can be used to explain the weight loss (to 1.3764kg). When the proportion of carbon fibers in the composite is raised, the composite becomes lighter because carbon fibers are less dense than S-Glass fibers. This weight loss may have benefits like increased fuel efficiency or a lighter overall system. Numerically it can be discussed that it’s linearly raised the weight reduction as a result of raised carbon fiber percentage to 79.42% when compared to the original steel bumper.

5.5. Simulation Results of a Hybrid Composite With 40% Carbon

Based on the distinctive features of the carbon and S-Glass fibers within the composite, the observed changes in the mechanical properties after altering the carbon percentage to 40% while keeping the complementary S-Glass percentage to obtain a total fiber content of 60% may be justified $f_f(0.24_c+0.36_s)+m_f(0.4)=1$.

The composite's mechanical characteristics significantly changed as a result of changing the carbon percentage. The equivalent (von-Mises) stress dropped to 22,832MPa, showing that the material's strength properties have improved. The total deformation, however, increased marginally, reaching 10,892mm, indicating increased flexibility and deformability. However, the internal energy dropped to 19,287J, indicating a decline in the composite's internal energy reserves. Additionally, the composite's weight lowered to 1.3661kg, which may have benefits for the system's overall performance and structural load.

And lastly, the acceleration increased to -4046 mm/s^2, indicating a faster rate of velocity change as a result of applied forces. These findings demonstrate the significance of material composition in achieving the desired performance parameters by highlighting the impact of variable carbon content on the mechanical behavior of the composite.

5.5.1. Assessment of Equivalent Stress and Total deformation

The increased carbon content is responsible for the decrease in equivalent (von-Mise) stress, which was 22,832MPa. It is possible that by increasing the proportion of carbon fibers in the composite, the material's total strength was improved, leading to a lower stress value. Carbon fibers offer outstanding strength and stiffness capabilities.

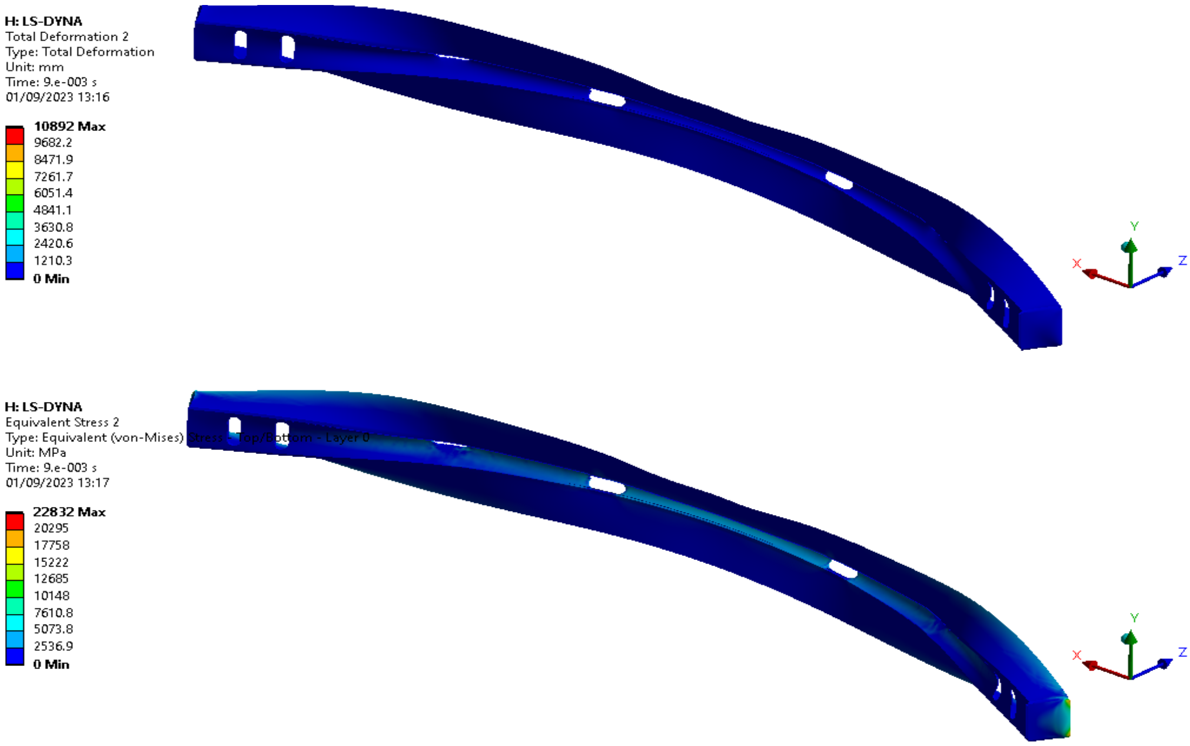

Figure 5.9: Total deformation and Equivalent Stress for 40% Carbon

The higher carbon content explains the modest rise in total deformation (to 10,892 mm). Carbon fibers are renowned for their exceptional flexibility and deformation resistance. The composite may have grown more malleable with a higher percentage of carbon fibers, resulting in a marginally higher overall deformation under applied loads.

5.5.2. Simulation Results of Acceleration and Internal Energy

The change in the composite's mechanical characteristics is probably what caused the acceleration to increase (to -4046 mm/s^2). The increased acceleration may have resulted from the higher carbon content making the material more elastic and malleable, allowing for a quicker change in velocity under applied forces.

The alteration in the composite's composition is probably what caused the decrease in internal energy (to 19,287J).

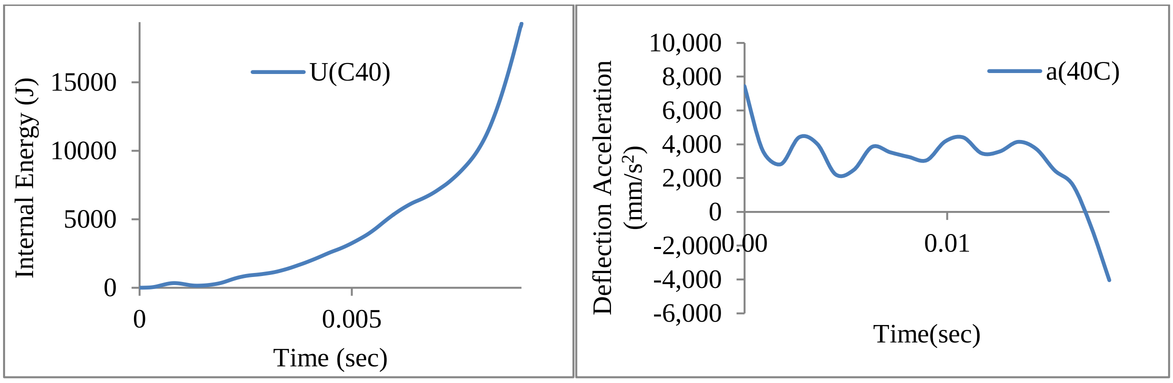

Figure 5.10: Internal energy and Directional Acceleration for 40% Carbon

Since carbon fibers have significant energy absorption capacities, raising their percentage may have had an impact on the composite's capacity to store energy, resulting in a reduced internal energy value.

5.5.3. Simulation Result for Weight Change

Because carbon and S-Glass fibers have different densities, the weight was reduced (to 1.3661kg). When the proportion of carbon fibers in the composite is raised, the composite becomes lighter because carbon fibers are less dense than S-Glass fibers. This weight loss may have advantages like increased reliability of the system generally and less structural load. Among the optimizations made on these thesis the maximum amount of carbon fiber percentage used 40%, and that was resulted in 79.58% weight reduction from the original reference case i.e. weight of steel bumper.

5.6. Simulation Results of a Hybrid Composite With 15% Carbon

The observed changes in the mechanical properties after changing the carbon percentage to 15% while maintaining the complementing S-Glass percentage to generate a total fiber content of 60% may be justified based on the unique characteristics of the carbon and S-Glass fibers inside the composite $f_f(0.09_c+0.51_s) + m_f(0.4)=1$.

5.6.1. Assessment of Equivalent Stress, Strain and Total deformation

Under applied stress, the material changes significantly when the carbon content is set at 15%. The equivalent stress, which reaches a value of 55,004 MPa, indicates the strength of the internal forces that the material encounters. In addition to this stress, the strain (2391.478) shows how much the material has deformed and how it reacts to the applied pressures. The material's entire change in size or shape as a result of the combination of stress and strain is shown by the total deformation, which measures 879.76 mm. Together, these metrics show how the material behaves and behaves at the given carbon concentration, emphasizing its strength, ability to deform, and potential for a range of engineering uses.

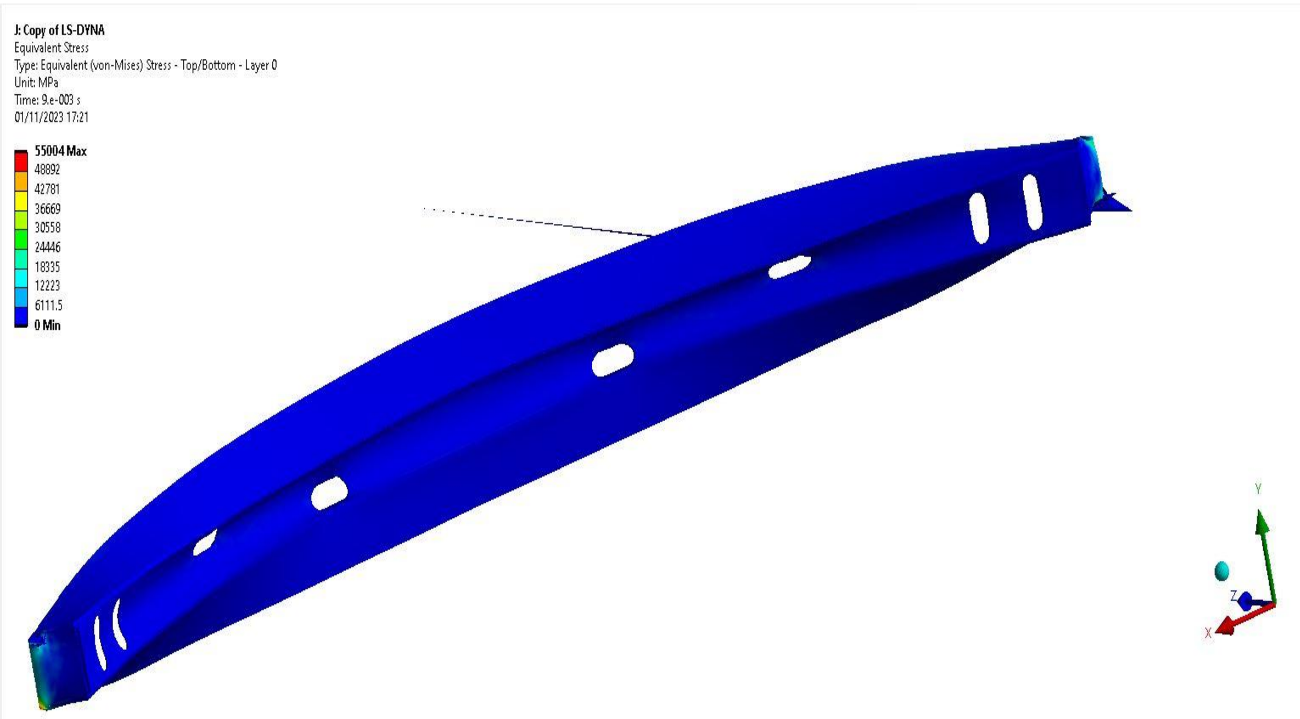

Figure 5.11: Equivalent Stress for 15% Carbon

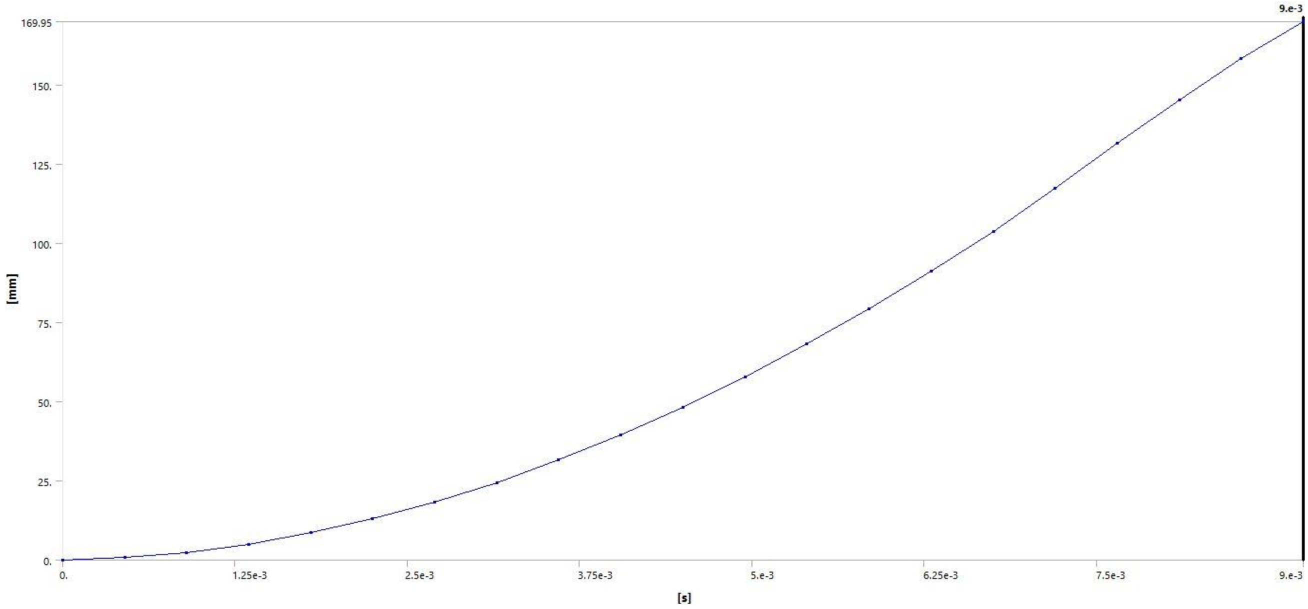

Figure 5.12: The total Deformation of 15% Carbon

5.6.2. Acceleration and Internal Energy Simulation Results

The material has a significant quantity of stored energy within its structure, as evidenced by its internal energy of 28,910 J. If the right circumstances are met, this energy can be released or changed. The material also undergoes a directional acceleration of -7352 mm/s^2, which denotes a change in velocity or a deceleration in the designated direction. Understanding the material's dynamic nature and how it reacts to outside forces is possible thanks to this acceleration value.

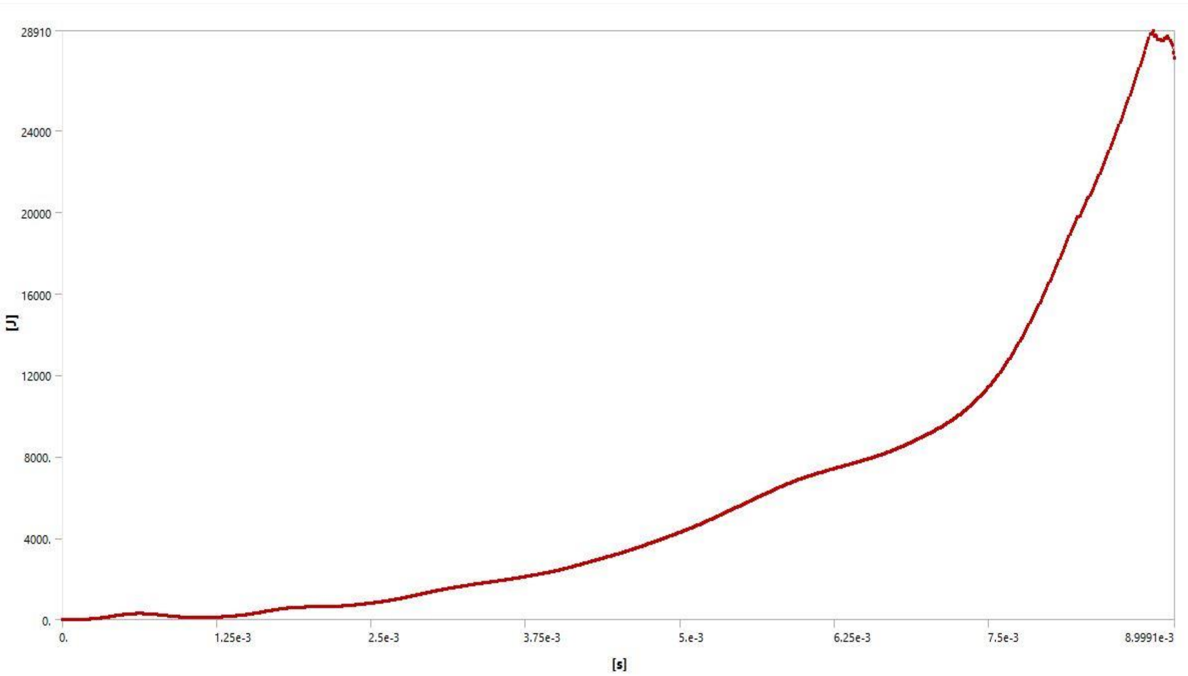

Figure 5.13: Internal Energy of 15% Carbon Percentage

5.6.3. Simulation Result for Weight Change

If the hybrid material's carbon content is set at 15%, the total weight stays at 1.4193 kg. This implies that the weight of the hybrid material is not greatly affected by the carbon concentration. It's crucial to remember, though, that a material's mass and the gravitational force acting on it are what ultimately define how much weight it has. Its weight may be more significantly influenced by other variables, such as the hybrid material's density and precise composition.

5.7. Simulation Results of a Hybrid Composite With 5% Carbon

The percentage of carbon is varied to 5% while keeping the S-Glass percentage complimentary to maintain the remaining overall percentage of 60% fiber content $f_f(0.03_c+0.57_s)+m_f(0.4)=1$.

5.7.1. Evaluation of the equivalent stress, strain, and total deformation.

The material shows noteworthy properties under applied stress when the carbon content is fixed at 5%. When the equivalent stress exceeds 34393 MPa, it indicates the internal forces that the material is subjected to. The strain of 1495.348, which goes along with this stress, illustrates how much the material has deformed and how it reacts to applied forces. The overall deformation, which is measured at 598.25 mm, shows how the combined effects of stress and strain have caused the material to change in size or shape overall. By highlighting the material's strength, deformation capacity, and potential uses in a range of engineering domains, these metrics taken together provide insight into the behavior and attributes of the material at the designated carbon content.

Figure 5.14: 5% Carbon Equivalent Stress

5.7.2. Internal Energy and Acceleration Simulation Results

The material displays particular properties concerning its directional acceleration and internal energy at a fixed carbon percentage of 5%. The quantity of stored energy within the structure of the material is represented by the internal energy, which has a measurement of 28966 J. Under the right circumstances, this energy can be changed or released. Concurrently, the material undergoes a directional acceleration of -7790 mm/s^2, signifying a change in velocity or deceleration in the designated direction. This acceleration number sheds light on the material's dynamic nature and how it reacts to outside influences.

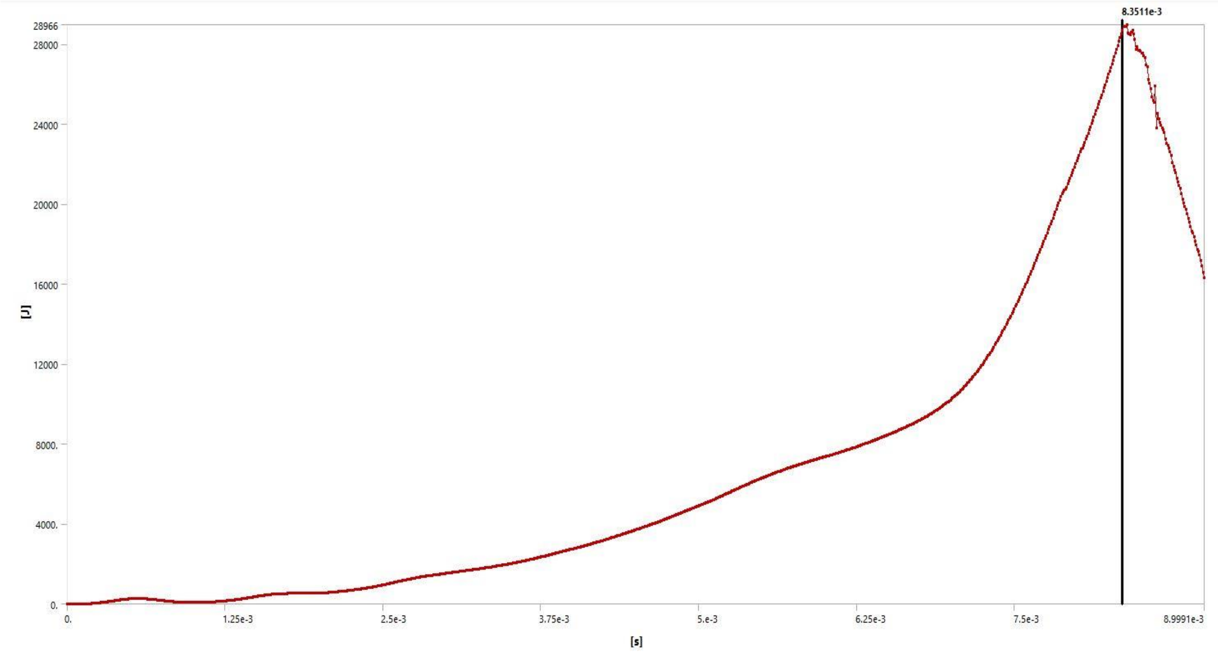

Figure 5.15: Internal Energy for 5% Carbon

5.7.3. Result for Simulation of Weight Change

The weight of the hybrid material rises to 1.4418 kg when the carbon proportion is fixed at 5%. This implies that the weight of the hybrid material is influenced by its carbon concentration. The gravitational force acting on an object and its mass are the main factors determining its weight. As a result, the increased weight suggests that the hybrid material's overall mass is influenced by the carbon addition. The hybrid material's weight is crucial to take into account for a number of reasons, including figuring out how stable it is, figuring out the forces at play in mechanical systems, and forecasting how it will behave in various gravitational settings.

5.8. Optimization using Grey Relational Analysis

The above-mentioned finite element results were optimized and compared using the Grey Relational Analysis technique, and the best performing percentage was chosen.

An extensive description of the precise numerical representations utilized in the analysis may be found in the document's appendix. The analysis's final conclusion has been gathered and provided in a thorough table for quick reference. The table offers a brief overview of the data, making it easy for readers to access and understand the conclusions drawn from the numerical representations. The outcomes of the whole simulation results are represented by the Grey Relational Coefficients in the following table, along with their ranked order.

Table 5.1: Grey Relational Coefficient and Result for carbon percentage

Concept	**Grey Relation Coefficient**					
	Von-Mise Stress	**Deformation**	**Internal Energy**	**Weight**	**Cost**	**Acceleration**
Steel 1006	0.832	1.000	0.500	0.500	1.000	0.500
C5	0.736	0.953	1.000	0.986	0.851	1.000
C15	0.500	0.930	0.998	0.990	0.785	0.952
C25	0.612	0.982	0.873	0.994	0.639	0.910
C30	0.701	0.966	0.798	0.996	0.584	0.751
C35	0.995	0.500	0.715	0.998	0.539	0.698
C40	1.000	0.500	0.713	1.000	0.500	0.697

R- Grade	**Rank**	**Concepts**
0.7220	**7**	Steel 1006
0.9210	**1**	**C5**
0.8591	**2**	**C15**
0.8350	**3**	**C25**
0.7993	**4**	**C30**
0.7409	**5**	**C35**
0.7351	**6**	**C40**

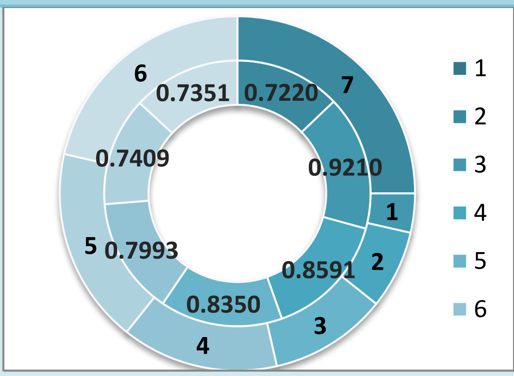

5.9. Justification on Varied Percentage Carbon Fiber Results

The original steel bumper beam's benchmark characterization serves as a standard by which the new composite materials can be measured. As a starting point for evaluating improvements, these initial parameters for stress, deformation, internal energy, weight, and acceleration are used.

The study's main emphasis is on adjusting the carbon content of the composite material. It is obvious that various characteristics alter as the amount of carbon fiber increases. In particular, equivalent stress declines, deformation grows, internal energy decreases, weight reduces, and acceleration exhibits an upward trend. The Grey Relational Analysis method's choice of the ideal carbon fiber content (5%) recommends that, based on the selected evaluation criteria, this composition is the best appropriate for the application. The findings demonstrate the intricate relationship between the carbon content and the mechanical characteristics of the composite material. These results highlight the significance of material engineering and design optimization, especially for bumper beam applications where structural integrity and energy absorption are crucial.

This research offers insightful information about the connection between carbon content and the effectiveness of composite materials used in bumper beams. The progress of car safety and design may effect from these results. The information gained in the investigation may have applications for the safety and design of automobiles. It provides information on how modifications to composite composition can impact bumper beam performance, possibly resulting in enhancements to vehicle safety and crash energy management. Complex and non-linear mechanical behavior can be seen in composite materials, especially those with different proportions of components like carbon fiber, S-glass fiber, and epoxy resin. Changing the mix, even slightly, can produce very diverse material reactions. In this instance, the change from 30% to 35% carbon fiber may be accompanied by a material behavior change that significantly alters performance.

It's possible that a smaller percentage of carbon fiber (5%) offered the best feasible mix of attributes for the particular performance standards and needs of the application. This material may be the best option because it strikes the ideal combination between stiffness, strength, and energy absorption. Compound mechanical behavior is frequently seen in composite materials. The unique synergy between the components of the 5% carbon composition (carbon, S-Glass, epoxy) may have produced improved performance. There are situations when the interactions between materials have unpredicted benefit.

In conclusion, the 5% carbon composition was ranked first since it outperformed others when compared to the criteria and study objectives. It emphasizes the complexity of the behavior of composite materials and the significance of taking particular application needs into account when selecting an ideal composition.

5.10. Simulation Results for Fiber Alignment of Various Angle

To determine the optimal fiber alignment for the best-performing carbon composite with 5% carbon fiber content, a number of tests are being conducted. The following two kinds of fiber alignments are being evaluated: **multi-directional** (45^0, 0^0, 45^0, 0^0, 45^0), (0^0, 90^0, 0^0, 90^0, 0^0), (-45^0, 45^0, -45^0, 45^0, -45^0), (-45^0, 45^0, 0^0, -45^0, 45^0) of four different laminae, with a distinct fiber alignment on each lamina and **unidirectional**, where all the lamina have the same fiber alignment but differ in angle by (0^0), (22.5^0), (45^0), (67.5^0) and (90^0). These tests focus on the mechanical properties of the composite rather than the inter-laminar interaction that typically influences overall performance. The goal is to understand how different alignment patterns affect the composite's mechanical properties while taking fiber alignment into account. In order to improve the mechanical performance of carbon composites with optimal carbon content, this work aims to identify the perfect fiber alignment.

The fiber alignment with the angle Zero was simulated again with other alignment angles because the end time taken to simulate the previous scenario has failed in the subsequent case, so the end time is then fixed to **0.0075sec**. The simulation taken for assessing various carbon percentages was endorsed by the default fiber alignment degree, i.e. zero.

5.10.1. Justification of Results for Fiber Alignment of Various Angle

The tested and simulated findings of fiber alignment in unidirectional laminate and multidirectional laminae configurations with varied ply angles and chosen carbon fiber percentages have, in conclusion, given important insights. According to the investigation, the performance of the 0-degree ply alignment was the best among the unidirectional laminate configurations. According to this conclusion, the highest strength and stiffness characteristics are produced when the fibers are aligned parallel to the direction of stress.

Additionally, in the unidirectional laminate configurations, the 22.5-degree ply alignment for each placed second, demonstrating its advantageous mechanical qualities. A balance between the advantages of unidirectional alignment and the capacity to disperse loads in numerous directions is provided by this angle.

Performance-wise, the multidirectional design with ply angles of (0, 90, 0, 90, 0) came in third. This arrangement improves load distribution along several axes by combining the benefits of unidirectional and multidirectional alignment. It's important to note that the simulations employed a specific carbon content of 5%. The mechanical characteristics of the laminate are considerably influenced by this %, and the findings are particular to this carbon fraction.

The relevance of fiber alignment in determining the mechanical performance of laminates is often highlighted by these findings. The study's findings can be a useful guide when building composite structures with the best fiber orientations possible to improve their performance in a variety of applications.

The mechanical properties of composite materials and the unique traits connected to each ply angle and configuration can be used to explain the ranking of the fiber alignment configurations. The possible causes of the observed ranking are broken down as follows:

1. **0^0 Ply Fiber Alignment (Unidirectional):** The alignment of fibers parallel to the loading direction gave the **0**-degree ply alignment the top ranking. With this design, the principal direction's load-bearing capacity is maximized, leading to greater strength and stiffness attributes. The laminate's weak areas are kept to a minimum thanks to the unidirectional alignment's effective stress transfer.
2. **The 22.5^0 ply Alignment (unidirectional):** came in second place, demonstrating its advantageous mechanical characteristics. This angle helps disperse the load in numerous directions, improving resistance to shear pressures and possibly strengthening the structural integrity overall, even if it is not aligned perfectly with the loading direction.
3. **(0, 90, 0, 90, 0) Ply Alignment (Multidirectional):** The multidirectional configuration with (0, 90, 0, 90, 0) ply angles placed third, indicating its beneficial qualities. Load distribution along many axes is made possible by this system, which blends unidirectional and multidirectional alignments. It strikes a balance between strength and agility by carefully arranging 0-degree and 90-degree plies.

The particular carbon percentage employed in the simulations may potentially have an impact on the observed ranking. The qualities of a material, such as strength, stiffness, and fracture toughness, can vary depending on the carbon content. Consequently, choosing a 5% carbon proportion may have contributed to the ranking that was found.

Table 5.2: Grey Relational Coefficient Result for Fiber Alignment

Fiber Orientation		Von-Mise Stress	Deformation	Internal Energy	Acceleration
		Grey Relation Coefficient			
Unidirectional	0^0	0.82540	0.50000	1.00000	0.97207
	22.5^0	0.72356	0.50384	0.97942	1.00000
	45^0	0.63225	0.55606	0.81078	0.82739
	67.5^0	0.50000	0.73093	0.62558	0.50000
	90^0	0.53074	1.00000	0.50000	0.55400
Multidirectional (for each lamina)	$45^0, 0^0, 45^0, 0^0, 45^0$	0.64265	0.54505	0.80958	0.87966
	$0^0, 90^0, 0^0, 90^0, 0^0$	1.00000	0.55971	0.78420	0.78015
	$(-45^0, 45^0, -45^0, 45^0, -45^0)$	0.77574	0.57383	0.76409	0.79027
	$(-45^0, 45^0, 0^0, -45^0, 45^0)$	0.74239	0.58106	0.72816	0.85597
		LB	LB	HB	LB

R- Grade	Rank	Fiber Orient.
0.8244	**1**	**0^0**
0.8017	**2**	**22.5^0**
0.7066	**7**	**45^0**
0.5891	**9**	**67.5^0**
0.6462	**8**	**90^0**
0.7192	**6**	**$45^0, 0^0, 45^0, 0^0, 45^0$**
0.7810	**3**	**$0^0, 90^0, 0^0, 90^0, 0^0$**
0.7260	**5**	**$-45^0, 45^0, -45^0, 45^0, -45^0$**
0.7269	**4**	**$-45^0, 45^0, 0^0, -45^0, 45^0$**

5.11. Validation of Results for Bumper Beam

The goal of a previous study on that particular vehicle type by (Abuye and Habtamu, published on International Journal of Scientific & Engineering Research) is to create a beam bumper that improves the bumper's crashworthiness and consequently increases vehicle safety. The research aims to study the impact behavior of an epoxy composite vehicle bumper beam reinforced with s-glass fibers and composed of 60% fiber and 40% matrix in volume. Significant improvements in collision performance are anticipated by substituting composite bumper beams for the present Lifan 520 model bumper beams. It is interesting to note that the internal energy absorption of composite materials is 38.7% higher than that of steel; whereas steel absorbs energy at a pace of 1200.9 J, the internal energy absorption of composite materials occurs at a rate of 1960 J. The LS-DYNA program is used for analysis in order to calculate the overall deformation and internal energy absorbed by the materials, leading to an optimal design for the new automobile bumper. The goal of this project is to develop a beam bumper that dramatically increases crashworthiness and raises vehicle safety using cutting-edge composite materials and sophisticated analysis methodologies. The next table shows the results of the previously and recently produced materials.

Table 5.3: Validation of the Optimized Material

	Previously Developed Composite	**Newly Optimized Composite**
Internal Energy	1980 **J**	28,966 **J**
Weight	-	1.4418 **Kg**
Equivalent Stress	213.76 **MPa**	34,393 **MPa**
Deformation	1.84 **mm**	598.25 **mm**

The results obtained from the measurements of the previously developed material indicate internal energy absorption of 1980 J, an equivalent stress of 213.76 MPa, and a deformation of 1.84 mm. These values demonstrate certain capabilities of the material in terms of energy absorption and deformation under impact conditions. However, the newly developed material showcases significant advancements in performance. It exhibits impressive internal energy absorption of 28,966 J, an equivalent stress of 34,393 MPa, and a deformation of 598.25 mm.

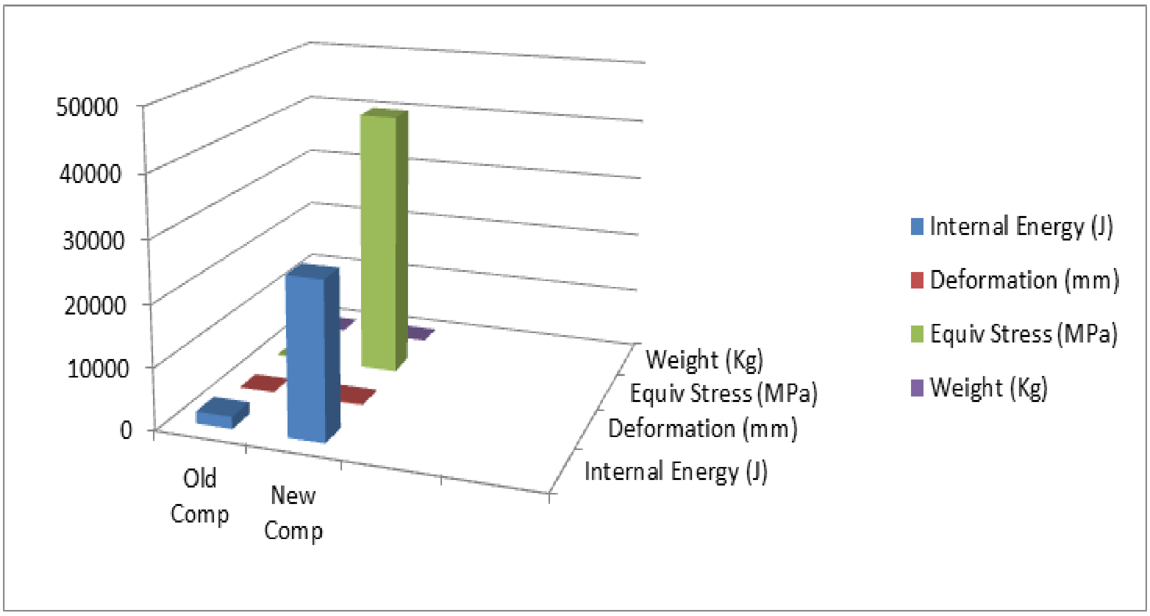

Figure 5.16 Parametric Validation

These results highlight the substantial enhancement achieved in energy absorption and deformation capabilities compared to the previous material. Additionally, the weight of the newly developed material is measured at 1.4418 Kg, which is an important consideration for practical applications where weight reduction is desired. The newly discovered material's better characteristics point to its potential for superior crashworthiness and increased safety in a variety of automotive applications.

CONCLUSIONS AND RECOMMENDATIONS

6.1. Summary

The Thesis focuses on the design optimization of a bumper beam for the Lifan 520, transitioning from its original steel composition to a hybrid material comprising Carbon-S-Glass fiber Epoxy Resin. Utilizing unidirectional fiber arrangement in laminates, the study maintains a total fiber-matrix ratio of 60% fiber and 40% matrix. The optimization strategy involved varying the percentage of carbon fiber while adjusting the S-Glass content to maintain the 60% total fiber target. Four different carbon percentages 5%, 15%, 25%, 30%, 35%, and 40%, were evaluated against parameters including internal energy, deformation, equivalent stress, and directional acceleration. The Greys Relational Analysis Technique facilitated the optimization process, with the 5% carbon composition emerging as the top performer. Further investigations considered the impact of fiber orientation by rearranging laminates in both unidirectional and multidirectional configurations, disregarding interlaminar interactions. Notably, a unidirectional alignment at 0 degrees secured the top position, followed by 22.5 degrees, while a multidirectional arrangement (0, 90, 0, 90, 0) degrees claimed the third spot. Additional comparisons encompassed a range of angles for unidirectional laminates (0, 22.5, 45, 67.5, and 90 degrees) and various multidirectional combinations (-45, 45, 0,-45, 45), (45, -45, 45, -45, 45), and (45, 0, 45, 0, 45). By rearranging laminates in unidirectional and multidirectional topologies while ignoring interlaminar interactions, subsequent studies examined the effect of fiber orientation. Additional comparisons included a variety of multidirectional combinations (-45, 45, 0, -45, 45), as well as a range of angles for unidirectional laminates (0, 22.5, 45, 67.5, 90) degree.

6.2. Conclusion

A detailed analysis of this MSc Thesis reveals important advancements in the bumper beam design of the Lifan 520. A hybrid composite made of Carbon-S-Glass fiber and epoxy resin is used in place of steel, significantly improving the material's properties and performance potential. The careful optimization procedure carried out using the Greys Relational Analysis Technique emphasizes the crucial part that material composition plays in getting the best outcomes. Notably, the composition with 5% carbon emerges as the best option, exhibiting remarkable qualities in a variety of criteria. Additionally, the investigation of various fiber orientations both unidirectional and multidirectional produces insightful information about the complex interaction between material configuration and performance results. The results offer vital pointers for advancing composite materials in the future and using them in automobile safety engineering.

A significant development in composite material science is presented by this thorough analysis, particularly in relation to bumper beam design. In terms of structural effectiveness and crash performance, the switch from conventional steel to a hybrid composite material marks a considerable advancement. Greys Relational Analysis Technique-guided thorough optimization concluded in the selection of the 5% carbon composition, proving its unquestionable fit for the specified use. Furthermore, a careful examination of various fiber orientations, including both unidirectional and multidirectional configurations, provides insightful information on how differently they affect material behavior. These findings contribute to our understanding of composite materials and have consequences for how automobile safety engineering will develop going forward. Future advancements in material choice and design optimization within the automotive sector will be built on the findings of this research.

6.3. Recommendations

- It is recommended to take into account a computer with increased processing speed and higher capacity to achieve improved mesh quality and shorter processing times. The effectiveness and efficiency of mesh production can be greatly improved by using a computer system with more processing capability. This update would speed up simulations and analysis by producing meshes of greater quality and reducing processing times.
- It is advised to take the beam bumper's impact at its top speed into account, and more investigation is required to determine how well the beam bumper absorbs energy in collisions involving various load configurations and loading positions. A fuller knowledge of the bumper's capacity to absorb energy and lessen the impact of crashes can be obtained by looking into these elements.
- It is indicated that employing fiber alignment with (0, 90, 0, 90, 0) degree would be advantageous if the manufacturing process is not time-consuming, expensive, and complex.

6.4. Future Work

- It would be beneficial to carry out future studies that concentrate on systematically altering the proportion of carbon content below a particular threshold, i.e. 5%, in order to create a more optimum carbon range. This strategy would involve running simulations with varying carbon content percentages below the threshold and analyzing the effects on various aspects of interest.
- Another future work would be focus on the interlaminar interaction between laminae. The goal can be to comprehend the dynamic interactions and bonding processes that occur at the interfaces between neighboring layers of composite materials. We can better understand stress transmission mechanisms and improve the design and production of composites by studying interlaminar interaction.

REFERENCES

Infinitihelp website. (2016). Retrieved from http://infinitihelp.com/diy/gcoupe/projects/images/infi.

Principle of Corrosion Engineering and Corrosion control. (2006).

581-01.pdf, James Jones. (2023).

AlecuA. (2014). Mechanics Course. Politehnica University of Bucharest: Bucharest.

Andersson R, S. E. (2002). The Applicability of Stainless Steel for Crash Absorbing Components. SAE Technical Paper.

Ashenafi Abuye, H. M. (2017). Automobile Bumper Beam Analysis to Improve Energy Absorption. International Journal of Scientific & Engineering Research.

ASTM. (2021). "Standard Specification for Glass Fiber strands". Annual Book of ASTM standards, D 578-98.

B.I. Yakobson, M. C. (1997). Computational Materials Science 8, 341.

Berrahou Mohamed, A. K. (2022). Effect of fiber orientation of the different types of composite plates notched of U-Shaped repaired by composite patch. Materials Research.

Butler M, W. J. (2002). Using Terocore Brand Structural Foam to Improve Bumper Beam Design. SAE Technical Paper.

C.Y. Li, T. C. (2003). Composites Science and Technology, Elsevier.

C.Y. Li, T. C. (2004). Mechanics Of Materials, Elsevier.

Chamis, C. C. (2021). Haybrid Composites - State of the art review; Analysis, Design, Application and Fabrication,. NASA Technical Memorandum, NASA TM.

Chou, T. W. (2010). Mechanical Behaviour of Hybrid Composite . American Society of Mechanical Engineers.

Chou, T. W. K. (2010). Mechanical Properties of Composites. Annu. Rev. Mater. Sci.,, 10:229-59.

Composite Materials Handbook (CMH-17), R. G. (2019).

Courtesy of Zweben. (2011).

Deac S C, P. A. (2017). Modeling and simulation of cars. International Conference on Applied Sciences, IOP Conference Series.

Donaldson, D. B. (2001). ASM Handbook, Vol 21: Composites . asminternational.

Dr.Shivanand N. Pujar, D. K. (2022). Effect of Fibre Volume Fraction and Fibre Reinforcement Orientation (Various Layup Sequence) on Mechanical Properties of Epoxy-based E-Glass fibre Reinforced Bio-material Used as Implant (Human Bone -Tibia) - Finite Element Method. International Journal of Creative Research Thoughts SSN: 2320-2882.

Du Bois P, C. C. (2004). Vehicle Crashworthiness and Occupant Protection . 2000 Town Center Southfield, Michigan: American Iron and Steel Institute .

Du Bois, P. (December 2001). 'Crashworthiness Engineering With LS-DYNA,' In FEA Information International News for the World-Wide Engineering Community,.

E. Hernandez, C. Goze, P. Bernier, and A. Rubio (18 May 1998). Physical Review Letters. American Physical Society 80, 4502.

E.C.E.(United Nation). (20 March 1958). Uniform Provisions concerning the approval of vehicles with regard to their front and rear protective devices. Regulation No. 42., Geneva.

Ed., F. W. (New York 2010). Fiberglass and Glass Technology, Journal of Environmental Protection, Springer.

Engineering fundamentals page on high-carbon steel. (June, 2016).

Engineering fundamentals page on medium-carbon steel. (Aug, 2016).

Ever Barbero. (2011). Introduction to Composite Materials Design. Boka Raton London New York: CRC Press Tyler and Francis Group.

Feraboli, P. (2009). Development of a Modified Flat Plate Test and Fixture Specimen for Composite Materials Crush Energy Absorption. (Vol. 43, No. 19, 2009, pp. 1967–1990).

George C. Jacob, J. F. (2004). Crashworthiness of automotive composite material systems.

Gergely C, S. P. (2015). Demonstration of pseudo ductility in unidirectional discontinuous carbon fibre/epoxy prepreg composites. Compos Sci Technol., 106:110-9. http://dx.doi.org/10.1016/j.compscitech.2014.10.022.

Gergely Czel, M. J. (2015). Demonstration of pseudo-ductility in unidirectional hybrid composites made of discontinuous carbon/epoxy and continuous glass/epoxy plies. Elsevior, Composites Part A (72) 75-84.

Gibson, R. F. (1994). Principles of Composite Material Mechanics, Third Edition.

Gigante, M. (2022, Nov 30). Finite Element Analysis: What and How does it Work.

Gupta, P. (1988). Glass Fibers for Composite Materials, Fiber Reinforcements for composite materials. A.R. Bunsell, Ed., Elsevier Publishers, 19-72.

Heinz Heisler. (2002). 'Advanced Vehicle Technology', 2nd Ed. Butterworth Heinemann.

Hosseinzadeh R.M, S. M. (68(2005)). Parametric study of automotive composite bumper beams subjected to low-velocity impacts J. Composite Stuct. Elseviour, 419-427.

Hsin-HungWu. (2002). A Comparative Study of Using Grey Relational Analysis in Multiple . Quality Engineering, 15(2):209-217.

Idicula, M. (2006). Thermophysical Properties of natural fiber reinforced polyester composites. ResearchGate.

IlieS. (2012). Modeling the impact phenomena of vehicles,. Bucharest: Publishing house AGIR.

J.N.Reddy. (2004). Mechanics of laminated composite plates and shell and shell theory and analysis, Second edition.

JFA Madeira, V. I. (2019). Characterization and optimization of hybrid carbon–glass epoxy composites under combined loading,. Journal of Composite Materials, Vol. 53(18) 2593–2605.

Jones, R. M. (1999). Mechanics of Composite Materials, Second Edition . Blacksburg, Virginia 24061-0219.

K.L. Loewenstein, B. P. (1993 3rd Edition). The Manufacturing Technology of Continous Glass Fibers. Tokyo: Elsevior.

Katkar A.D., D. B. (2015). Bumper Design Enhancement through Crash Analysis. Kolhapur, India.

Kaw, A. K. (2006). ‘Composite Materials’ second edition.

Kuo Y, Y. T. (2008). The use of grey relational analysis in solving multiple attribute. . Computers & Industrial Engineering, 55(1):80-93.

LChung., D. D. (2010). Composite Materials: Science and Applicatios. State University of New York, Buffalo: Springer.

Li CY, C. T. (2004). Elastic properties of single-walled carbon nanotubes in transverse directions. International Journal of Solids and Structures, 40 2487.

Loughlana J, A. M. (2008). Multi-cell carbon fibre composite box beams subjected to torsion with variable twist. In Thin Wall Structure (pp. 46: 914–924).

Lowenstein, K. (Amsterdam (1983)). The manufacturing technology of continuous glass fibers. Elsevier.

Min. Feng Yu, Bradley S. A. (2000). Physical Review Letters, Volume 84, 5552 (June 2000). Johnson Space Center.

M.M. Davoodi, S. S. (11 April 2012). Development process of new bumper beam for passenger car. Elsevier Ltd.

MalenD. (2011). Fundamentals of Automobile Body Structure Design. SAE International USA.

Mallick, P. (2007). Fiber reinforced composites: Materials, Manufacturing, and Design. CRC Press, third edition.

Mallick, P. K. (2007 Third Edition). Fiber Reinforced Composite Materials, Manufacturing, and Design. Dearborn, Michigan: Taylor & Francis Group.

Marzbanrad JM, A. M. (2009). Design and analysis of automotive bumper beam in low speed frontal crashes. Elseviour, 902- 911.

Masoumi A, M. H. (2011). Comparison of steel, aluminium and Composite bonnet in terms of pedestrian head impact. Tehran, Iran: College of Engineering, University Of Tehran.

Md Abdul Maleque, M. S. (2013). Materials Selection and Design.

Mehmet Bulut, M. A. (2 February 2018). A comparative study on the tensile and impact properties of Kevlar, carbon, and S-glass/epoxy composites reinforced with SiC particles, IOP Science Mater. Res., DOI 10.1088/2053-1591/a991.

Michael Heine, T. H. (January 2008). Carbon Fibers . ResearchGate.

Mohamad Fotouhi, P. S. (July 2016). Detection of fibre fracture and ply fragmentation in thin-ply UD carbon/glass hybrid laminates using acoustic emission,. Science Direct, Volume 86, Pages 66-76.

Mohammad Irshad Ali and J. Anjaneyul. (2018). Effect of fiber-matrix volume fraction and fiber orientation on the design of composite suspension system. IOP Conf. Ser.: Mater. Sci. Eng., 455,012104.

Mohapatra, S. (2005). Rapid Design Solutions for Automotive Bumper Energy Absorbers using Morphing Technique. Bangalore, India. Altair CAE users Conference.

Morgan, T. E. (1999). Engineering Thermoplastic Energy for Bumpers. SAE Paper.

Mueller, D. H. (2003). Journal of Industrial Textiles Vol. 33, No.2.

N Kumar, P. A. (2020). Advances in Mechanical Engineering,. Select Proceedings of ICRIDME 2018, Springer.

Nishimura, N., & Murase, k. (2012). Ultrasonic detection of spall damage induced by low-velocity repeated impact. Central European Journal of Engineering 2, 650-655.

Nitin S. Gokhale, S. S. (2007). Practical Finite Element Analysis’. India: Finite to Infinite.

Classification of Carbon and Low-Alloy Steel. (Nov-2001). Total Material, the world's most comprehensive materials database.

Nukman Yusoff, S. M. (April 2010). Material selection of polymeric composite automotive bumper beam using Analytical hierarchy Process. Journal of Central South University of Technology, 244−256.

O. G. Lademo, T. B. (May 2019). A model for process-based crash simulation. Norwegian University of Science and Technology Trondheim Norway 2008: PP. 376–388.

Olagoke Olabisi. (Spring 2000). Emerging Nonmetallic Materials Technology in The Exploration. Saudi ARAMCO Journal of Technology.

P. Zhang, Y. H. (2002). International Journal of Solids and Structures, IJSS.

Pakkar M S. (2017). An Integrated Approach to Grey Relational Analysis, Analytic Hierarchy Process andData Envelopment Analysis, Social Science Electronic Publishing, 9(1):71-86.

Pascault JP, W. R. (2010). Epoxy Polymers: New Materials and Innovations. Wenheim: Wiley-VCH.

Prince M Patel, H. N. (2013). Properties of Carbon Fiber and its Application . International Journal of Engineering Research and Technology (IJERT), ISSN: 2278-0181.

Putu Suwarta, M. F. (20-25th August 2017). Fatigue Behaviour of Pseudo-Ductile Thin Ply Hybrid Composites. 21st International Conference on Composite Materials.

RadesM. (2008). Mechanical vibrations. Bucharest: Publishing House Printech.

Raiano, M. (2013, December 28). Retrieved May 18, 2023, from www.aerospacengineering.net.

Raiano, M. (2014, January 10). Retrieved May 19, 2023, from www.aerospacenginering.net.

Ramazan Karakuz, E. E. (2010). Damage Prediction in glass/epoxy laminates subjected to impact loading. Turkey.

Sapuan, S. M. (2004). A note on the conceptual design of polymeric composite automotive bumper system. J. Mater. Production Tech, Vol.159, pp.145-151.

Satish Pathy, J. D. (2022). LS-DYNA Analysis for Structural Mechanics. DYNAmore, Gmbh, Germany: ANSYS®, LS-DYNA® and LS-PrePost® are registered and protected trademarks of ANSYS.

Seo, S.-J. P.-K. (2011). Interface Science and Composites. Department of Chemistry, Inha University South Korea: Interface Science and Technology Volume 18.

Shi K. (2017). Research on the Network Information Security Evaluation Model and Algorithm Based on Grey Relational Clustering Analysis. Journal of Computational & Theoretical Nanoscience, 14(1):69-73.

Shindo, A. (Amesterdam 2000). Polyacrylonitrile (PAN)-based Carbon Fibers. Comprehensive Composite Materials Elsevier, Page 1.

Strong. (A B 2007). Fundamentals of composites manufacturing [M]. Michigan: Society of Manufacturing Engineers (SME).

Suddin M N, H. M. (2007). A prototype of KBS for material selection in bumper beam design (J). Suranaree Journal Science Technology, 14: 215−222.

Tejasagar Ambati, K. S. (2012). Simulation of vehicular frontal crash-test. 2231–5950, Volume-2, Issue-1.

Witteman, W. (2000). Improved Vehicle Crashworthiness Design by Control of the Energy Absorption for Different Collision Situations. Doctoral dissertation, Eindhoven University of Technology.

Yang W, H. Y. (2011). Fire and mechanical performance of nanoclay reinforced glass-fiber/PBT composites containing aluminum hypophosphite particles, IJARIIE JOURNAL, Composites Part A;42 (7):794-800.

YG TG, M. V. (2021). A new study on flax-basalt-carbon fiber reinforced epoxy/bioepoxy hybrid composites,. Wiley Online Library.

Yonggang, W. L. (2015, Vol. 7(6)). Design and analysis of automotive carbon fiber composite bumper beam based on finite element analysis. Creative Commons.

Zhang Jingwen, E. A. (2017). Light weight replacement and the optimization design of bumper beam based on crash safety,. Engineering. CAE.CN, Vol. 12 No. 5.

Zhou L, W. Y. (2017). A transformer fault diagnosis method based on grey relational analysis and integrated weight determination. Electrical Insulation.

Zhu, H. S. (2008). Evaluation of Failure Criteria for Fiber Composites using FE Micromechanics, . Journal of composite Materials, 8 vol 18.

APPENDICES

Appendix A: Grey Relational Coefficient of Steel and Varied Carbon Percentage

Table A.1. Simulation Results of Parameters

Concept	Normalized Data					
	Von-Mise Stress	**Deformation**	**Internal Energy**	**Weight**	**Cost**	**Acceleration**
Steel 1006	0.798	1.000	0.000	0.000	1.000	0.000
C5	0.641	0.951	1.000	0.986	0.825	1.000
C15	0.000	0.925	0.998	0.990	0.726	0.949
C25	0.367	0.981	0.854	0.994	0.435	0.901
C30	0.574	0.964	0.746	0.996	0.288	0.668
C35	0.995	0.001	0.602	0.998	0.143	0.568
C40	1.000	0.000	0.598	1.000	0.000	0.566

Table A.2. Normalized Data of Simulation Results

Concept	Delta					
	Von-Mise Stress	**Deformation**	**Internal Energy**	**Weight**	**Cost**	**Acceleration**
Steel 1006	0.202	0.000	1.000	1.000	0.000	1.000
C5	0.359	0.049	0.000	0.014	0.175	0.000
C15	1.000	0.075	0.002	0.010	0.274	0.051
C25	0.633	0.019	0.146	0.006	0.565	0.099
C30	0.426	0.036	0.254	0.004	0.712	0.332
C35	0.005	0.999	0.398	0.002	0.857	0.432
C40	0.000	1.000	0.402	0.000	1.000	0.434

Table A.3. Delta of Normalized Data

Concept	Grey Relation Coefficient					
	Von-Mise Stress	**Deformation**	**Internal Energy**	**Weight**	**Cost**	**Acceleration**
Steel 1006	0.832	1.000	0.500	0.500	1.000	0.500
C5	0.736	0.953	1.000	0.986	0.851	1.000
C15	0.500	0.930	0.998	0.990	0.785	0.952
C25	0.612	0.982	0.873	0.994	0.639	0.910
C30	0.701	0.966	0.798	0.996	0.584	0.751
C35	0.995	0.500	0.715	0.998	0.539	0.698
C40	1.000	0.500	0.713	1.000	0.500	0.697

Appendix B: Grey Relational Coefficient of Fiber Alignment

Table B.1 Simulated Fiber Orientation Data

	Simulated Result Data			
Fiber Orientation	**Von-Mise Stress (MPa)**	**Deformation (mm)**	**Internal Energy (J)**	**Acceleration (m/s^2)**
0	14120	209.64	100450	1.6200
22.5	14806	209.38	100070	1.5990
45	15609	206.2	96229	1.7515
67.5	17292	198.86	89625	2.3300
90	16826	192.58	82364	2.1875
45,0,45,0,45	15506	206.82	96196	1.6990
0,90,0,90,0	13269	206	95473	1.8050
(-45,45,-45,45,-45)	14432	205.25	94866	1.7930
(-45,45,0,-45,45)	14665	204.88	93698	1.7220
QA	LB	LB	HB	LB

Table B.2 Normalized Data for Fiber Alignment Simulation Result

	Normalized Data			
Fiber Orientation	**Von-Mise Stress**	**Deformation**	**Internal Energy**	**Acceleration**
0	0.788466319	0	1	0.971272230
22.5	0.617946806	0.015240328	0.978989273	1.000000000
45	0.418344519	0.201641266	0.766615061	0.791381669
67.5	0	0.631887456	0.401470751	0.000000000
90	0.115833955	1	0	0.194938440
45,0,45,0,45	0.443947303	0.165298945	0.764790446	0.863201094
0,90,0,90,0	1	0.213364596	0.724814774	0.718194254
(-45,45,-45,45,-45)	0.710912255	0.257327081	0.691252903	0.734610123
(-45,45,0,-45,45)	0.652995277	0.27901524	0.626672564	0.831737346

Table B.3 Delta of Normalized Data for Fiber Alignment

	Delta			
Fiber Orientation	**Von-Mise Stress**	**Deformation**	**Internal Energy**	**Acceleration**
0	0.2115337	1.0000000	0.0000000	0.0287277702
22.5	0.3820532	0.9847597	0.0210107	0.0000000000
45	0.5816555	0.7983587	0.2333849	0.2086183311
67.5	1.0000000	0.3681125	0.5985292	1.0000000000
90	0.8841660	0.0000000	1.0000000	0.8050615595
45,0,45,0,45	0.5560527	0.8347011	0.2352096	0.1367989056
0,90,0,90,0	0.0000000	0.7866354	0.2751852	0.2818057456
(-45,45,-45,45,-45)	0.2890877	0.7426729	0.3087471	0.2653898769
(-45,45,0,-45,45)	0.3470047	0.7209848	0.3733274	0.1682626539

Appendix C: Parametric Results for Simulation of Different Fiber Orientation (Uni and multi directional arrangement)

- **All the lamina were arranged 0^0**

1. Total Deformation

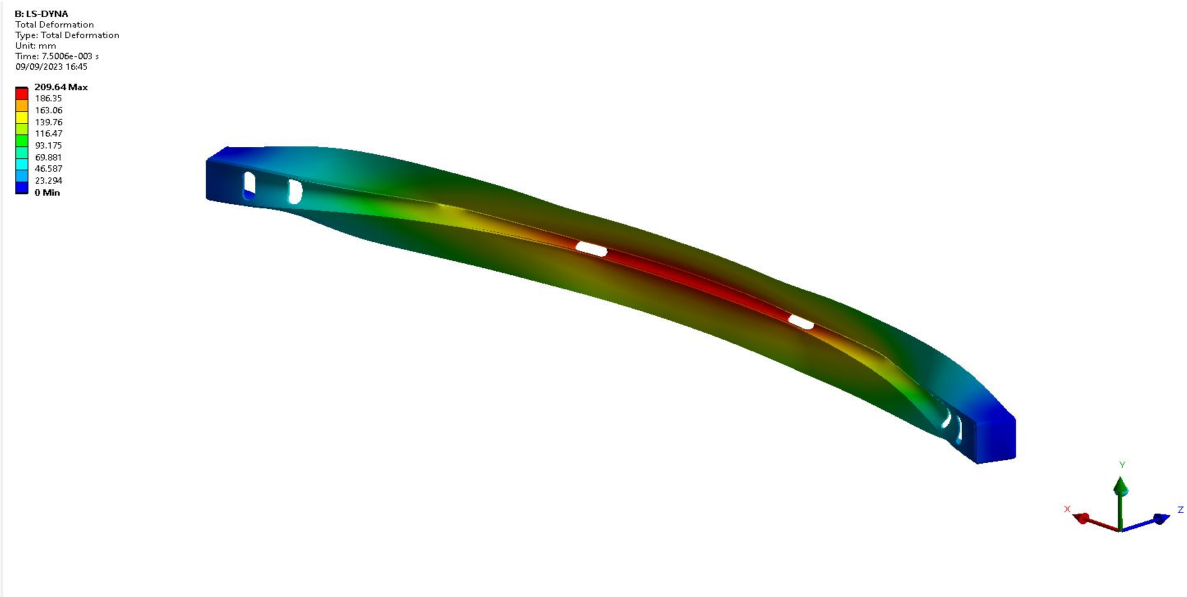

Figure C.1 Total Deformation for 0^0

2. Internal Energy

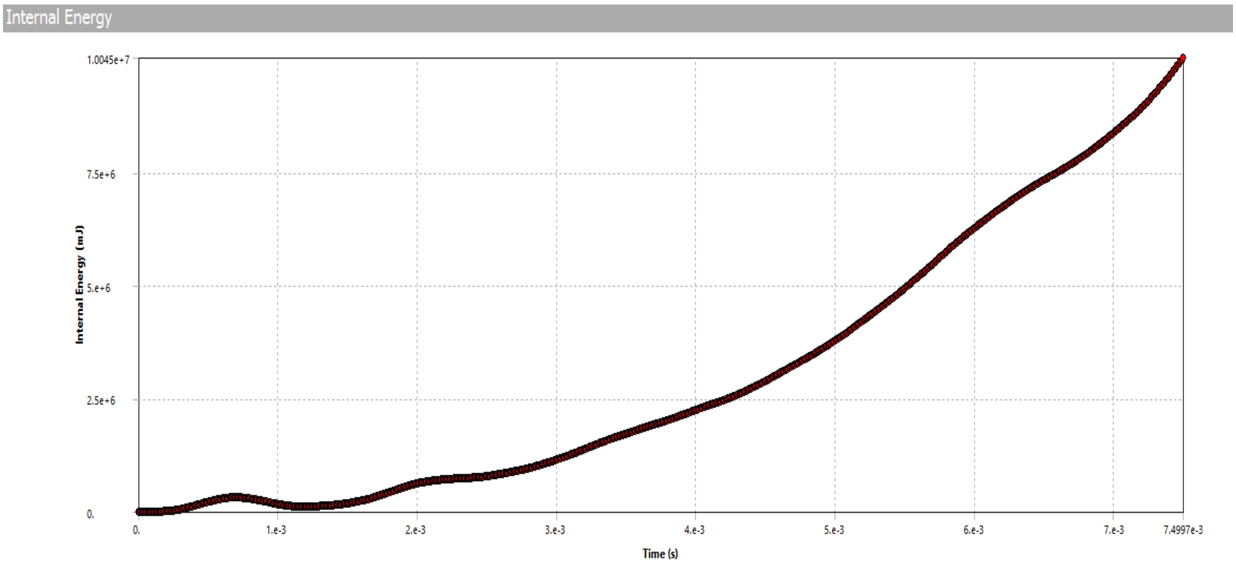

Figure C.2 Internal Energy for 0^0

3. Equivalent (von-Mises) Stress

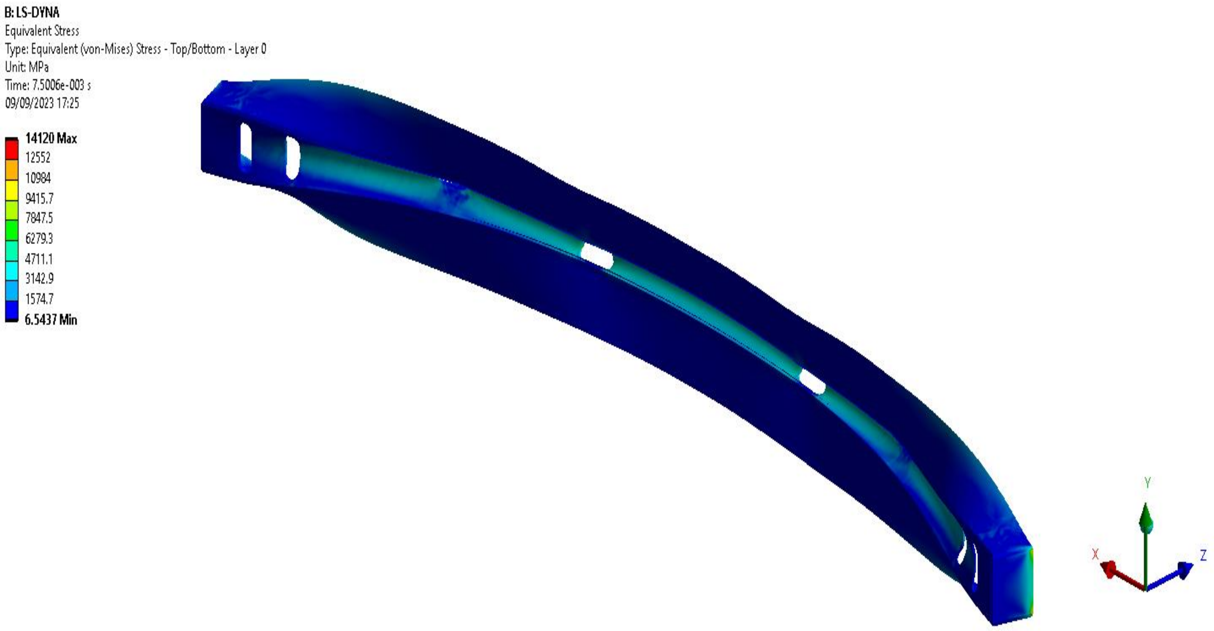

Figure C.3 Equivalent Stress for 0^0

4. Directional Acceleration

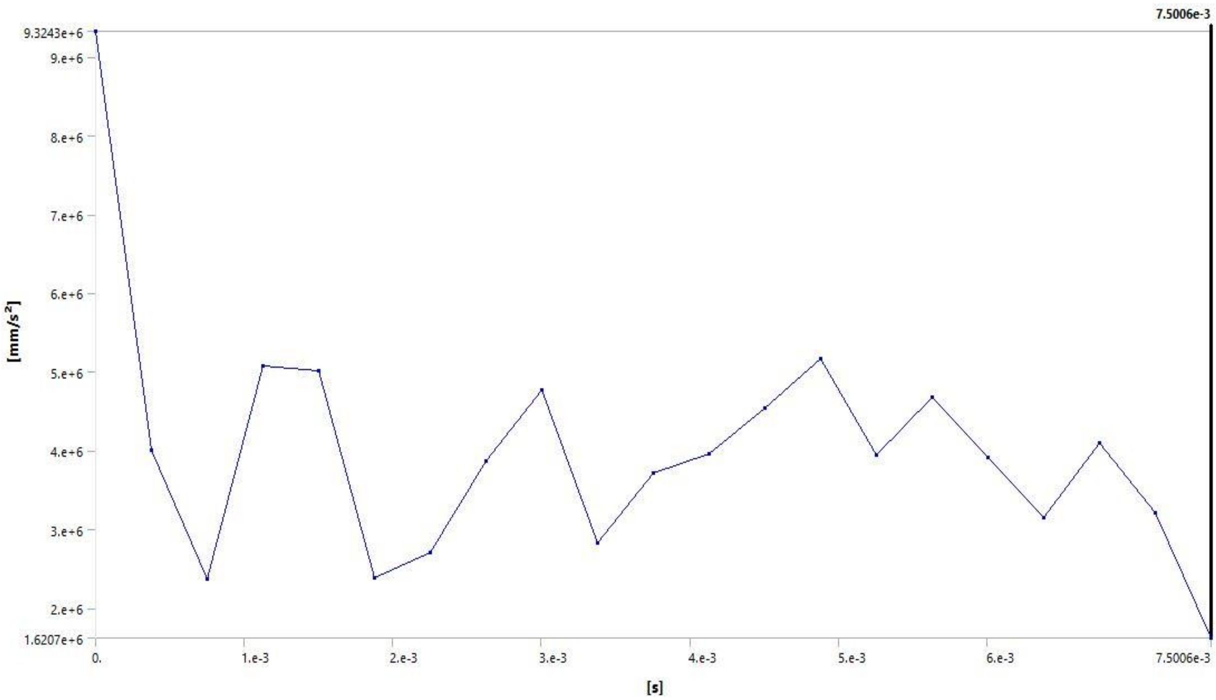

Figure C.4 Directional Acceleration for 0^0

- **All the lamina were arranged 22.5^0**

1. Total Deformation

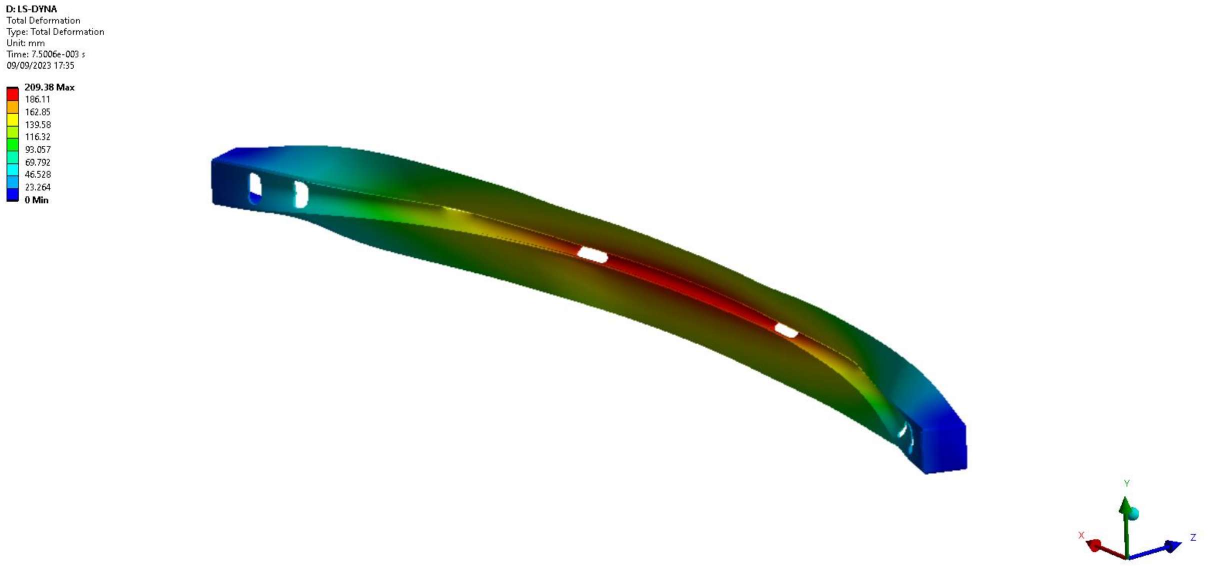

Figure C.5 Total Deformation for 22.5^0

2. Internal Energy

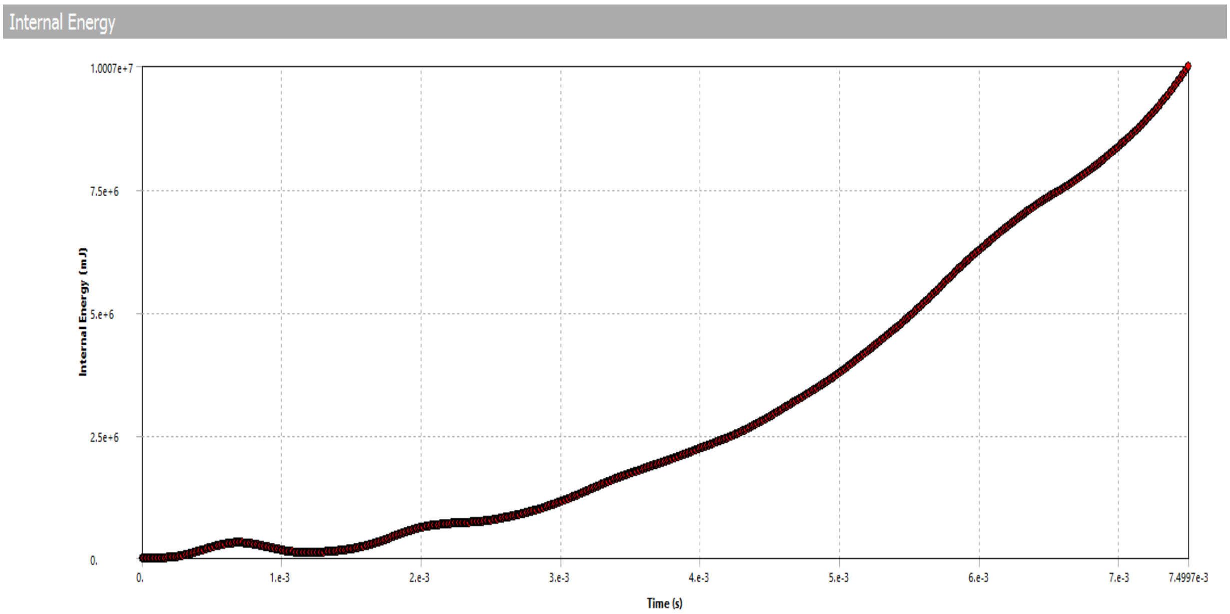

Figure C.6 Internal Energy for 22.5^0

3. Equivalent (von-Mises) Stress

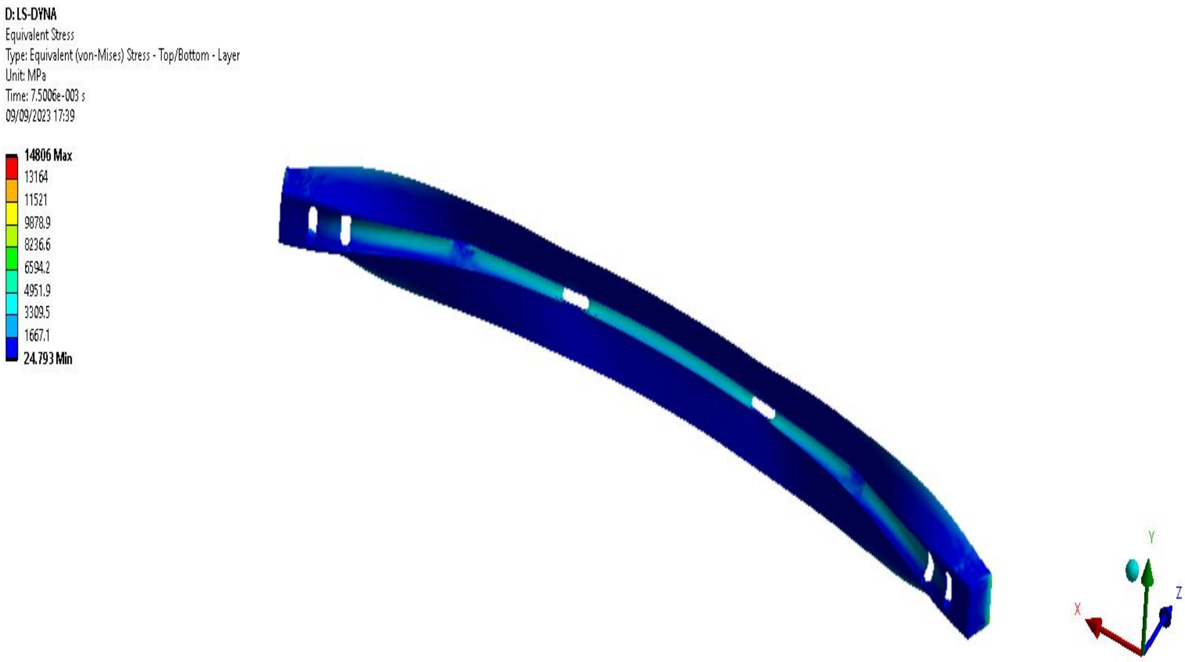

Figure C.7 Simulated result of Stress for 22.5^0

4. Directional Acceleration

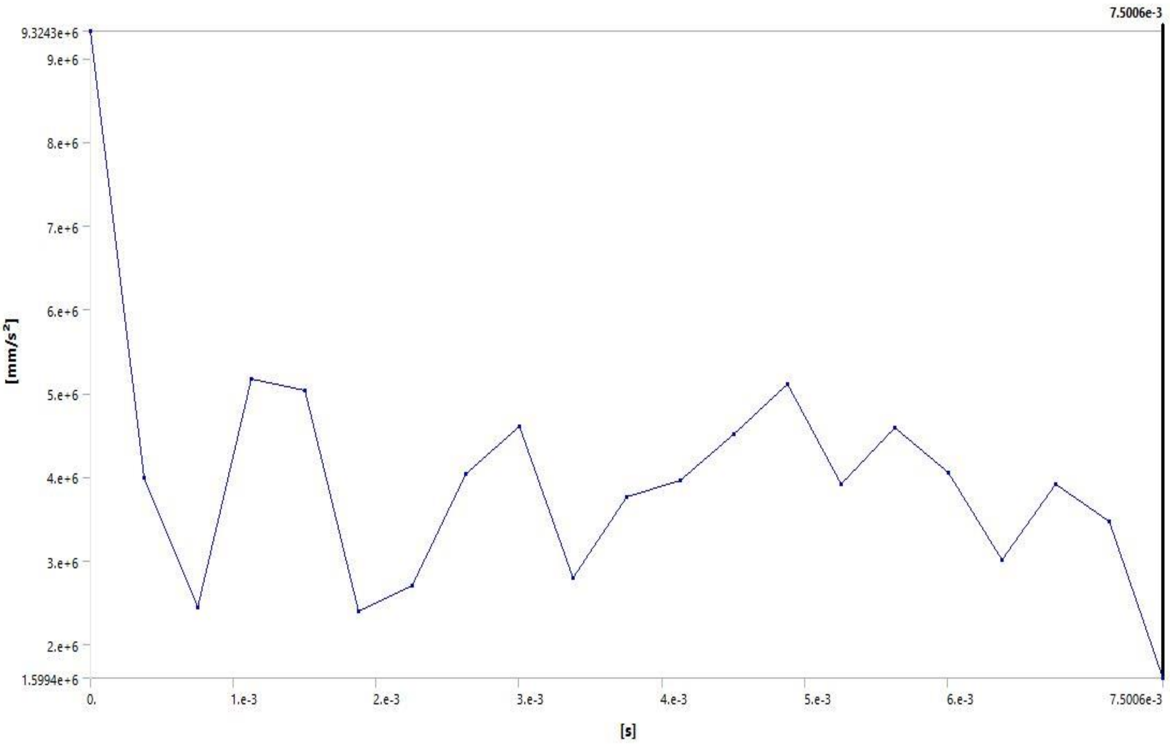

Figure C.8 Acceleration for 22.5^0

➢ All the lamina were arranged 45^0

1. Total Deformation

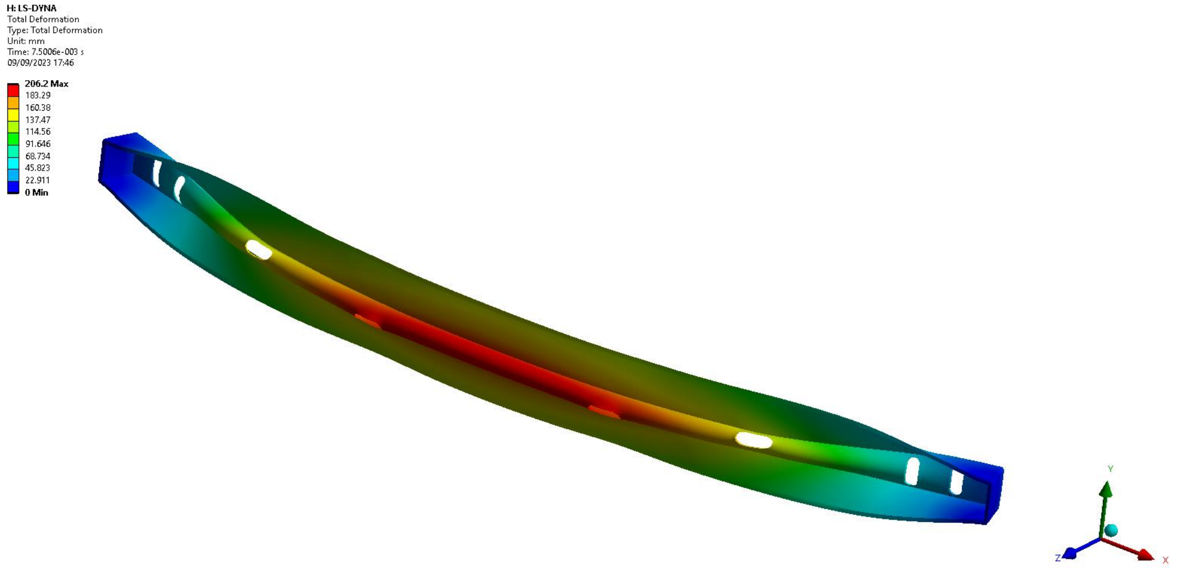

Figure C.9 Deformation for 45^0

2. Internal Energy

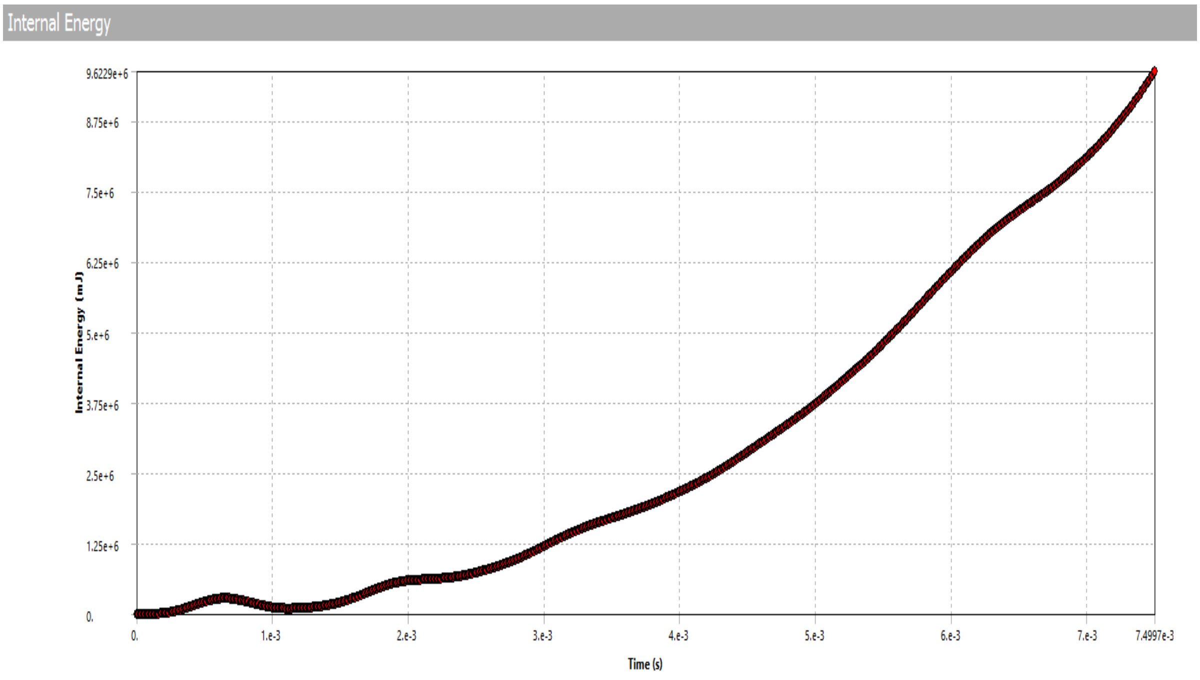

Figure C.10 Internal Energy for 45^0

3. Equivalent (von-Mises) Stress

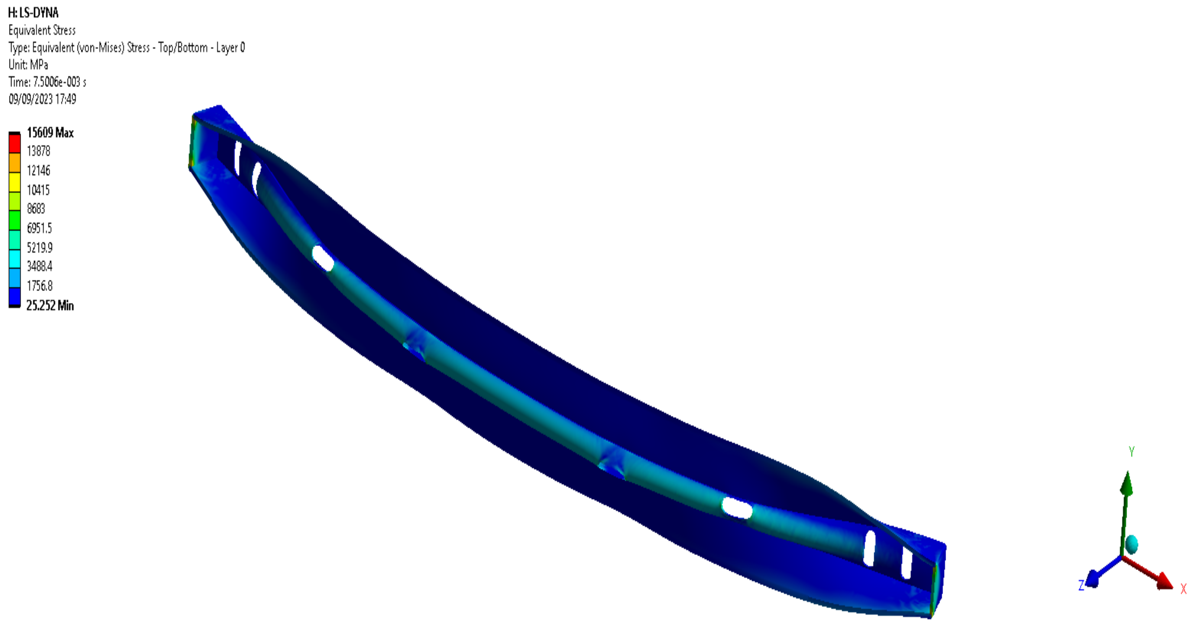

Figure C.11 Von-Mises Stress for 45^0

4. Directional Acceleration

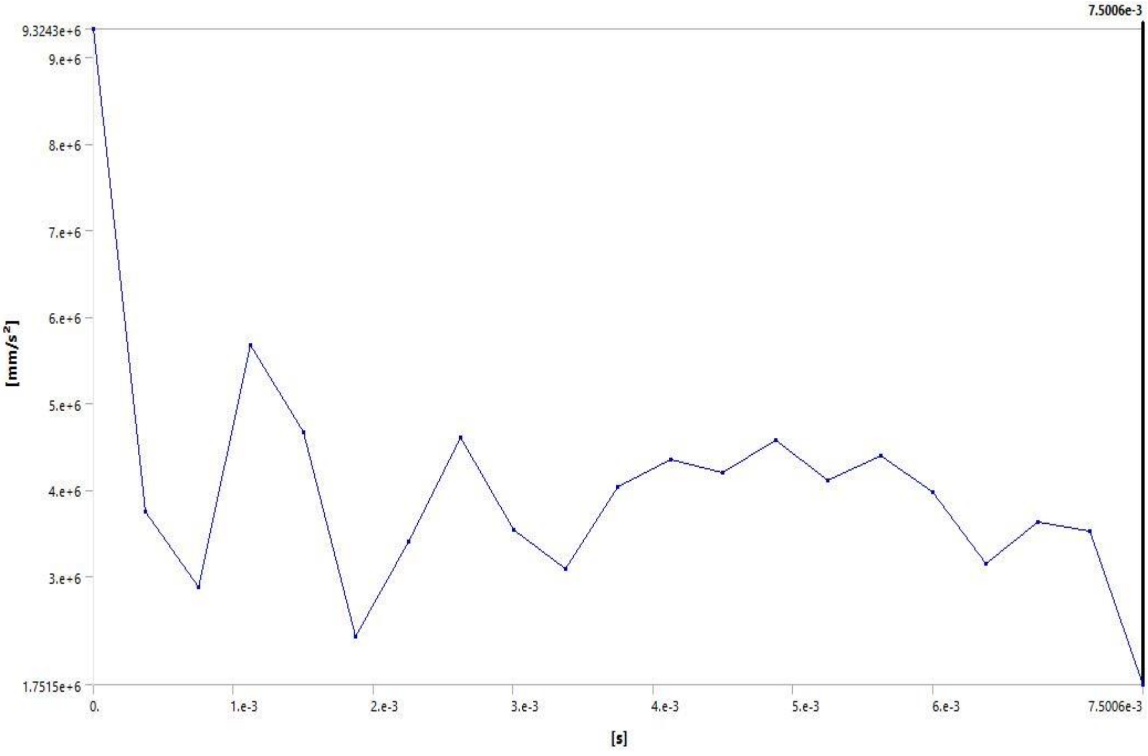

Figure C.12 Directional Acceleration for 45^0

- **All the lamina were arranged 67.5^0**

1. Total Deformation

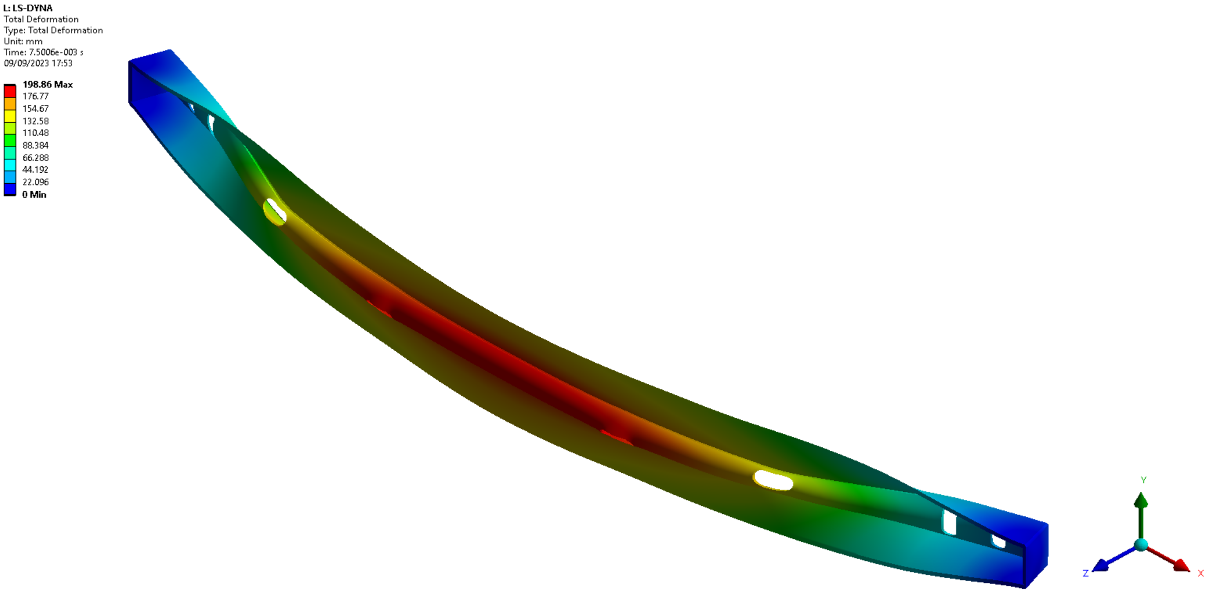

Figure C.13 Total Deformation for 67.5^0

2. Internal Energy

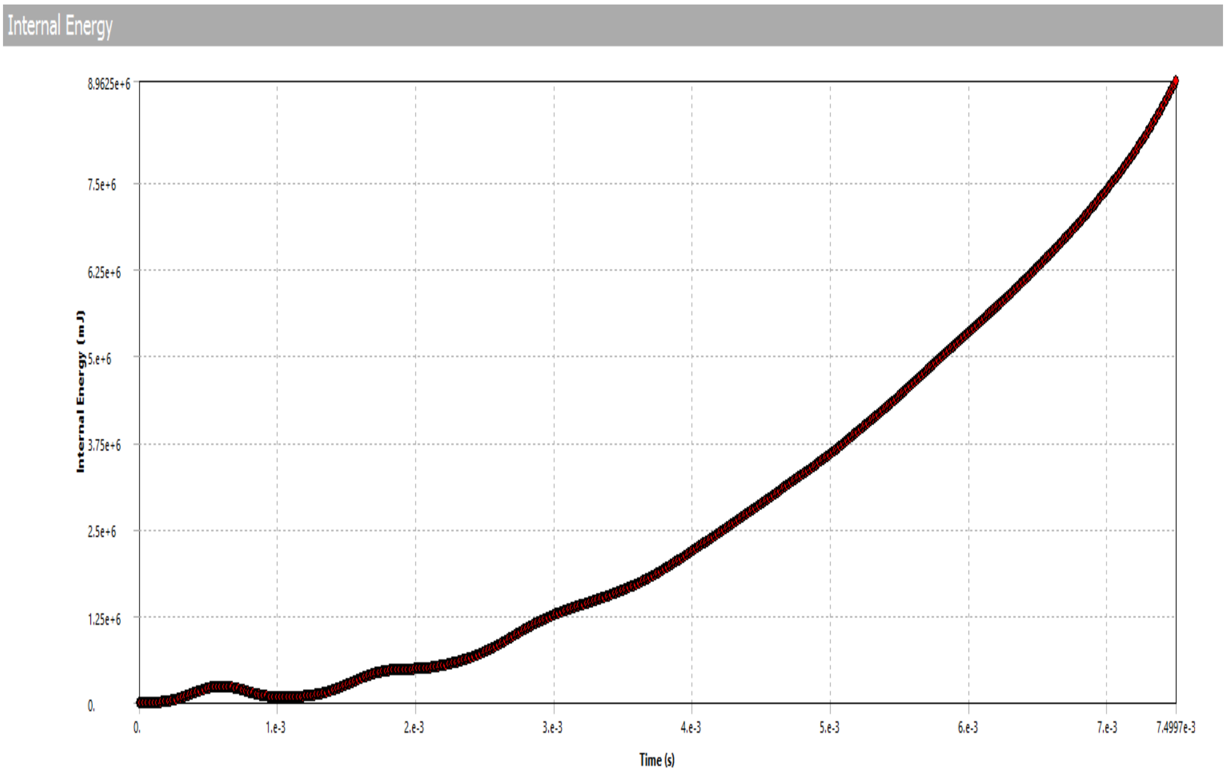

Figure C.14 Internal Energy for 67.5^0

3. Equivalent (von-Mises) Stress

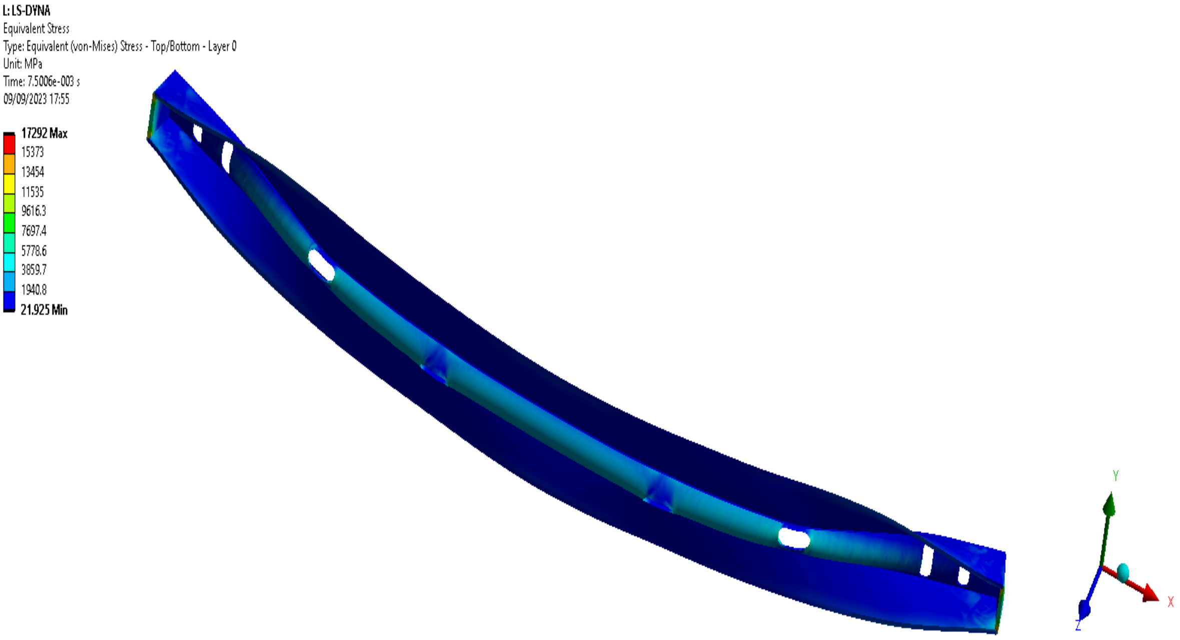

Figure C.15 Equivalent Stress for 67.5^0

4. Directional Acceleration

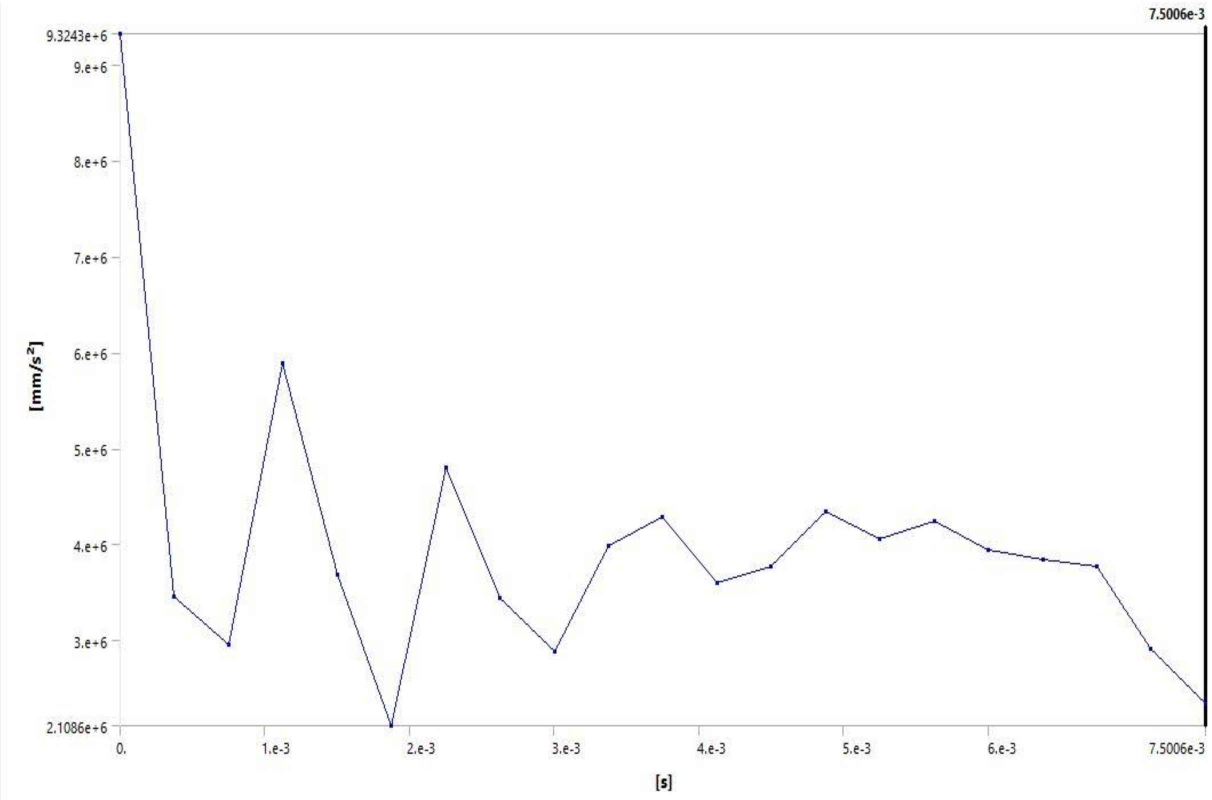

Figure C.16 Directional Acceleration for 67.5^0

- **All the lamina were arranged 90^0**

1. Total Deformation

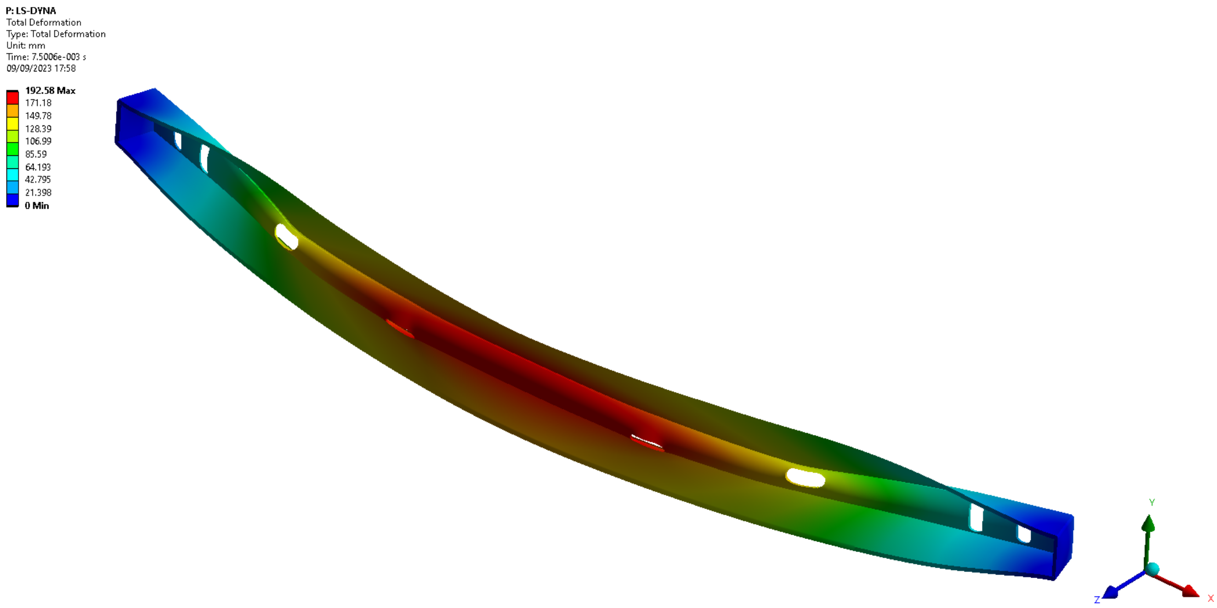

Figure C.17 Deformation for 90^0

2. Internal Energy

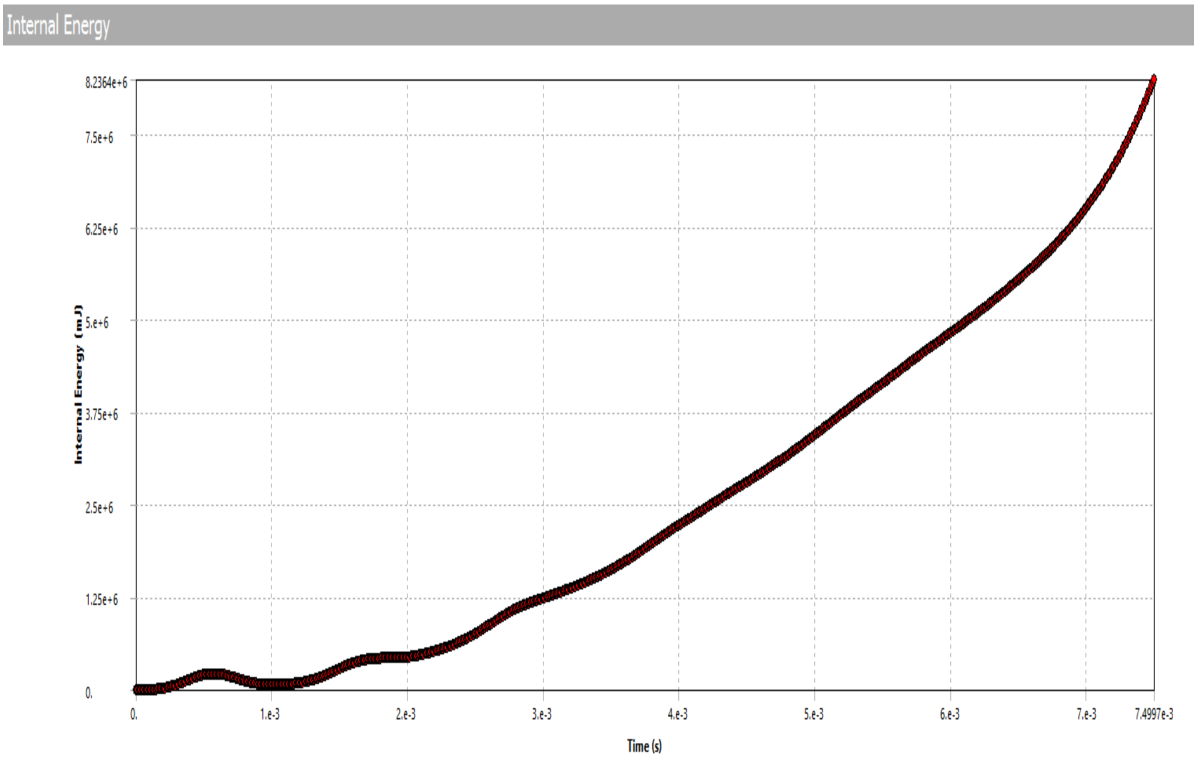

Figure C.18 Internal Energy Absorbed for 90^0

3. Equivalent Stress

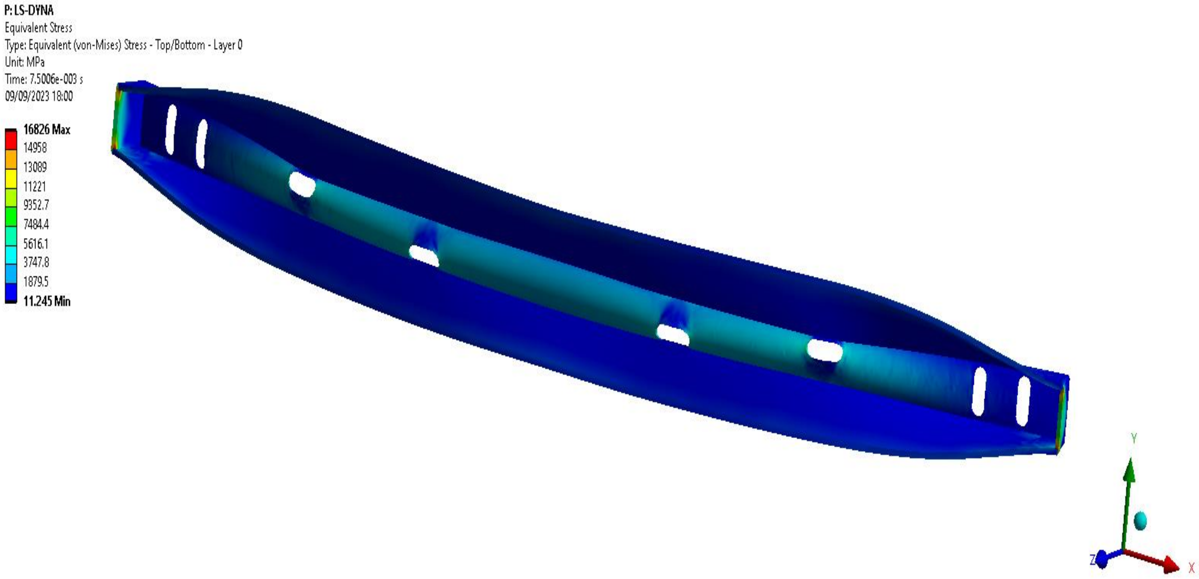

Figure C.19 Equivalent Stress for 90^0

4. Directional Acceleration

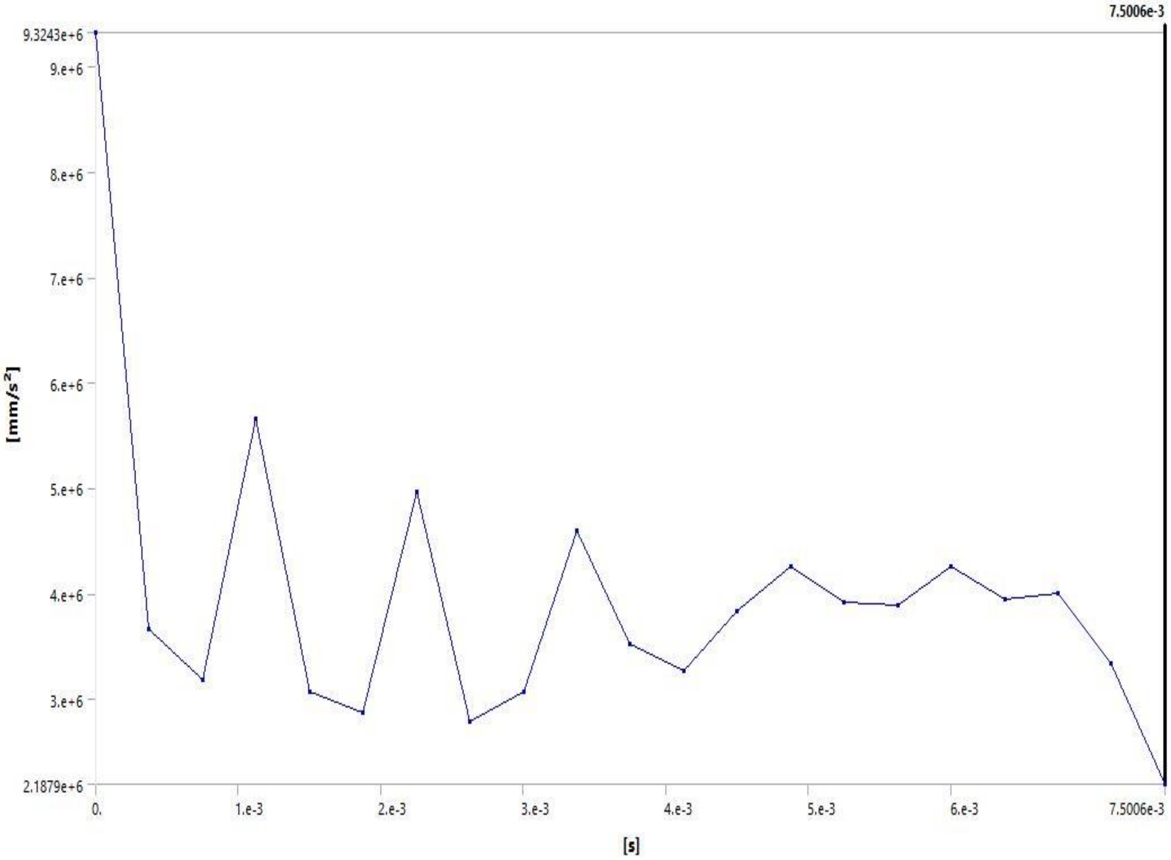

Figure C.20 Directional Acceleration for 90^0

- **Each lamina was arranged 45^0, 0^0, 45^0, 0^0, 45^0 Respectively**

1. Total Deformation

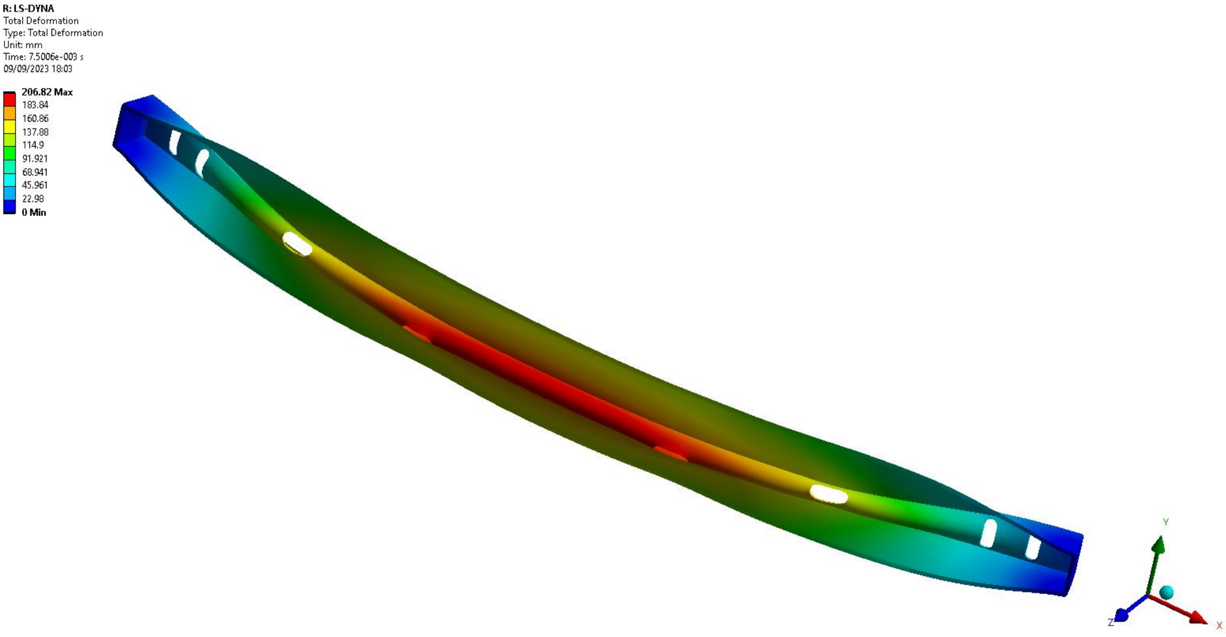

Figure C.21 Total Deformation for 45^0, 0^0, 45^0, 0^0, 45^0

2. Internal Energy

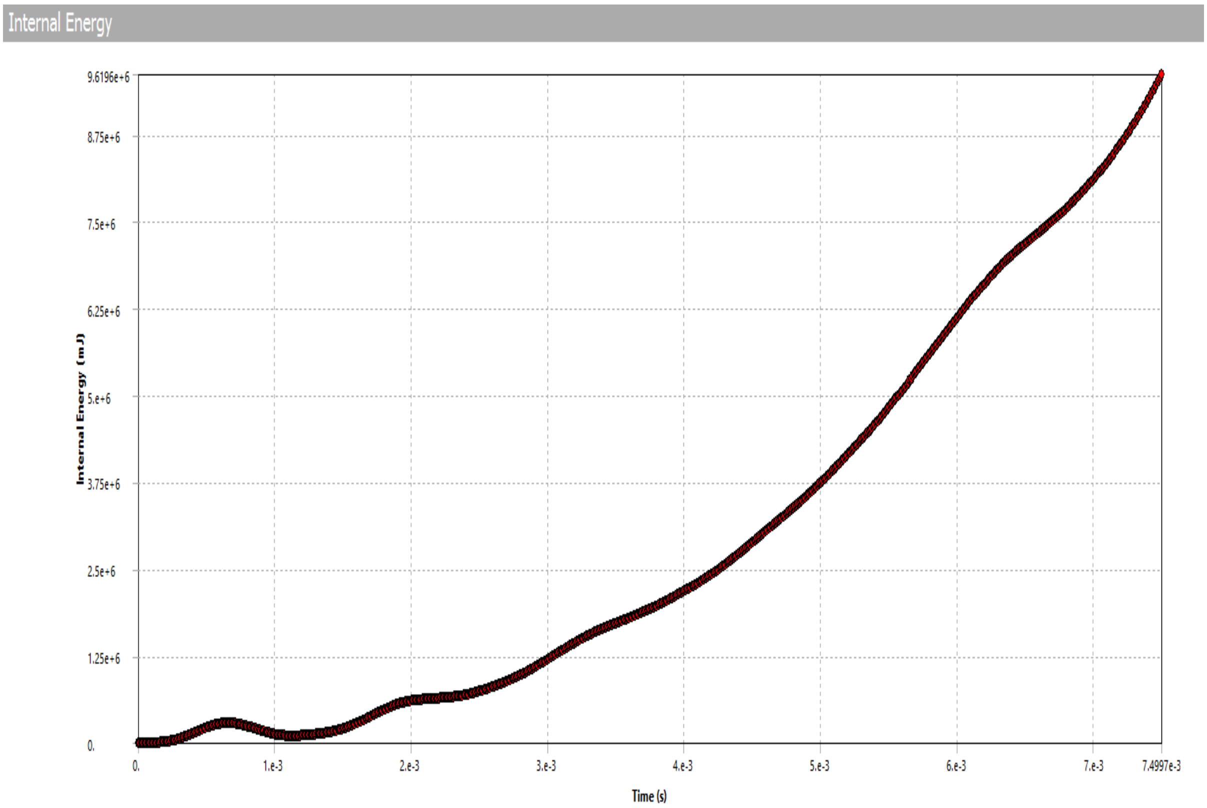

Figure C.22 Internal Energy for 45^0, 0^0, 45^0, 0^0, 45^0

3. Equivalent Stress

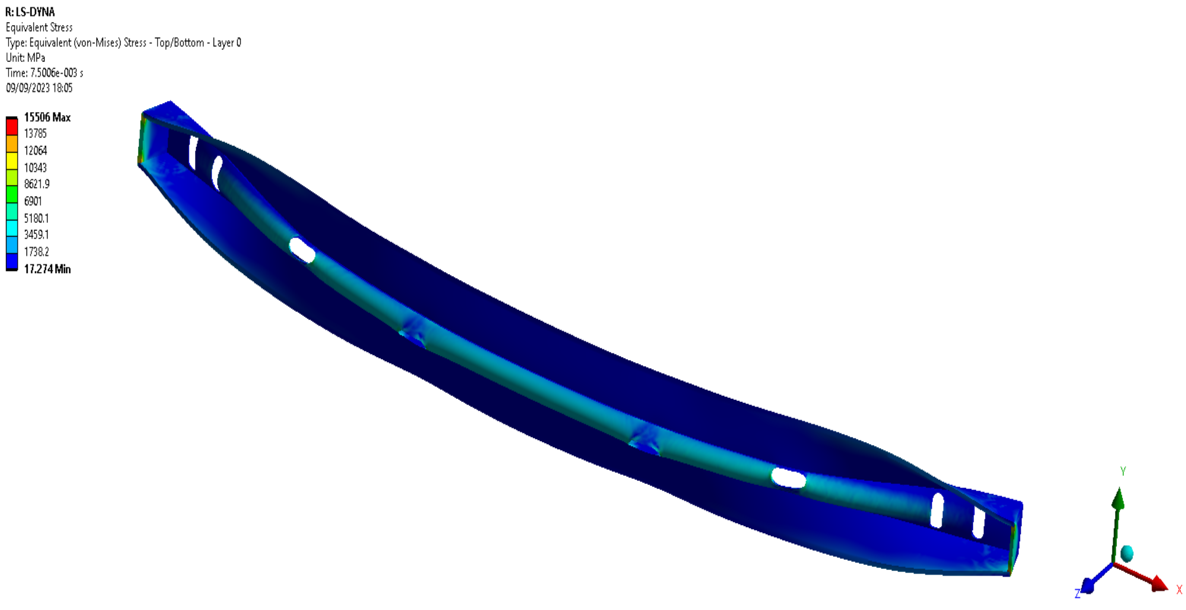

Figure C.23 Von-Mises for 45^0, 0^0, 45^0, 0^0, 45^0

4. Directional Acceleration

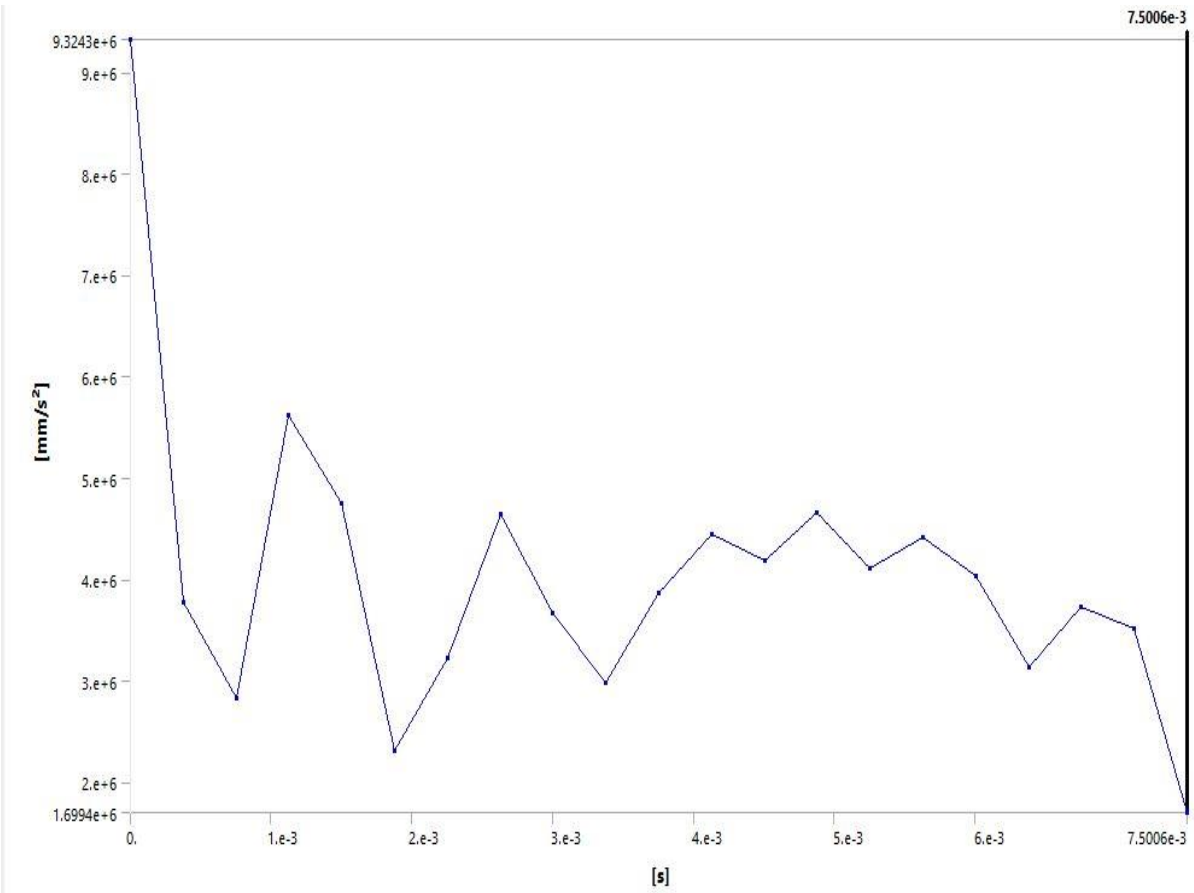

Figure C.24 Acceleration for 45^0, 0^0, 45^0, 0^0, 45^0

➢ Each lamina was arranged 0^0, 90^0, 0^0, 90^0, 0^0 Respectively

1. Total Deformation

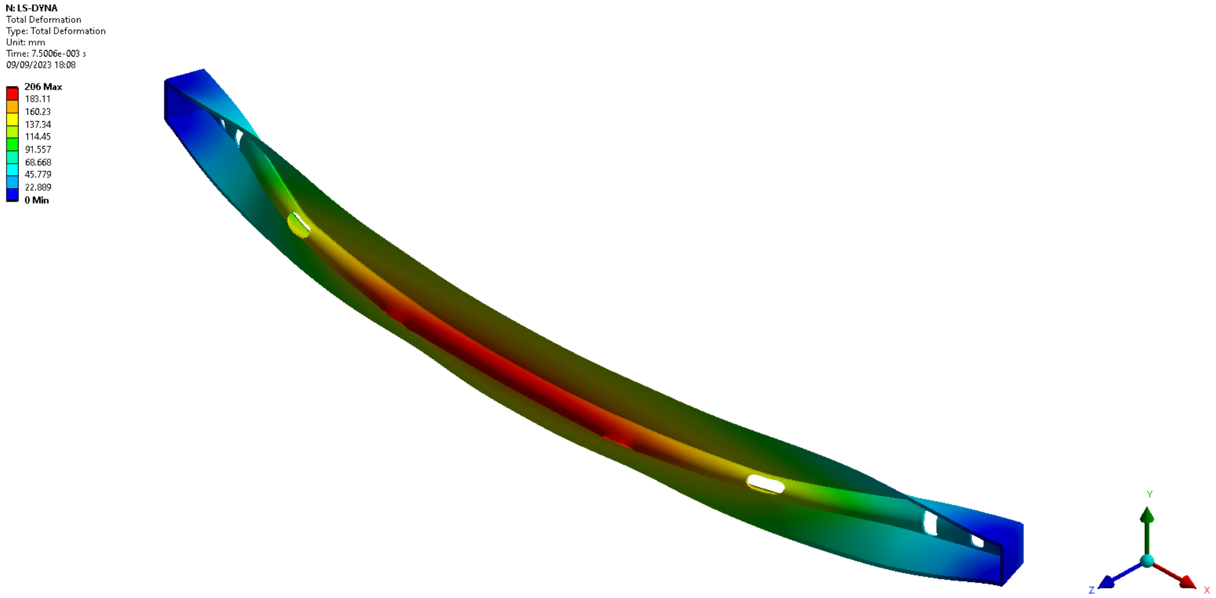

Figure C.25 Total Deformation for 0^0, 90^0, 0^0, 90^0, 0^0

2. Internal Energy

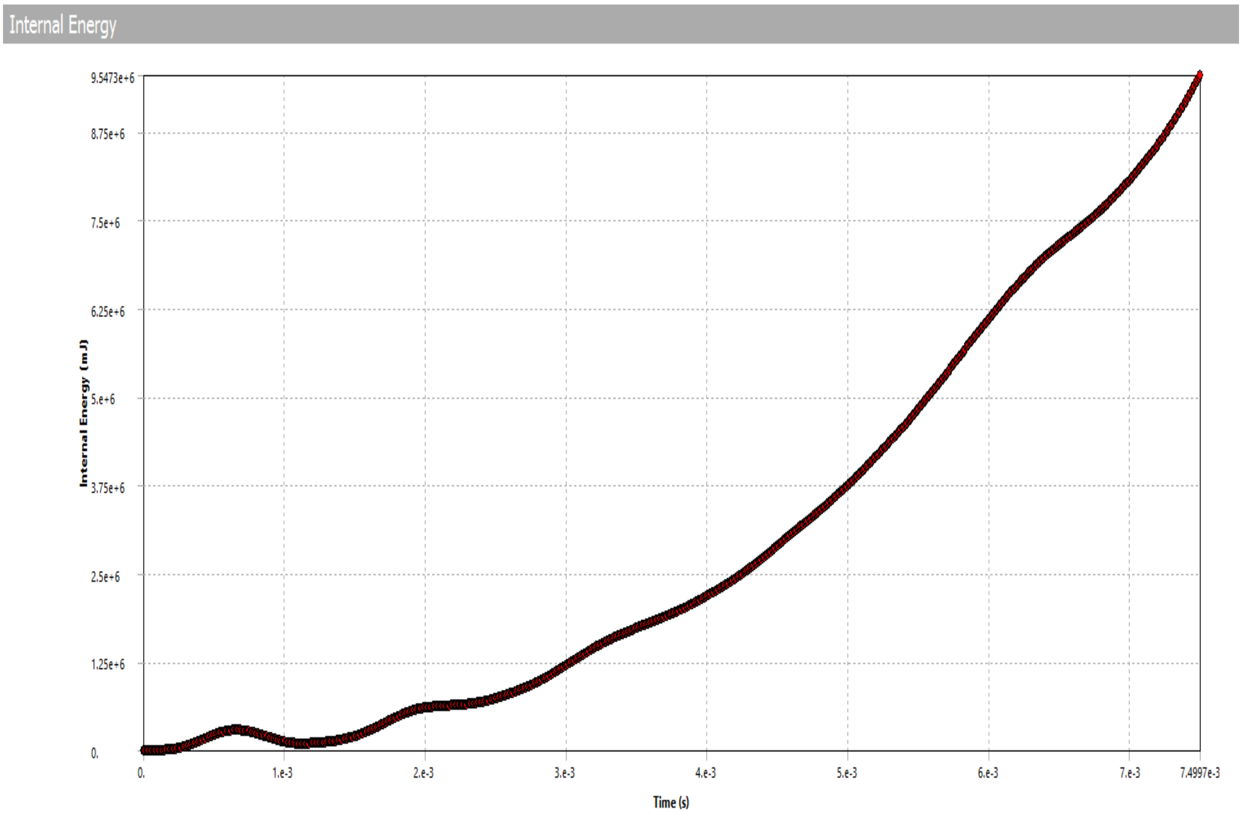

Figure C.26 Internal Energy for 0^0, 90^0, 0^0, 90^0, 0^0.

3. Equivalent Stress

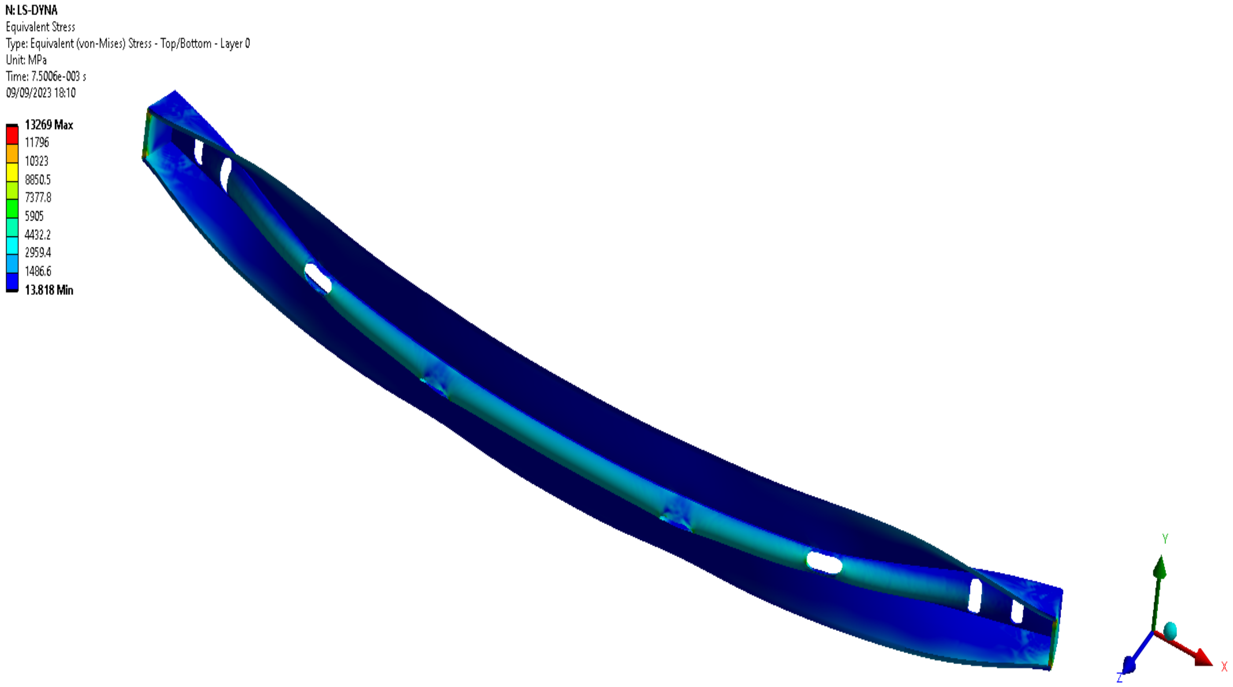

Figure C.27 Equivalent Stress for 0^0, 90^0, 0^0, 90^0, 0^0

4. Directional Acceleration

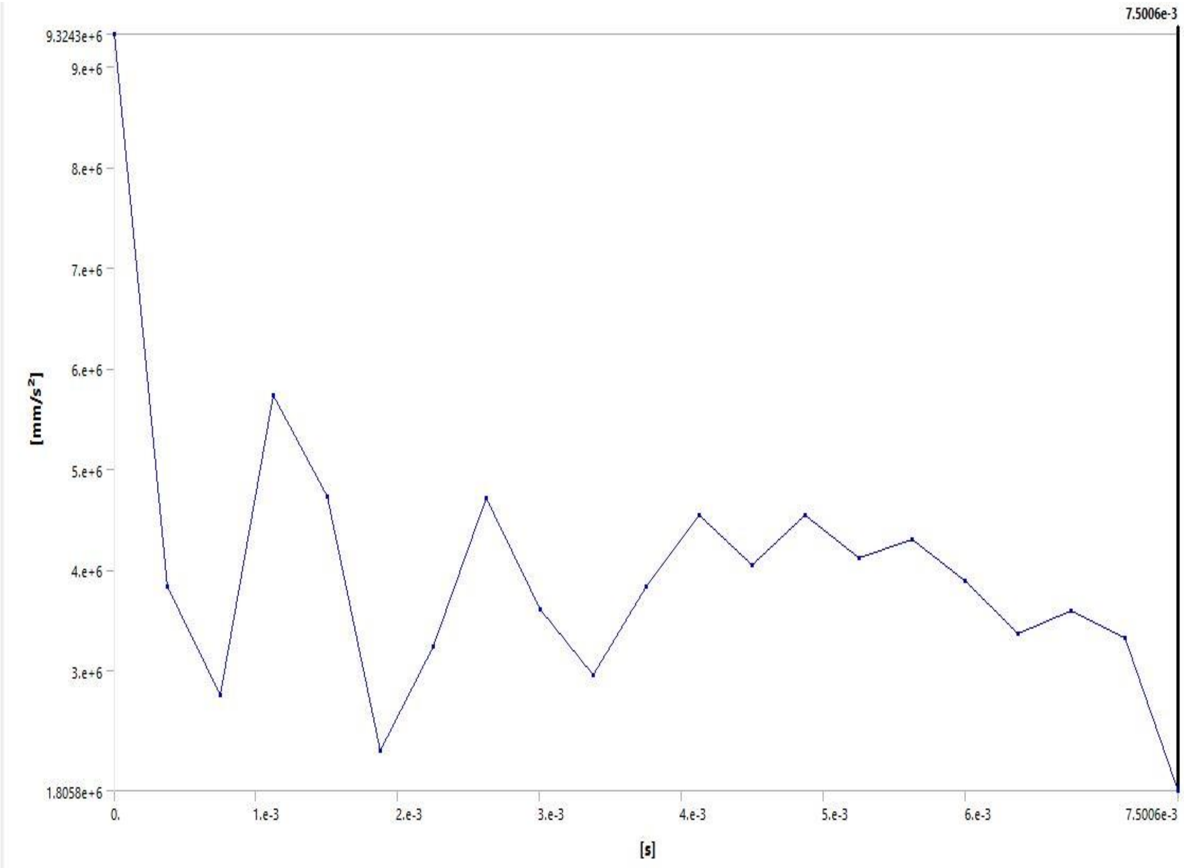

Figure C.28 Directional Acceleration for 0^0, 90^0, 0^0, 90^0, 0^0

➢ **Each lamina was arranged -45^0,45^0,-45^0,45^0,-45^0 Respectively**

1. Total Deformation

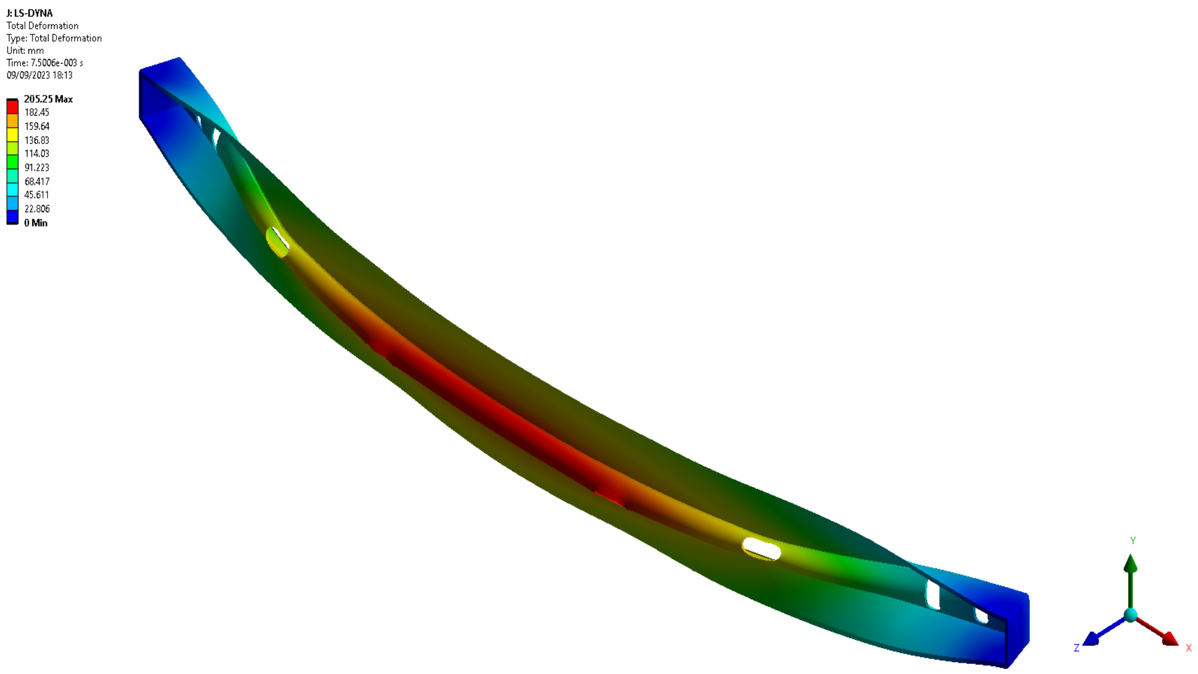

Figure C.29 Total Deformation for -45^0, 45^0,-45^0, 45^0,-45^0

2. Internal Energy

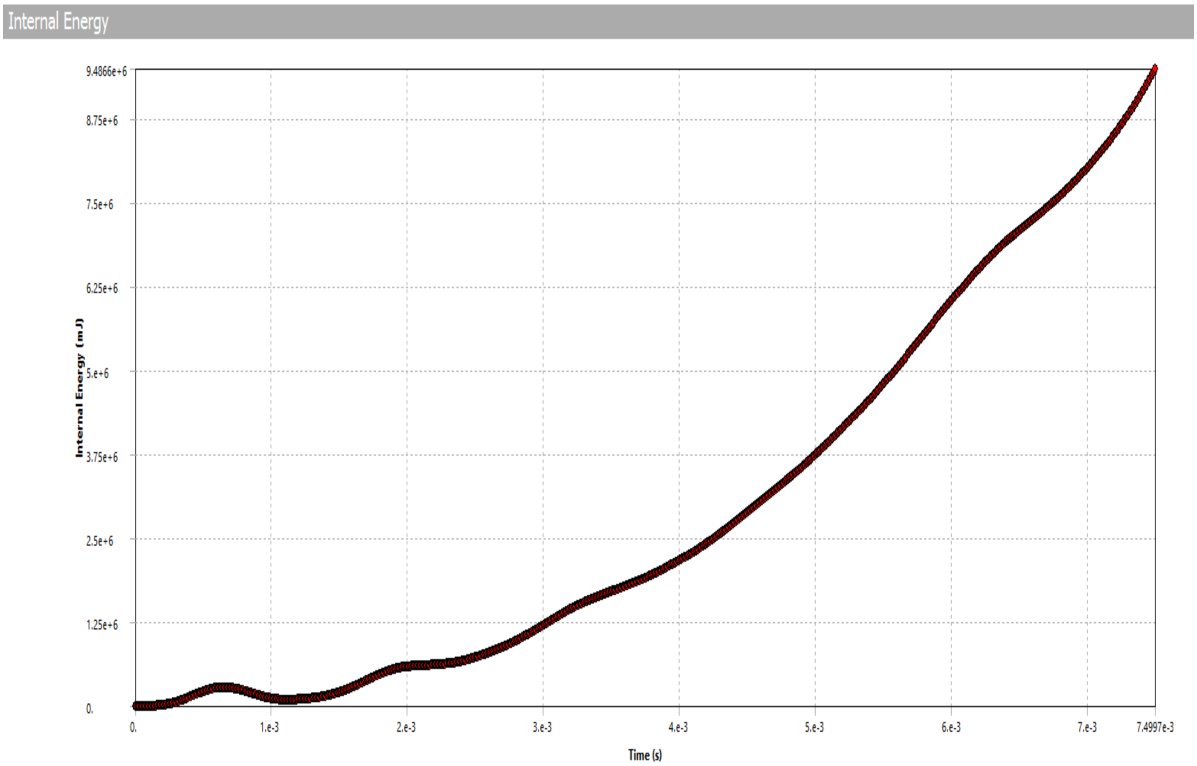

Figure C.30 Internal Energy for -45^0, 45^0,-45^0, 45^0,-45^0

3. Equivalent Stress

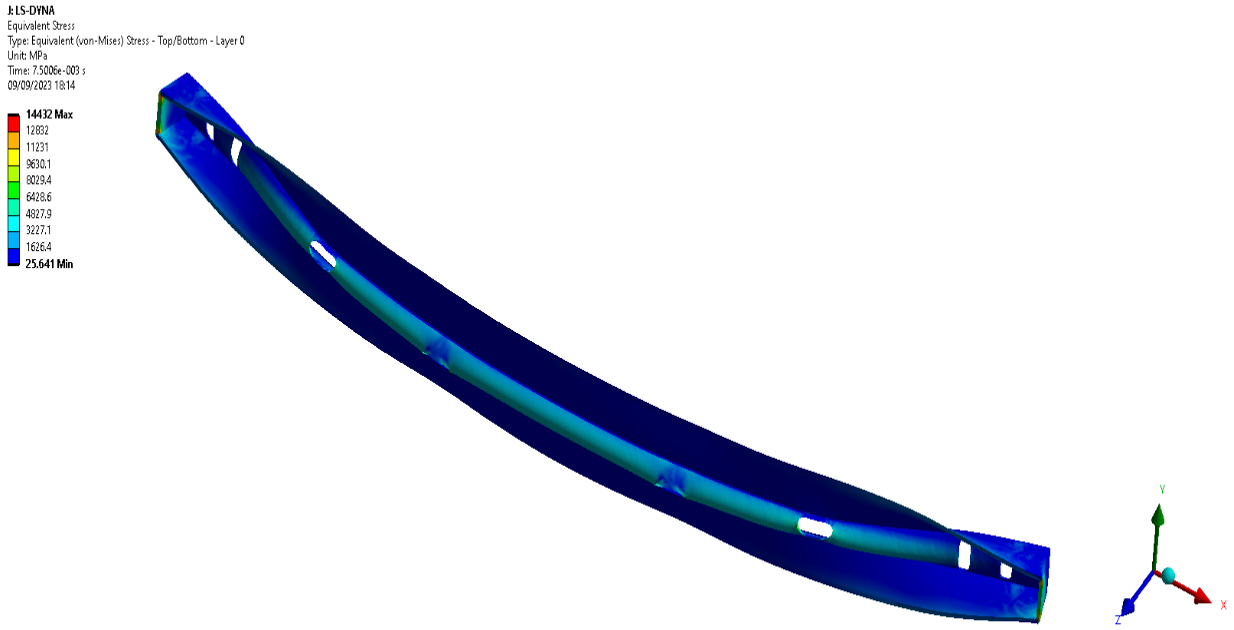

Figure C.31 Equivalent Stress for -45^0, 45^0,-45^0, 45^0,-45^0

4. Directional Acceleration

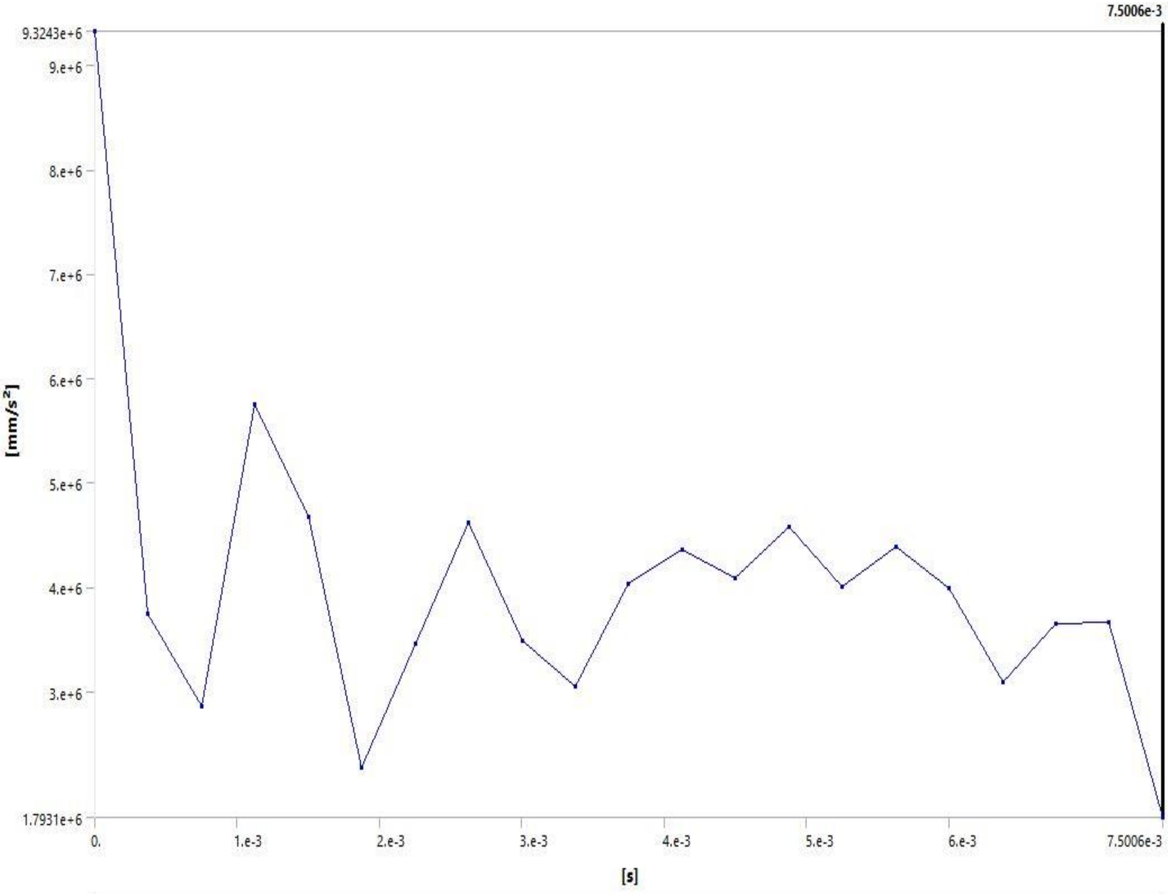

Figure C.32 Directional Acceleration for -45^0, 45^0,-45^0, 45^0,-45^0

- **Each lamina was arranged -45^0, 45^0, 0^0,-45^0, 45^0 Respectively**

1. Total Deformation

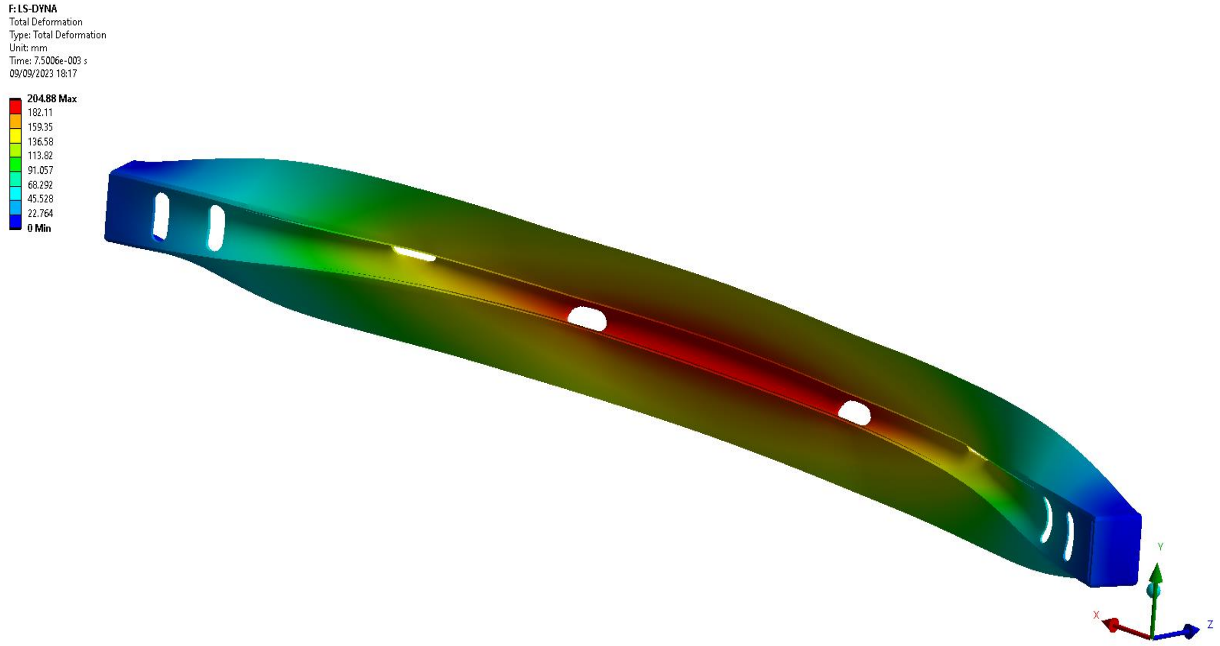

Figure C.33 Total Deformation for -45^0, 45^0, 0^0,-45^0, 45^0

2. Internal Energy

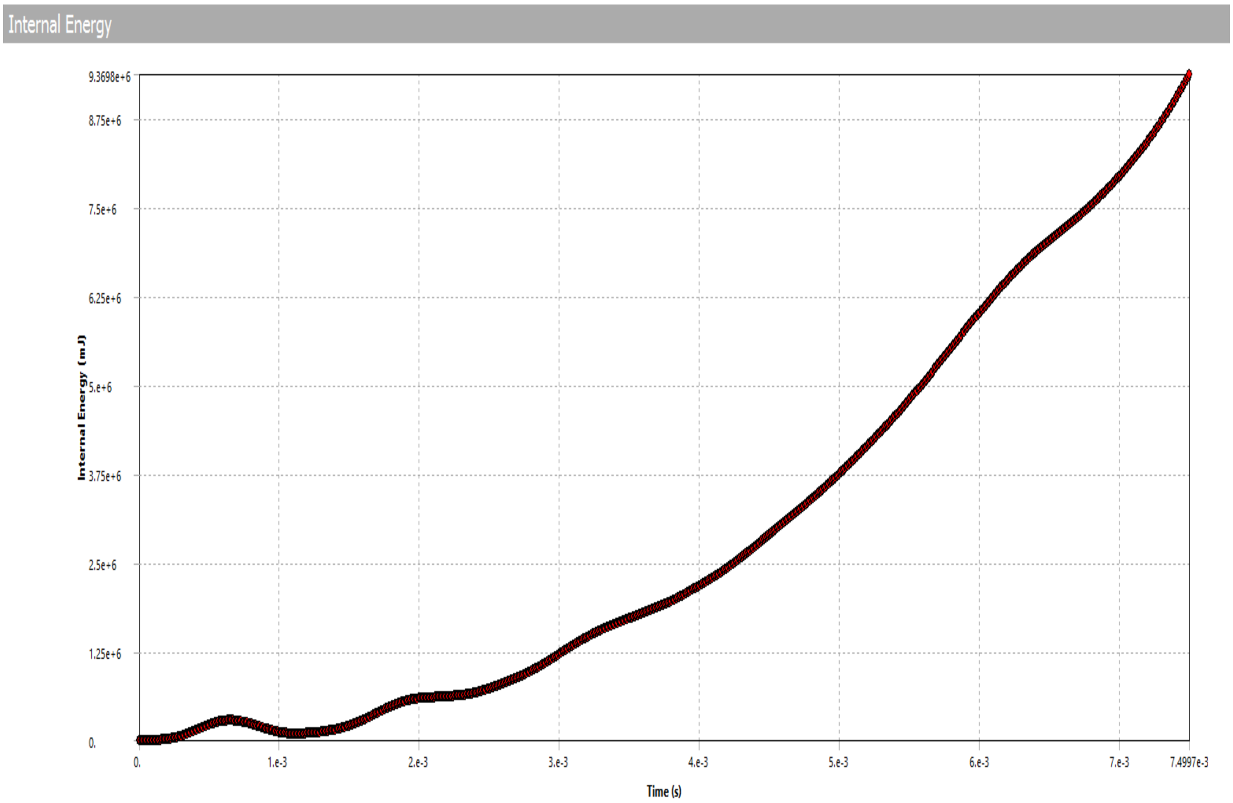

Figure C.34 Internal Energy for -45^0, 45^0, 0^0,-45^0, 45^0

3. Equivalent (Von-Mises) Stress

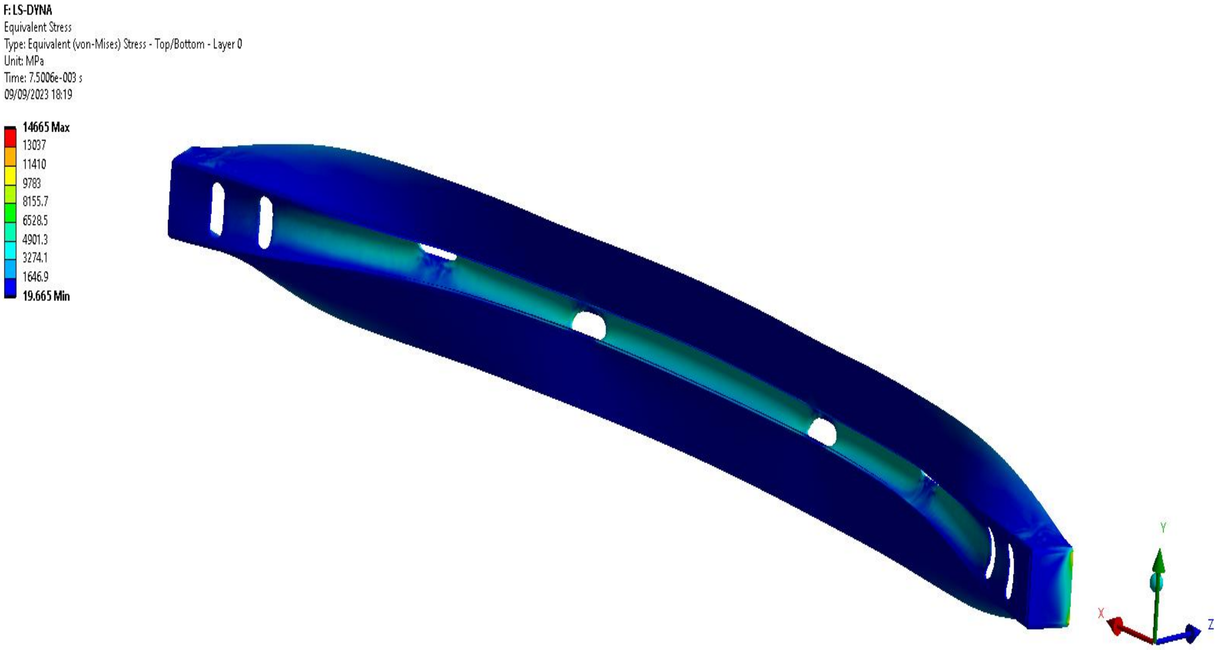

Figure C.35 Equivalent Stress for -45^0, 45^0, 0^0,-45^0, 45^0

4. Directional Acceleration

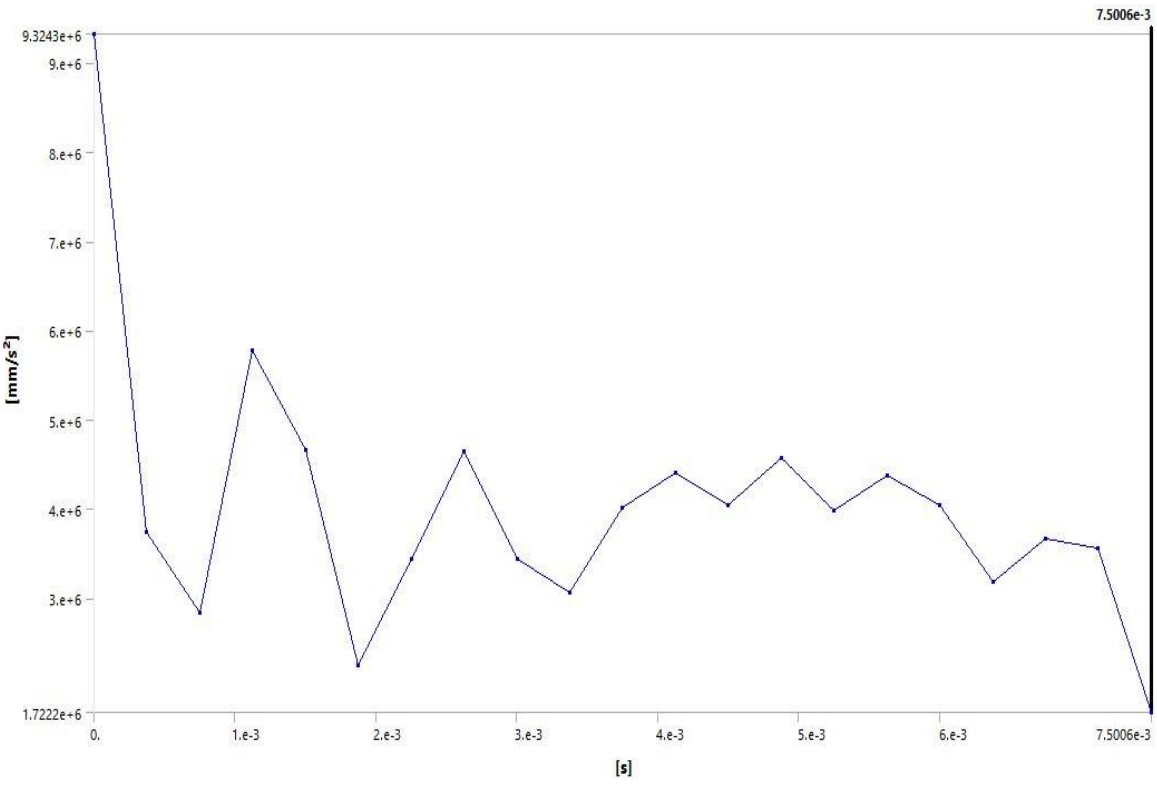

Figure C.36 Directional Acceleration for -45^0, 45^0, 0^0,-45^0, 45^0